This is to certify that the
dissertation entitled

ORGANOFUNCTIONAL SILICA MESOSTRUCTURES WITH

IMPROVED ACCESSIBILITY AND APPLICATIONS AS HEAVY

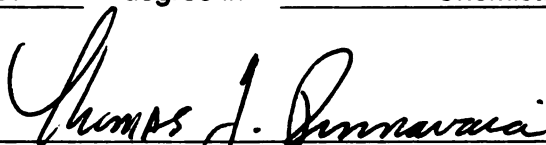METAL ION ADSORBENTS

presented by

Xin Sun

has been accepted towards fulfillment
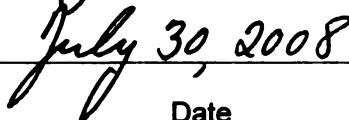of the requirements for the

Ph.D. degree in Chemistry

Thomas J. Pinnavaia
Major Professor's Signature

July 30, 2008
Date

PLACE IN RETURN BOX to remove this checkout from your record.
TO AVOID FINES return on or before date due.
MAY BE RECALLED with earlier due date if requested.

DATE DUE	DATE DUE	DATE DUE

ORGANOFUNCTIONAL SILICA MESOSTRUCTURES WITH IMPROVED
ACCESSIBILITY AND APPLICATIONS AS HEAVY METAL ION ADSORBENTS

By

Xin Sun

A DISSERTATION

Submitted to
Michigan State University
in partial fulfillment of the requirements
for the degree of

DOCTOR OF PHILOSOPHY

Department of Chemistry

2008

ABSTRACT

ORGANOFUNCTIONAL SILICA MESOSTRUCTURES WITH IMPROVED ACCESSIBILITY AND APPLICATIONS AS HEAVY METAL ION ADSORBENTS

By

Xin Sun

Effective approaches to the removal of toxic metals from contaminated water have involved the use of solid adsorbents, such as activated carbons, ion exchange resins, and functionalized silica-based materials including silica gels, clays and mesoporous silicas. The advantages of functionalized mesoporous silicas for environmental remediation are their high surface areas, well-defined pore size, and the ability to covalently link organic groups to the framework to allow for the selective adsorption of specific toxic heavy elements.

The overall goal of this work is to design functionalized mesostructured silica materials for use as heavy metal ion (i.e. Pb^{2+}) adsorbents. The approaches investigated include the incorporation of organosilanes, heteroatoms, and surfactants into the framework structure. The hydrogen bonded supramolecular assembly of a neutral alkylamine surfactant and a nonionic silica sources was used to form wormhole mesostructures.[1,2] The key objective was to improve the accessibility of the functional sites within the mesostructured silica framework.

Mesoporous amine-functionalized organosilicas were synthesized via several routes. A hydrophobic *t*Boc-protected amine group or a nitrile group was incorporated into the framework by direct assembly of an organosilane and tetraethylorthosilicate (TEOS) in the presence of dodecylamine as a surfactant. The amine groups were formed inside the mesopores of organosilica framework by Boc deprotection or nitrile reduction.

The obtained mesostructure showed a much higher structural order and much higher accessibility of the amine groups in comparison to derivatives synthesized by the conventional direct co-condensation of TEOS and an amino-functional organosilane. The resulting mesostructures had a Pb^{2+} trapping capacity of 0.23-0.48 mmol g^{-1}.

An attempt also was made to utilize the structure-directing surfactant for the removal of heavy metal ions from solution. As-made mesophases containing intercalated tallow amine surfactants showed good affinity towards Pb^{2+} ions, having a maximum trapping capacity of 1.2 mmol g^{-1}. However, it remained a concern that the surfactant was not irreversibly bound inside the mesopores. This problem was solved by introducing an epoxide organic moiety into the silica synthesis process in order to immobilize the amine surfactant inside the mesopores through the formation of covalent bonds. This modification also reduced the hydrophobic nature of the mesopore environment. A mesophase containing 5 mol % immobilized dodecylamine surfactant had a Pb^{2+} trapping capacity of 0.33 mmol g^{-1}.

In addition, the alumination of mesostructured silica using lithium aluminum hydride, in-situ generated sodium aluminate and sodium aluminate solution as aluminum sources also was investigated. The tetrahedrally coordinated Al sites incorporated into the mesophases served as the cation exchange sites. The resultant adsorbents showed excellent Pb^{2+} trapping capacities of 0.75-1.0 mmol g^{-1}.

(1)   Pauly, T. R.; Liu, Y.; Pinnavaia, T. J.; Billinge, S. J. L.; Rieker, T. P. *J. Am. Chem. Soc.* **1999**, *121*, 8835-8842.

(2)   Kim, Y.; Lee, B.; Yi, J. *Sep. Sci. Technol.* **2004**, *39*, 1427-1442.

ACKNOWLEDGEMENTS

This dissertation would not have been realized without the help, support, guidance and efforts of a lot of people. First and foremost I want to thank Dr. Tom J. Pinnavaia, my doctoral advisor, for instilling in me the qualities of being a good scientist and chemist. I shall never forget his encouragement for independent thinking and inspiring discussions during the past five years. I also really appreciate his support on my internships and all his advices for my career launching. He is one of the rare advisors that students dream that they will find.

Additionally, I would like to thank my group members, former and present, for their friendships. I am grateful for the rewarding discussions with Dr. Zhaorong Zhang and Dr. Hui Wang. I also want to thank DK, Christ and Susan for making our office and lab an attractive and fun place to go everyday.

I must acknowledge as well all the friends I made at Michigan State University. They made East Lansing feel like a second home to me. I would especially like to thank Meng Li for her great friendship and help during the past years.

Finally, I would like to thank my family. My parents showed great understanding and support on my decision of pursuing my Ph.D. study abroad. They have always been having faith in me. I also want to give my special thanks to my husband, Lingyun, my best friend I have known for fourteen years. I am deeply grateful for his patience, support and love.

TABLE OF CONTENTS

LIST OF TABLES

LIST OF FIGURES

ABBREVIATIONS

AA	Atomic absorption
AP	Aminoprpyl
APTMS	Aminopropyltrimethoxysilane
APTES	Aminopropyltriethoxysilane
BET	Brunauer-Emmett-Teller
BJH	Barrett-Joyner-Halenda
Boc	3-*tert*-butyloxycarbomate
CMC	Critical micelle concentration
CN	Butyonitrile
CNTES	4-(Triethoxysilyl)butyronitrile
CP	Cross polorization
CTA	Cetyltrimethylammonium
CTAB	Cetyltrimethylammonium bromide
DDA	Dodecylamine
EtOH	Ethanol
FT-IR	Fourier transform infrared spectroscopy
HMS	Wormhole mesostructured silica synthesized with amine surfactant using hydrogen bonding interactions under neutral condition
HR-STEM	High-resolution scanning transmission electron microscopy
I^0	Neutral silicate precursors, which are obtained under neutral reaction conditions

I^+	Cationic silicate precursors, which are obtained under acidic reaction conditions
I^-	Anionic silicate precursors, which are obtained under basic reaction conditions
IUPAC	International Union of Pure and Applied Chemistry
LAH	Lithium aluminum hydride
LCT	Liquid crystal templating
MAS	Magic angel spinning
mmol	Millimoles
MP	Mercaptopropyl
MPTMS	Mercaptoprypyltrimethoxysilane
N^0	Non-ionic surfactants (such as alkyl poly(ethylene oxide))
NHtBoc	3-*tert*-butyloxycarbonylaminopropyl
NHtBocTES	3-*tert*-butyloxycarbonylaminopropyltriethoxysilane
NMR	Nuclear magnetic resonance
P/P_0	Relative pressure P=pressure P_0=saturation pressure
PEO	Polyethylene oxide
PMOs	Periodic mesoporous organosilicates
ppm	Parts per million
PTMS	Phenyltrimethoxysilane
Q^2	Incompletely condensed silica sites $Si(OSi)_2(OH)_2$
Q^3	Incompletely condensed silica sites $Si(OSi)_3(OH)_1$
Q^4	Completely condensed silica sites $Si(OSi)_4$

S^0	Neutral surfactants (such as alkyl amine surfactants)
S^+	Cationic surfactants (such as alkylammonium surfactants)
S^-	Anionic surfactant (such as carboxylic salt surfactants)
S_{BET}	Specific surface area in m^2 g^{-1} obtained from the linear part of the adsorption isotherm using the Brunauer-Emmett-Teller equation
SEM	Scanning electron microscopy
SO_3H	Sulfonic acid moiety
T^2	Functionalized Q^2 site $RSi(OSi)_2(OH)$
T^3	Functionalized Q^3 site $RSi(OSi)_3$
TBOS	Tetrabutyl orthosilicate
TEOS	Tetraethyl orthosilicate
TEM	Transmission electron microscopy
TGA	Thermogravimetric Analysis
TLCT	True liquid crystal templating
TMB	Trimethylbenzene
VTES	Vinyltriethoxysilane

Chapter 1

Introduction

1.1 Mesoporous silica molecular sieves background

Porous materials have properties suitable for a variety of applications such as adsorbents, ion exchangers, catalysts, etc. They possess accessible void space within their interior structure, as in zeolites and mesoporous silicas. Such porosity is described as "framework porosity", whereas the aggregation or intergrowth of small particles often results in the formation of "textural porosity" between the grains. According to the classification made by IUPAC,[1] porous solids can be arranged in three main categories, depending on their pore size (diameter, d).

1. Microporous materials with pores < 2 nm

2. Mesoporous materials with pores in the intermediate range between 2-50 nm

3. Macroporous materials with pores > 50 nm

The dimensions and accessibility of pores of microporous materials, including zeolites and related crystalline molecular sieves, are restrained to their sub-nanometer scale. This limits the application of microporous material systems to small molecules. During the past decade, an important effort has been focused on obtaining molecular sieves showing larger pore sizes. The introduction of supramolecular assemblies as templating agents (liquid-crystalline self-assembled surfactant micellar aggregates, rather than single surfactant molecules in the case of zeolite templating) permitted a new family of mesoporous silica and aluminosilicate compounds (M41S) to be obtained. These mesophases were first developed by research groups at Mobil Corp.[2,3] Several studies have investigated the mechanism of MCM-41, a mesostructured amorphous silica. It was

1

found that two different pathways are involved.[2,4,5] In the true liquid crystal templating (TLCT) pathway, the concentration of the surfactant is so high, much higher than the critical micelle concentration (CMC), that under the prevailing conditions (temperature, pH) a lyotropic liquid-crystalline phase is formed without requiring the presence of the precursor inorganic framework materials. On the other hand, it is also possible that liquid crystal templating (LCT) forms as a cooperative self-assembly of the structure directing agents and the already added inorganic precursors even below the CMC, in which case a liquid-crystal phase with hexagonal, cubic, or laminar arrangement can develop. The two mechanism pathways are shown in Figure 1.1.

In either case, an attractive interaction between the template and the silica precursors is needed to ensure the condensation of a continuous framework without phase separation taking places. The resulting organic-inorganic mesostructure could be alternatively viewed as an array of structured micellar rods embedded in a silica matrix. The removal of the surfactants, usually by calcination method, will produce the open, mesoporous silica framework. Generally, there are two types of interactions between the surfactant head groups and the inorganic precursors, namely, electrostatic interaction and hydrogen bonding interactions. These two types of interactions lead to different structures as described in the sections below.

2
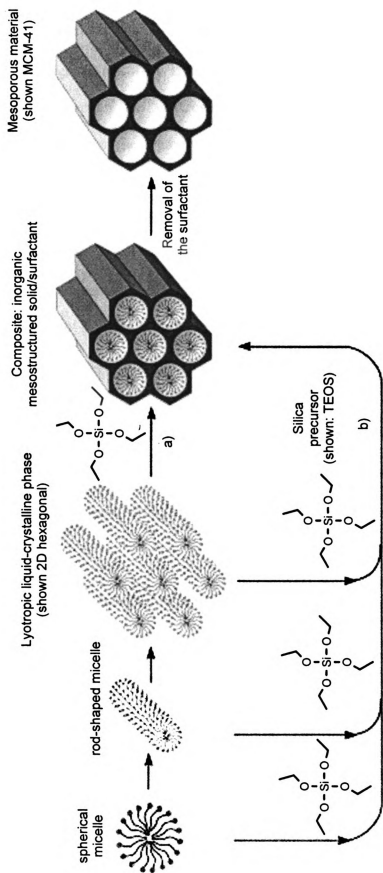
Figure 1.1. Formation of mesoporous materials by structure-directing agents through true (a) liquid-crystal template mechanism, or (b) cooperative liquid crystal template mechanism.[6]

3

1.1.1 Electrostatic interaction pathways

Hexagonal MCM-41 is the first example of a mesostructure silica material synthesized through the electrostatic interaction between the positively charged ammonium surfactant head group (S^+) and the negatively charged silicate precursors (I^-) under basic synthetic conditions. Cubic MCM-48 and lamellar MCM-50 were also synthesized via this S^+I^- pathway.[3]

The SBA series[7,8] of mesostructures was obtained by similar electrostatic interactions between the surfactant and inorganic precursor, except that a counter ion X^- to mediate the interaction between the protonated inorganic silica species and protonated surfactant of the same charge under acidic synthetic conditions, denoted the $S^+X^-I^+$ pathway.

Although mesoporous metal oxides also have been successfully made through the electrostatic interactions by anionic surfactant, no pure siliceous mesostructure has been made using an anionic surfactant via either S^-I^+ or $S^-X^+I^-$ pathway.

1.1.2 Hydrogen-bonding interaction pathways

Other synthesis routes rely on nonionic or neutral surfactants, where the main interactions between the template and the inorganic species are H-bonding or dipolar interactions, giving rise to the so-called neutral path. Tanev and Pinnavaia first synthesized mesostructured silica termed HMS using neutral primary alkylamine surfactant micelles (S^0) and an unchanged silica species (I^0), such as tetraethylorthosilicate.[9] As in the assembly of HMS mesostructures, MSU-X

4

mesostructures utilize a hydrogen-bonding interaction between an uncharged silica species (I^0) and the non-ionic surfactant (N^0).[10]

The different possible hybrid inorganic-organic interfaces are schematized in Figure 1.2.
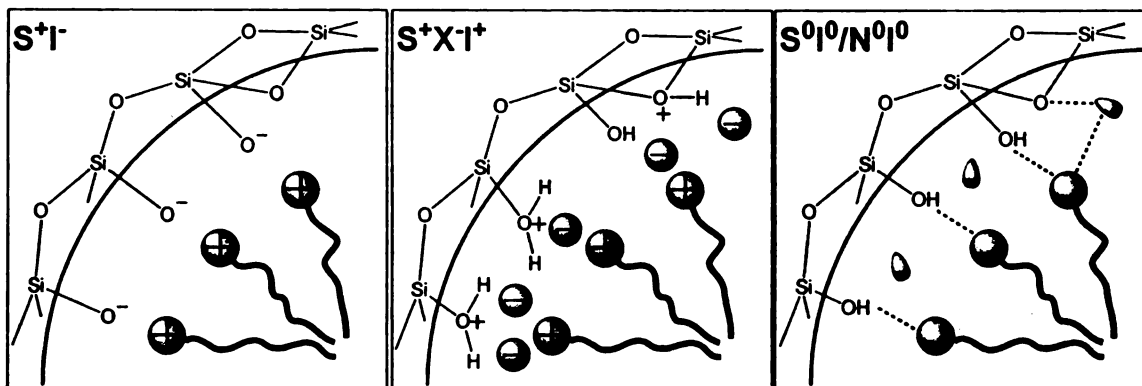
Figure 1.2. Schematic representation of interactions between the silica precursors and the head group of the surfactant molecules with consideration of the possible synthetic pathway in basic, acidic and neutral conditions

All mesostructured silicas possess extremely high surface areas and easily accessible, uniformly sized pores. Most importantly, the pore sizes exceeded those attainable in zeolites and they could be tuned in the nanometer range by choosing an appropriate surfactant templating system, sometimes augmented by a co-solvent or swelling agent[11].

1.2 Organic functionalization of mesoporous silicas

All mesostructured silicas possess extremely high surface areas and easily accessible, uniformly sized pores. Most importantly, the pore sizes exceeded those attainable in zeolites and they could be tuned in the nanometer range by choosing an

appropriate surfactant templating system, sometimes augmented by a co-solvent or swelling agent[11].

To further expand the use of mesoporous silicas, organic functional groups have been incorporated into the framework of the structures. By the choice of organic moiety, mesoporous derivatives can be designed to selectively trap toxic metal ion pollutants (such as mercury[12], arsenic[13], and lead[14]), as supports to immobilize enzymes[15-18], or as chemical sensors[19]. In general, there are two different pathways by which the organic functionality can be incorporated into the mesostructures: 1) the subsequent modification of the pore surface of a purely inorganic silica material ("grafting" pathway), and 2) the simultaneous co-condensation of corresponding silica and organosilica precursors ("direct assembly" pathway).

1.2.1 Incorporation of the organic functionality by grafting

Grafting is a method of covalently linking reactive organosilane species with surface silanol groups (terminal Si-OH groups). A typical synthesis involves two steps. First, pure inorganic mesostructured silica is synthesized through the methodologies mentioned before (electrostatic or electrically neutral pathways). Secondly, an organosilane reagent is allowed to react with the pre-formed mesostructured silica by condensation reaction, also called silylation, with surface silanol groups on the framework surface (Fig. 1.3). This also is called the post-synthesis functionalization method. The organosilanes used here must have hydrolysable group such as alkyloxy or haloid attached to the organosilicon sites.
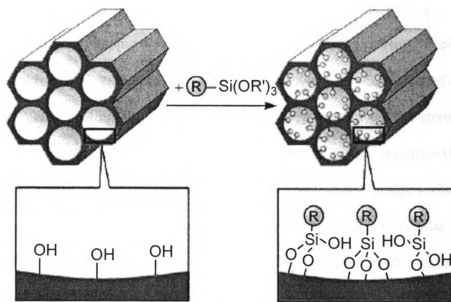
Figure 1.3. Schematic diagram for the grafting pathway used in the preparation of organic functionalized silica materials[6]

If a high surface coverage of functional groups is desired, it is important to maintain a large number of surface silanol groups after removal of the surfactants. Surfactant removal is carried out either by calcination or by appropriate solvent or ion exchange extraction methods. Calcination promotes condensation of unreacted silanol groups, and many surface groups are lost at typical calcination temperatures (400-600°C). The calcined mesoporous silicate can be rehydrated in boiling water and then removing the excess water by azeotropic distillation, e.g., with toluene or benzene.

Mesoporous materials have been grafted with a variety of organic functional groups, depending on the properties and applications sought. Grafting with groups that exhibit little or no reactivity, such as alkyl chain or phenyl group, can be used to tailor the pore size of the mesoporous solids and increase the surface hydrophobicity which can be used for organic pollutant removal from aqueous system. Reactive functional groups like alkyl thiols, alkyl amines, nitriles, etc. also have been grafted to the framework.

7

In order to have uniform distribution of surface organic groups through the grafting method, some unique methods have been used. A strategy of imprint coating was first designed by Dai to have specific ligand position towards the formation of a complex (Fig. 1.4).[20] This coating methodology allows precise control of the stereochemical arrangement of ligands on the surfaces of mesopores, which in turn optimizes the binding of a targeted metal ion. Moreover, a well-defined amine-functionalized silica surface displaying evidence of isolated amine sites was prepared using a molecular patterning technique.[21-23] A tritylimine patterning agent, which can be removed afterwards, was used to spatially position the amine sites a minimum distance from each in order to have single well paced organic functional sites (Fig. 1.5).
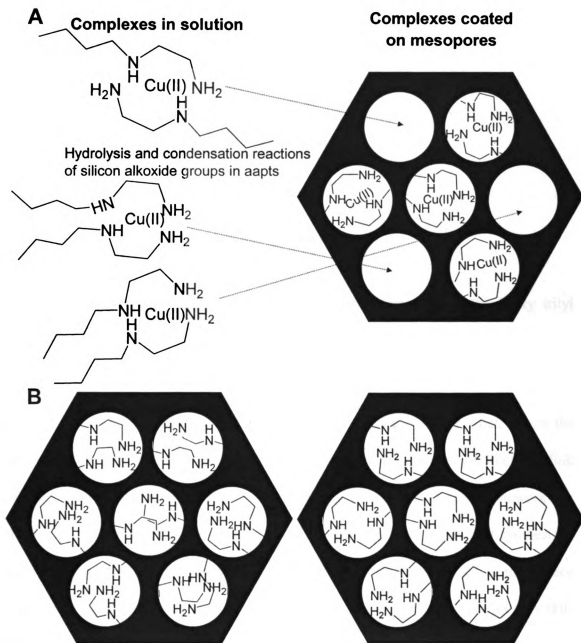
Figure 1.4. (A) Schematic diagram of the imprint-coating process: first the complexes are introduced between target metal ions and bifunctional ligands, then the siloxane groups in the bifunctional ligands are hydrolyzed, and finally covalently coated on the mesopore surfaces. (B) Schematic representation of the difference between the cavities generated by conventional coating (left) and imprint coating (right).[20]
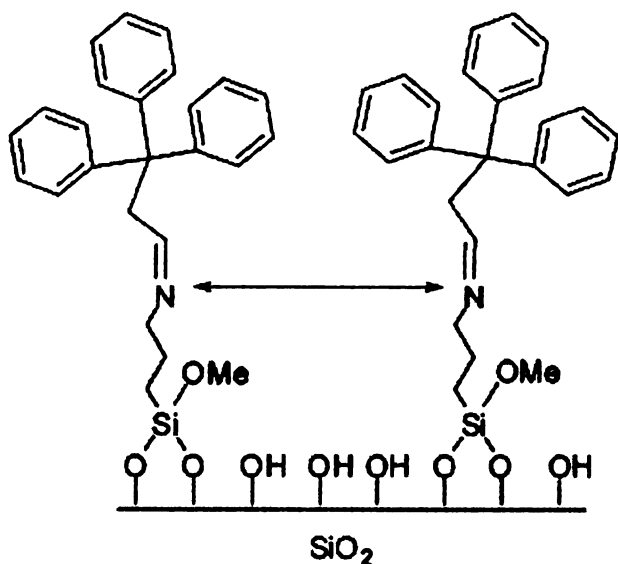
Figure 1.5. Single site distribution of amine groups obtained using the bulky trityl protecting group as a spacer.[22]

The original structure of the mesoporous support is generally maintained after grafting. However, there are some drawbacks of the grafting pathway. First, due to the differences in geometrical conformation, the functional groups are not likely to link completely to the surface. Under certain conditions the O-Si bond to the framework can break due to hydrolysis processes, causing functionality lost of the post-synthesized materials. Second, the functional groups may not be uniformly distributed on the surface of the framework. And if the loading percentage goes higher, the organosilanes may self-polymerize. Still further, because of the large number of sequential steps, the grafting pathway is time consuming.

1.2.2   Incorporation of the organic functionality by direct assembly

Another approach to synthesize organically functionalized mesoporous materials is the direct-assembly pathway, in which silica precursor tetraethyl orthosilicate (TEOS)

and organosilane $(R'O)_3Si\text{-}R$ (where R' is Et or Me and R is non-hydrolysable organic group) precursors co-condensate in the presence of structure directing agents leading to materials with organic residues anchored covalently to the pore walls (Fig. 1.6). The co-condensation of a silicon tetraalkoxide as a precursor such as TESO, which constructs the pore wall, is indispensable because the three-connected organosilane itself can not build an infinite framework. The removal of surfactant by using solvent extraction generates the mesoporous silicate with surface functionalization.
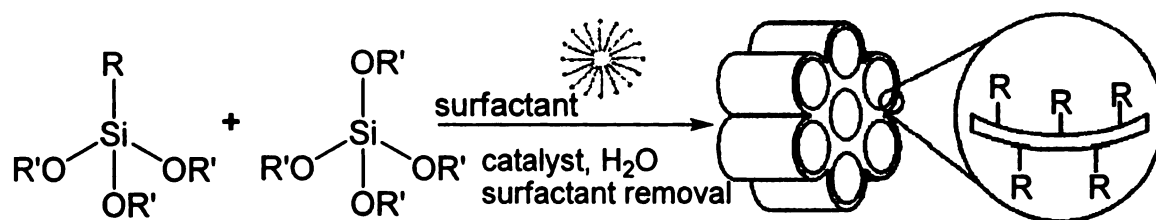
Figure 1.6. Schematics of direct-assembly pathway, where R is the functional group and OR' is a hydrolysable group,[24] for the synthesis of an organofunctional mesoporous silica from co-condensation pathway.

This one-pot direct assembly method has been commonly used to prepare organic functionalized mesoporous silica materials through various synthetic conditions. Mann et al. first used a cationic surfactant as the structure directing agent to incorporate phenyl and n-alkyl chain into the silicate framework under basic condition, which was the reaction condition used for the synthesis of MCM related mesoporous silica materials.[25,26] It was reported that numerous kinds of organic groups, such as aminopropyl, mercaptopropyl, glycidyloxypropyl, imidazolidinyl, vinyl, methyl, and ethyl, have been successfully incorporated into the MCM-41 silicate framework through the S^+I^- route.[27-33] Acidic conditions were used for the incorporation of organic groups into SBA related

hexagonal or cubic structure silica materials through $S^+X^-I^+$ route.[34-39] Compared to basic conditions, the interactions between the surfactant and the silicate surface under acidic conditions are weaker. Therefore, the surfactant could be extracted with ethanol, instead of an acid/alcohol mixture, which is the method used for materials synthesized via S^+I^- route, although some structural disordering was observed after this process.

Macquarrie first used the neutral synthetic conditions to incorporate aminopropyl and cyanoethyl groups and obtained wormhole structured organic-inorganic hybrid materials via the S^0I^0 route (HMS).[40] Pinnavaia and Mercier subsequently extended the incorporation to other functional groups, including vinyl, imidazole, mercaptopropyl, phenyl, octyl, butyl, etc.[41-45] Neutral N^0I^0 assembly strategy was also utilized to successfully synthesized mercaptopropyl functionalized hybrid materials.[46-48] Due to the weak hydrogen bonding interaction between the surfactant and the silicate surface, the structure directing surfactants can be readily removed by alcohol extraction.

Since the organic functionalities are direct components of the silica matrix, pore blocking which might happen via the grafting method is not a problem in the direct assembly method. Furthermore, the organic units are generally more homogeneously distributed than in materials synthesized with the grafting process. It allows for a greater loading of the organic group, fewer steps in the overall synthesis, and facile recovery of the surfactant. Until recently, direct-assembly was limited to organosilanes and TEOS, since the two are miscible. However, this process has recently been extended to the use of sodium silicate as the inorganic silica source.[49,50]

1.2.3 Advances improving the structural integrity and accessibility of the organic functionality incorporated through the direct assembly method

The direct assembly method is considered superior to the grafting method in order to obtain mesostructured silica materials with a high organic functionality loading and a homogeneous distribution of organic moiety. However, the direct assembly method also has some disadvantages. In general, the degree of mesostructure orderness of the products decreases with increasing concentration of (R'O)$_3$SiR in the reaction mixture and consequently the content of organic functionalities in the modified silica phases does not normally exceed 40 mol%. Usually, basic conditions may be favorable to forming crossed frameworks in a sol-gel derived material, and in turn, ordered mesostructures can be well maintained even with the addition of three-connected organosilanes. On the contrary, the cross linkage of silicate species in an acidic solution is easy to be disrupted by the three connected bonds, leading to the destruction of the final mesostructures. Wei el al. observed a decease of the surface area and pore volume while increasing the thiol functional moiety in the SBA-15 mesostructure and concluded that the molar concentration of mercaptopropyl organosilane should be limited to less than 20% in order to functionalize SBA-15 silicas without a significant change of pore structure.[51] Chong also observed a disordered mesostructure caused by the strongly adverse effect of aminopropyltrimethoxysilane (APTES) on the formation of SBA-15 even at aminopropyl organosilane loading of 10%.[37] The introduction of amine organic moiety in to 3D wormhole mesostructure of HMS silica also sacrificed the structural integrity of the mesophase.[41,52]

Furthermore, increasing the proportion of organosilane in the reaction mixture favors homo-condensation reactions, which is caused by different hydrolysis and condensation rates of the structurally different precursors. It is a constant problem in co-condensation because the homogeneous distribution of different organic functionalities in the framework cannot be guaranteed. The binding site of the organosilane may, or may not, be accessible, and some of them in fact may be buried within the walls of the silica. An exaggerated schematic is shown in Figure 1.7.

= organosilane moiety
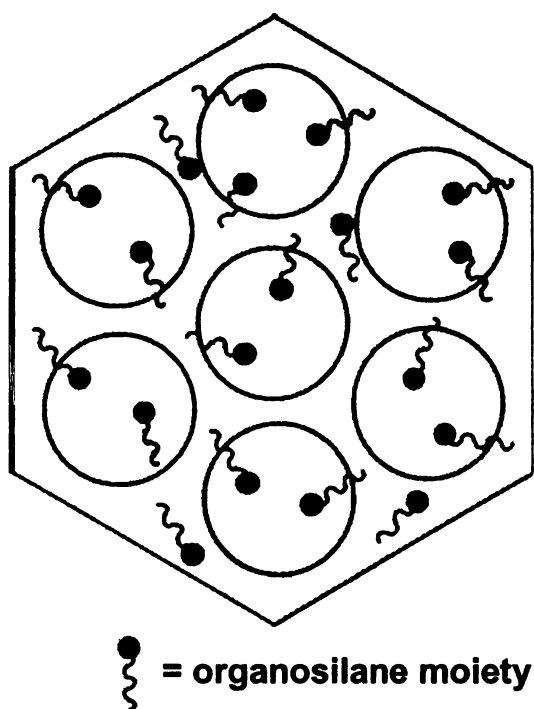
Figure 1.7. An exaggerated schematic showing the functional organosilane distribution arising via co-condensation.

Hermans et al. utilized high-resolution scanning transmission electron microscopy (HR-STEM) technique whereby the accessibility of the organo-functionalized sites can be determined through directly visualized images.[53] Several separate simple transition metal clusters which have specific coordinating ability with different organic groups

14

introduced into the mesostructures were used for this purpose. According to the HR-STEM images, they concluded that the thiol functional groups were accessible and mainly located within the channels of the MCM-41 nanoparticles. In contrast, most of the amino functional sites were unavailable due to embedding within the silica walls during the co-condensation synthesis. Yokoi et al. compared the results from the elemental analysis and the argentometric titration of the amino functionalized MCM-41 and revealed that all the amino moieties incorporated were not present on the surface, but some of them were in the wall of the hexagonal channels.[54] Rosenholm also studied amino-functionalized mesoporous SBA-15 silicas prepared by direct assembly and post-grafting.[55] Special focus was put on the accessibility of the introduced function which was determined by a surface imine formation, followed by UV-vis spectrophotometry. They observed a decrease not only in the relative but also the absolute number of accessible amine groups per unit area with an increasing amino organosilane molar fraction for the co-condensation materials.

The spatial orientation of the organic functional groups and the interactions with the surfactant in the mesoporous channels will certainly affect the accessibility. This is illustrated by the carboxylate-, sulfonate- , and tiolated mesostructured MCM-41 silica made by direct assembly method by Lin's group.[56] The precursors used for these materials are shown in Figure 1.8. The amount of chemically accessible organic ligands in -SO$_3$H modified mesoporous silicas is higher than those of –COOH and –SH functionalized materials, despite a lower loading of organic groups in the former. It could be attributed to the competition of the anionic species, i.e., Br⁻, silicate, and organosilane

during the formation of organosilicas. The least hydrated sulfonate group gave rise to the highest loading of chemically accessible organic groups.
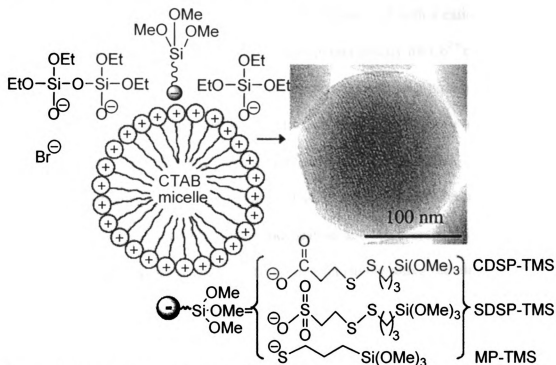
Figure 1.8. Schematic representation of the utilization of an anionic organoalkoxysilane for controlling the functionalization of an organosilica made by direct assembly pathway. The MCM-41 type mesoporous channels are illustrated by the parallel stripes shown in the TEM micrograph.[56]

Several groups have already made some progress on improving the structural integrity and the accessibility of organic groups introduced by direct assembly methods. Wang et al found that the TEOS prehydrolysis prior to the addition of amino organosilane was essential to obtain well-ordered mesoporous materials SBA-15 with amino (i.e., monoamine and diamine) functionality.[57,58] The Tatsumi group used anionic surfactant successfully synthesized functionalized mesostructured silica with the assistance from the protonated amine functional groups under synthetic conditions.[59,60] The 40% amino functionalized materials synthesized with an anionic surfactant still showed mesoporosity

and a high surface area and pore volume. The results from CHN elemental analysis and argentometric titration suggested that almost all the aminopropyl moieties were on the surface in contrast to the MCM-41 type materials synthesized with a cationic surfactant. Thus, the resultant material showed a higher adsorption capacity for Co^{2+} cations.[61]

Voss et al proposed an "all-in-one" approach using silsesquioxane surfactant precursors for the functionalization of the channel walls with primary amine groups.[62] The monomer is made by a hydroboration/aminolysis sequence on the base of a commercial monomer, with the template bound to the functionalization site by hydroboration and released after silica condensation and aminolysis. This combination ensures both the placement of the amine groups exclusively along the channel interface as well as optimal use of the template. The increased accessibility of amine groups was verified by Cu(II) binding experiment.

Chong et al. studied the effect of 3-aminopropyltriethoxysilane (APTES), 3-mercaptopropylmethoxysilane (MPTMS), phenyltrimethoxysilane (PTMS), vinyltriethoxysilane (VTES), and 4-(triethoxysilyl)butyronitrile (CNTES) on the SBA-15 mesostructure made by the direct assembly method.[63] Among the organosilanes studied, the disruptive effects on the formation of the SBA-15 mesostructure followed the order VTES< CNTES< PTMS< MPTMS< APTES. Such different effects are interpreted in terms of their different behaviors under acidic synthetic conditions and in terms of steric molecular sizes and shapes, which all have a direct impact on the interactions of P123 with silicate species and on micellation of the P123 template. Therefore, a post-modification of the functionalized mesoporous materials by direct synthesis could be an alternative to obtaining ordered mesoporous materials with large and/or hydrophilic

functional groups, which often have large disruptive effects on the formation of the mesostructure.

Mehdi et al. synthesized ordered mesoporous silicas with large-pore diameters incorporating aminopropyl groups in variable quantity via the co-condensation of tetraethyl orthosilicate (TEOS) and 3-tertbutyloxycarbonylaminopropyltriethoxysilane templated with nonionic surfactant P123 under acidic conditions. The deprotection of amino groups was then quantitatively achieved either by thermal treatment or acid hydrolysis followed by Et_3N treatment. Both routes led to exactly the same materials. They showed that the free amino centers are fully accessible, by using the condensation of the amine function with benzaldehyde.[64] The same group of researchers also synthesized ordered (hexagonal phase) mesoporous silica functionalized with iodopropyl groups [$I(CH_2)_3$] located in the pore channels by the co-condensation method.[65] The iodo group allows easier and faster chemical transformations, giving rise quantitatively to a variety of mesoporous materials with large and/or hydrophilic functional groups located within the channel pores that are difficult or impossible to obtain by other routes.

1.3 Characterization techniques

Mesostructured molecular sieves are typically characterized by a battery of techniques including X-ray diffraction (XRD), N_2 adsorption desorption, Transmission Electron Microscopy (TEM), ^{29}Si and ^{13}C Magic Angle Spinning Nuclear Magnetic Resonance (^{29}Si, ^{13}C MAS NMR), Thermogravimetric Analysis (TGA), Infrared Spectroscopy (IR), and elemental analysis.

XRD has turned out to be an invaluable tool for the determination of the shape and, in particular, the spatial distribution of the pores for highly ordered arrays such as in

MCM-41 and a more disordered arrangement of pores, for instance in HMS. For almost all types of mesoporous materials, no single crystal diffraction data have been observed. Therefore, only powder diffraction raw data are obtained as 1D plots of the coherent scattering intensity (i.e. counts) versus the scattering angle 2θ. The characteristic length scale d describing the pore system and the corresponding diffraction angle 2θ are related by the Bragg equation, $s=1/d=(2\sin\theta)/\lambda$, where λ is the wavelength and s is the corresponding scattering vector. Figure 1.9 shows the typical XRD patterns for MCM-41 and HMS mesostructure silicas. The successive four peaks at low angle indicate the hexagonal structure of MCM-41, while the single broad diffraction around 2θ of 2 degree suggests the wormhole structure of HMS.

Adsorption of a gas by a porous material is described quantitatively by an adsorption isotherm, the amount of gas adsorbed by the material at a fixed temperature as a function of pressure. Gas sorption represents a widely used technique for characterizing micro- and mesoporous materials and provides porosity parameters such as pore size distributions, surface areas, and pore volumes. The IUPAC classification of adsorption isotherms is illustrated in Figure 1.10.[1] The six types of isotherms are characteristic of adsorbents that are microporous (type I), nonporous or macroporous (type II, III, and VI) or mesoporous (type IV and V). At low P/P_0 adsorption in micropores takes places, which is supposed to be a process of volume filling rather than capillary condensation. In a mesoporous substrate, with increasing values of P/P_0, a liquid-like adsorbate film is formed on the pore walls. At a certain pressure, capillary condensation takes place, filling the mesopores with liquid, which is apparent in isotherms as a pronounced increase in the adsorbed amount. Figure 1.11 shows the typical N_2 adsorption desorption isotherms of

mesostructure HMS silica. The hysteresis at relative pressure P/P_0 of 0.3-0.4 indicates the existence of mesopores, while the uptake steps at high relative pressure (i.e. $P/P_0 > 0.8$) suggest the pores caused by spaces between inter-particles or called texture pores.

^{29}Si MAS NMR is performed to asses the degree of framework cross-linking and degree of organic functionalization. Two kinds of resonances bands denoted as Q^n and T^m are normally observed. The former with chemical shifts at about -90 ~ -110 ppm is assigned to the silicate species which connected with tetrahedrally coordinated silicate species and surface silanol groups, $Q^n = Si(OSi)_n(OH)_{4-n}$. While the latter with chemical shifts at about -60 ~ -80 ppm is characteristic of completely cross-linked organosilane, $T^m = RSi(OSi)_m(OH)_{3-m}$. Figure 1.12 shows the structural nature of different silicon sites. Quantitative assessment of the functional groups content of the mesoporous silica can be monitored by the means of measuring the integrated areas beneath of each Q^n and T^m band.

Electron microcopies such as TEM and SEM are indispensable tool for the investigation of mesoporous materials. The biggest advantage of these techniques is that they deliver an optical image of the samples, providing direct views of the topology and morphology of the materials.

TGA is typically done to determine if the surfactant is completely removed and to probe the thermal stability of the structures. TGA and elemental analysis are the primary methods to investigate the organic moiety loading in the organosilicas. ^{13}C MAS NMR is carried in conjunction with FT-IR for the characterization of the incorporation of organic functional groups in the mesostructures.

hkl	d(Å)
100	39.8
110	22.9
200	19.8
210	14.9
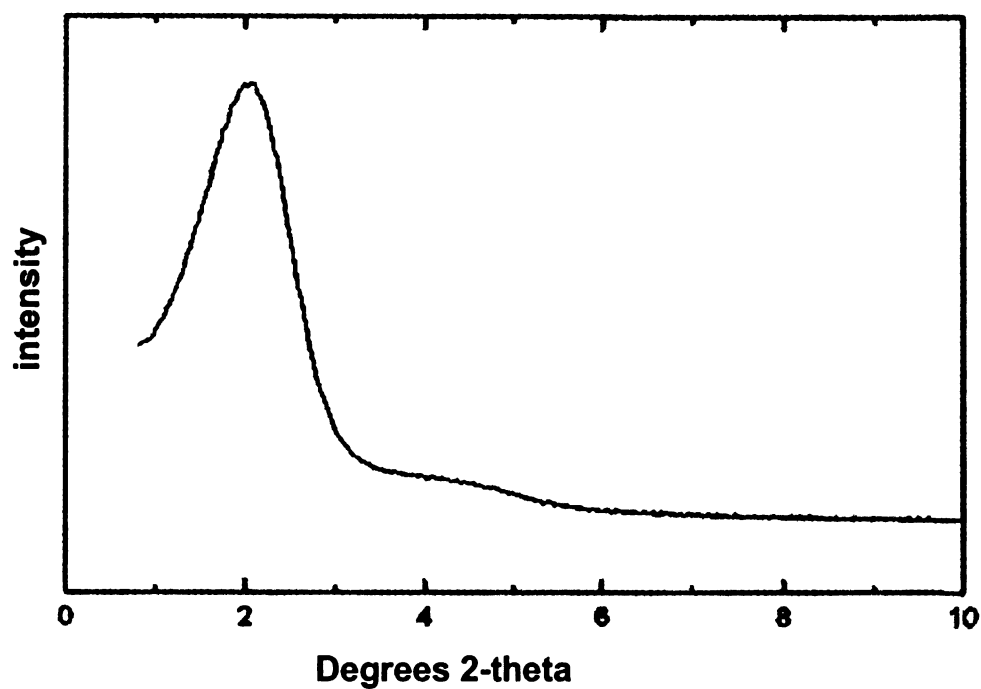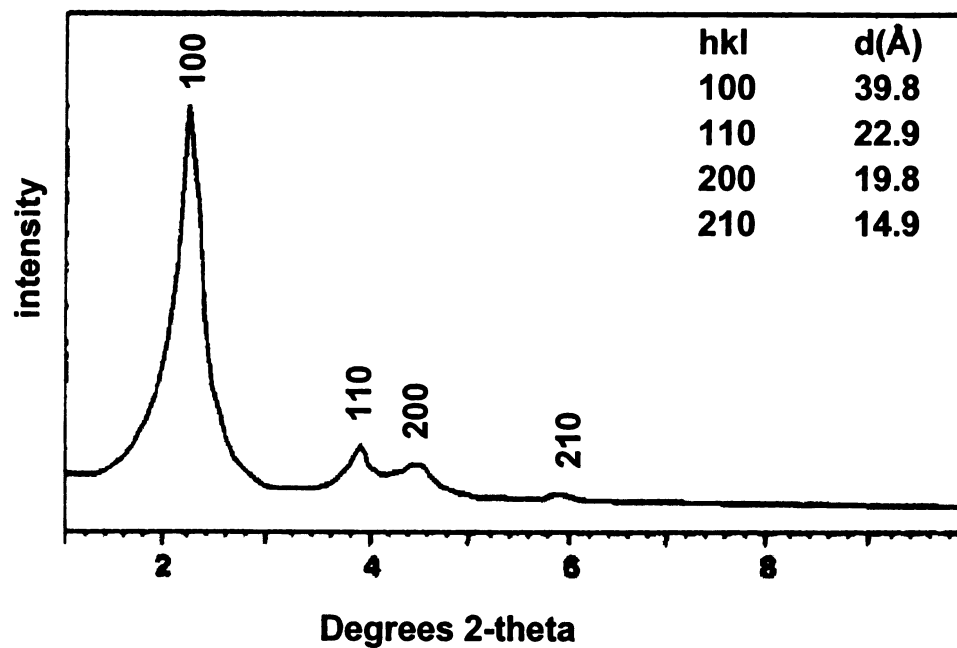
Figure 1.9. Typical XRD powder patterns for mesostructured silica materials: (A) hexagonal arrayed MCM-4[2] and (B) wormhole HMS[66]
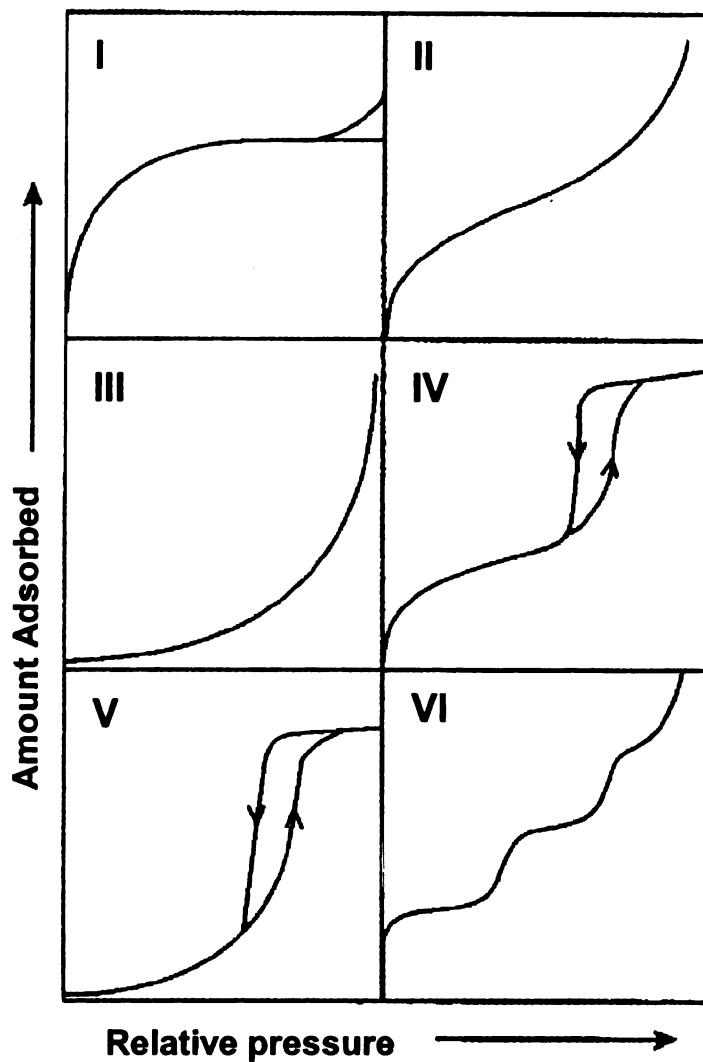
Figure 1.10. IUPAC classification of adsorption isotherms[1]

22
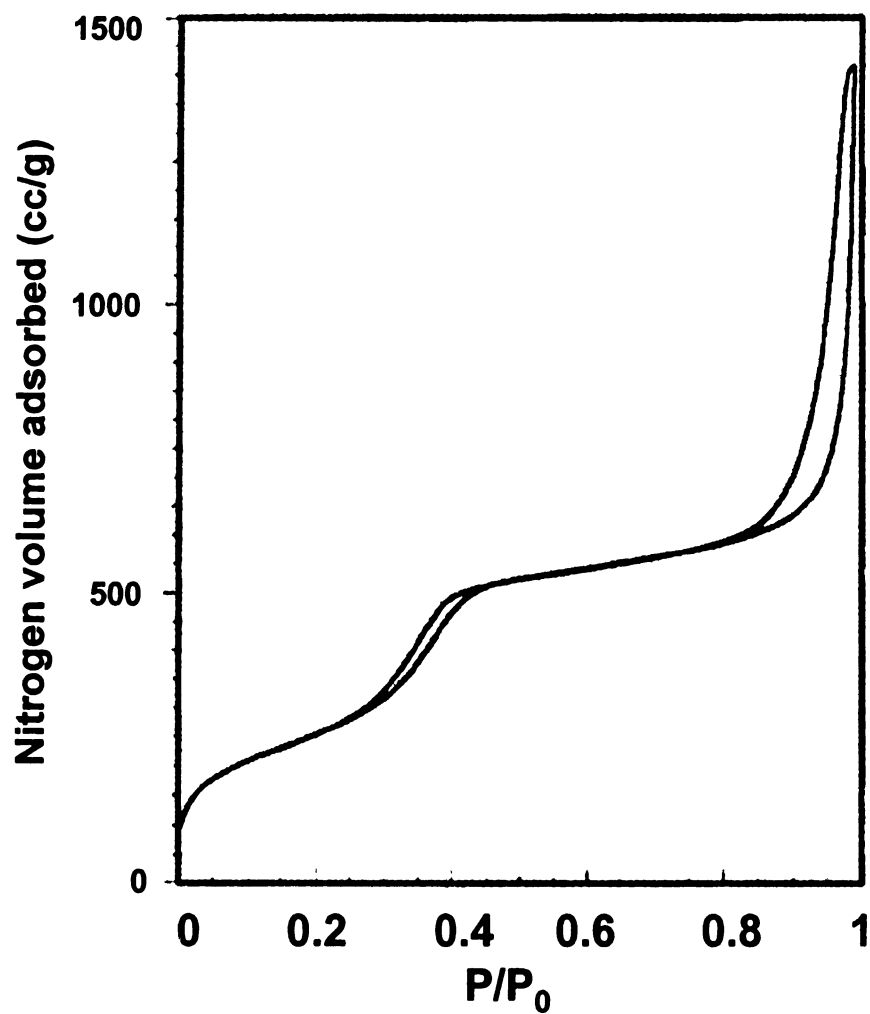
Figure 1.11. A typical N_2 adsorption-desorption isotherm for calcined mesostructured HMS silica.[67]
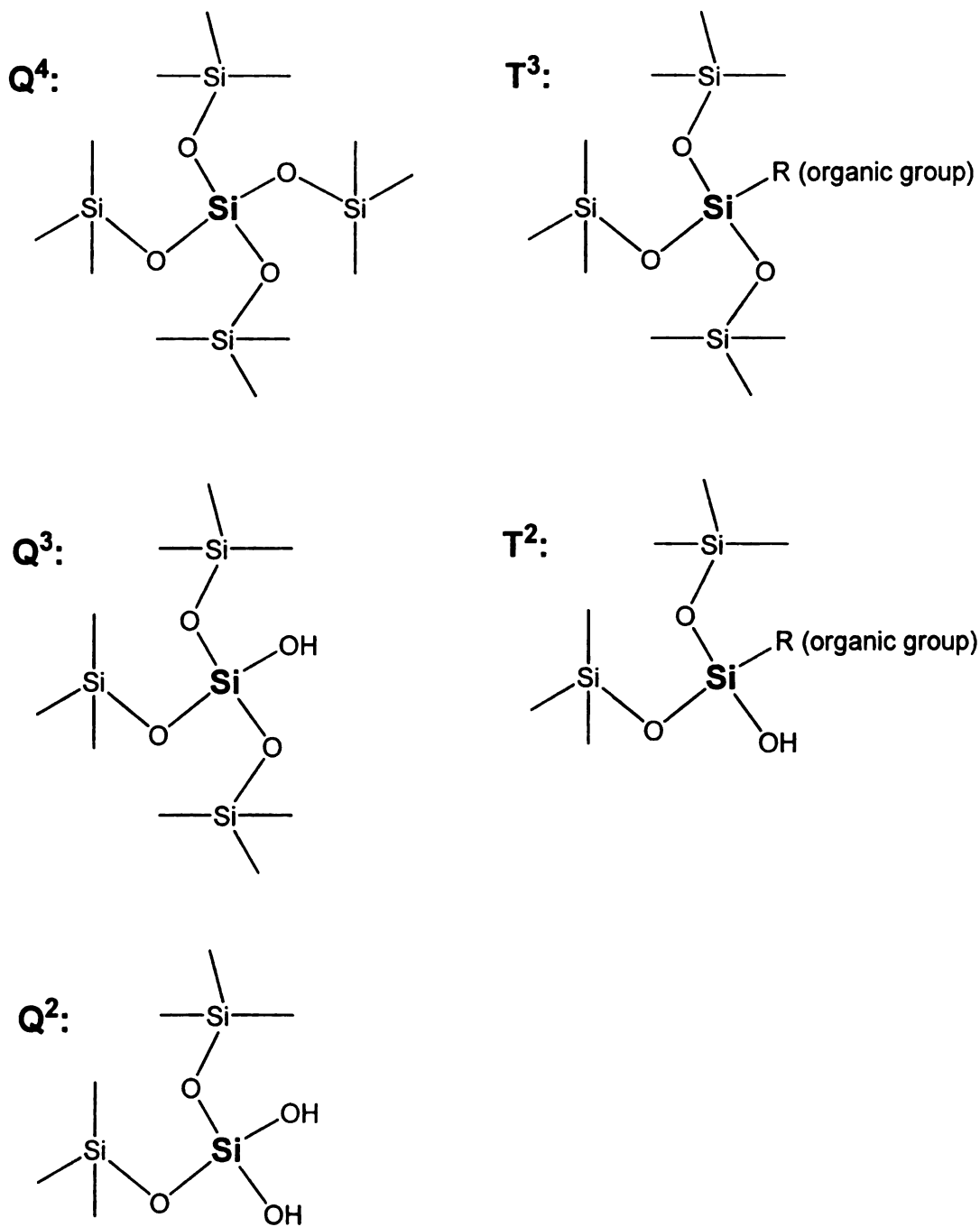
Figure 1.12. Schematic illustration of Q^n and T^m framework silicon sites in an organosilica framework. Q and T denote the binding of silicon to four and three oxygen centers, respectively, and n and m indicate number of oxygen that bridge to neighboring silicon centers.

1.4 Remediation of heavy metal cations with functionalized mesoporous silicas

1.4.1 Heavy metal trapping

"Heavy metal" is a general collective term applied to the group of metals and metalloids with an atomic density greater than 6 g cm^{-3} and includes such elements as Cu, Cd, Hg, Ni, Pb, Zn, Co, and Fe.[68,69] These metals contaminate the aqueous waste streams of many industries, such as metal plating facilities, mining operations and tanneries. The soils surrounding many military bases are also contaminated and pose a risk of metals groundwater and surface water contamination. Heavy metals are not biodegradable and tend to accumulate in living organisms, causing various diseases and disorders. Health agency guidelines set maximum acceptable heavy metal concentration in drinking water that are typically less than 3 ppm.[70,71] Treatment processes for metals contaminated waste streams include chemical precipitation, membrane filtration, ion exchange, carbon adsorption, and coprecipitation/adsorption.[72]

Organo-functionalized mesoporous materials are good adsorbents for either organic pollutants or heavy metal ions. If the incorporated organic group is an alkyl chain, it increases the hydrophobicity of the framework. Thus, this material can adsorb an organic pollutant which is hydrophobic, but yet the pollutant can have significant solubility in water from the standpoint of toxicity. With the incorporation of thiol or amine groups, the modified mesostructured silicas show good affinity to trap heavy metal ions. The modified mesostructured silicas used for environmental remediation especially for heavy metal removal are listed in the following table (Table 1.1):

Table 1.1. Modified mesostructured $(SiO_2)_{1-x}(SiO_{1.5}L)_x$ organosilicas for heavy metal ion trapping.

Author	Framework Notation	Functionalization Method	Organic functionality	Adsorbed Species	Adsorption capacity (mmol g^{-1})
Fryxell[14]	MCM-41	Grafting	-thiol (SH)	Hg^{2+}	1.05
Pinnavaia[12,73]	HMS	Grafting	-thiol	Hg^{2+}	1.55
Stein[31]	MCM-41	Direct-assembly	-thiol -SO$_3$H	Hg^{2+}	2.1 1.76
Mercier[42]	HMS	Direct assembly	-thiol	Hg^{2+}	0.65
Fryxell[74]	MCM-41	Grafting	-ethylenediamine chelating Cu^{2+}	CrO$_4$$^{2-}$ HAsO$_4$$^{2-}$	1.12 1.00
Mercier[46]	MSU-2	Direct assembly	-thiol	Hg^{2+}	2.3
Kawi[75]	SBA-15	Grafting	-thiol -amine (NH$_2$)	Hg^{2+} Cu^{2+}, Zn^{2+}, Cr^{3+}, Ni^{2+}	2.431 1.2 for Cu^{2+}
Mercier[43]	HMS	Direct assembly	-thiol -amine	Hg^{2+}, Ag$^+$, Au^{3+}, Pd^{2+}	0.65, 0.6, 0.7, 0.65 No binding
Yi[76]	HMS	Direct-assembly	-amine -thiol -amine & thiol	Hg^{2+}, Cd^{2+}, Cu^{2+}	No binding 1.51, 0.25, 0.21 0.38-0.76 for Hg^{2+}
Maginn[77]	MCM-41	Diret-assembly	-thiol	Hg^{2+} Ag$^+$	1.26 0.89
Markowitz[78]	SBA-15 MCF	Direct-assembly	-carboxylate -ethylenediaminetriacetic acid	Cu^{2+}	0.32 1.22
Fryxell[79]	MCM-41	Grafting	-ethylenediamine chelating Cu^{2+} ferrocyanide	Cs$^+$	1.35
Jaroniec[80]	MCM-41	Grafting	-amine -1-Allyl-3-propylthiourea	Hg^{2+}	0.0 1.5
Mercier[81]	MSU-X	Direct-assembly	-thiol	Hg^{2+}	1.49
Fryxell[82]	MCM-41	Direct-assembly	carbamoylphosphonate	Pu^{4+}	NM

Table 1.1. (cont'd)

Author	Framework Notation	Functionalization Method	Organic functionality	Adsorbed Species	Adsorption capacity (mmol g⁻¹)
Walcarius[83]	MCM-41	Direct-assembly	-thiol -amine	Hg^{2+}	0.6 0.01
Yoshitake[36,84]	MCM-41 SBA-1	Grafting	-mono, di, triamine	CrO_4^{2-}, $HAsO_4^{2-}$	MCM-41 SBA-1 N 0.5, 0.5; 0.9, 1.0 NN 0.9, 0.7; 1.7, 1.7 NNN 1.1, 0.9; 2.0, 2.1
Jaroniec[85]	MCM-41	Grafting	1-benzoyl-3-propylthiourea	Hg^{2+}	5
Yeung[86,87]	MCM-41	Grafting	-thiol -amine	Pb^{2+}, Cu^{2+}	0.25; 0.06 1.24; 0.81
Walcarius[88]	MCM-41	Direct-assembly	-thiol	Hg^{2+}	3.6
Yoshitake[89,90]	MCM-41	Grafting	mono,di,triamine with Fe^{3+} mono,di,triamine with Cu^{2+}	SeO_4^{2-}	0.7, 0.6, 1.5 0.5, 0.6, 0.5
Yoshitake[91]	MCM-41 MCM-48	Grafting	mono,di,triamine with Fe^{3+}, Co^{2+}, Ni^{2+}, Cu^{2+}	$HAsO_4^{2-}$	NN-Fe^{3+},Co^{2+}, Ni^{2+}, Cu^{2+} 1.5, 0.7, 0.5, 0.4; 2.1, 1.0, 0.9, 0.6
Bios[52]	HMS	Direct-assembly	-amine -diamine -triamne -thiol	Cu^{2+}, Ni^{2+}, Co^{2+}, Cd^{2+}	0.5 for Cu^{2+} 0.5 for Cu^{2+}
Shi[92]	SBA-15	Direct-assembly	(1,4)-bis(triethoxysilyl)propane	Hg^{2+}	13.5
Walcarius[93]	MCM-41 SBA-15 MCM-48	Grafting	-thiol	Hg^{2+}	1.4 1.0 1.4
Yi[94,95]	SBA-15	Grafting	imidazole	Pd^{2+}, Pt^{2+}	1.10 1.01

Table 1.1. (Cont'd)

Author	Framework Notation	Functionalization Method	Organic functionality	Adsorbed Species	Adsorption capacity (mmol g^{-1})
Tatsumi[54]	MCM-41	Direct-assembly Grafting	-mono, di, triamine	Co^{2+}, Fe^{3+}	N NN NNN Co (g) 0.71 0.27 0.07 Co (d) 0.27 0.38 0.57 Fe (g) 1.31 1.04 0.18 Fe (d) 0.56 0.57 0.60
Yi[38]	SBA-15	Grafting	-thiol	Pd^{2+}, Pt^{2+}	1.6 1.1
Jaroneic[96]	MCM-48	Grafting	1-benzoyl-3-propylthiourea	Hg^{2+}	6.7
Yi[97]	HMS SBA-15	Grafting	-thiol	Hg^{2+}, Pb^{2+}	1.2 (Hg); 0.2 (Pb) 0.4 (Hg)
Yoshitake[98]	MCM-41	Grafting	-diamine with Fe^{3+}	HAsO$_4^{2-}$, CrO$_4^{2-}$, SeO$_4^{2-}$, MoO$_4^{2-}$	1.56, 0.99, 0.81, 1.29
Walcarius[99,100]	SBA-15 SBA-16	Direct-assembly Grafting	-thiol	Hg^{2+}	0.27 (g), 1.15 (d) 0.42 (g), 1.37 (d)
Luan[101]	SBA-15	Grafting	-thiol	Hg vapor	80.6 ng Hg/g
Jaroneic[102]	MCM-41 SBA-15	Grafting Direct-assembly	2,5-dimercapto-1,3,4-thiadiazole	Hg^{2+}	SBA-15: 4.7 (g); 8.2 (d)
Shi[103]	SBA-15	Grafting	-mono, di, triamine	Hg^{2+}, Pb^{2+}, Cu^{2+}, Cd^{2+}, Zn^{2+}	For Hg^{2+}: 1.8(N),2.4(NN),3.5(NNN)
Li[104]	SBA-15 MCM-41	Direct-assembly	-amine	Cu^{2+}, Pb^{2+}, Zn^{2+}, Mn^{2+}, Fe^{2+}, Ag$^+$	0.3, 0.3, 0.3, 0.2, 0.3, 0.4 0.1, 0.1, 0.1, 0.1, 0.1, 0.2

NM-not mentioned

1.4.2 Lead trapping

The toxicity of lead is now well established and all over the world guidelines set the maximum acceptable concentration of lead in drinking water at very low levels. Environmental Protection Agency (EPA) requires the lead concentration at consumer taps lower than 15 ppm.

Although the adsorption of mercury (Hg^{2+}) by organo-functionalized mesostructured silicas has been studied exclusively in the past decade, there were only few studies on the removal of lead by mesostructured organosilicas. Yeung et al. showed thiol and amine functionalized MCM-41 synthesized by grafting method having Pb^{2+} capacities of 0.2 and 1.25 mmol g^{-1} respectively.[86,87] Thiol grafted HMS also showed trapping capacity towards lead of 0.2 mmol g^{-1}.[97] The incorporation of amine organic groups into the SBA-15 and MCM-41 mesostructured silicas by direct assembly method results in the adsorbents for many cations including Cu^{2+}, Pb^{2+}, Zn^{2+}, Mn^{2+}, Fe^{2+} and Ag^{+}. The lead trapping capacities for amine functionalized SBA-15 and MCM-41 are 0.34 and 0.13 mmol g^{-1}, respectively.[104]

Figure 1.13 shows the distribution of hydrolysis products $Pb_x(OH)_y$ in aqueous solution at different concentrations. The high concentration distribution 0.1 m corresponds to 2.1×10^4 ppm, whereas the low concentration distribution 10^{-5} m corresponds to 2.1 ppm. Considering the practical condition of lead trapping experiment, the distribution of hydrolysis products at low concentration is closer to the target contaminated water conditions. Thus, at pH lower than 6 which is the case for water containing heavy metal ions, the majority of the species is the Pb^{2+} cation. Therefore, the

design of mesostructured silica adsorbents should be focusing on the trapping mechanism of cation exchange, or complex formation toward divalent lead ions.
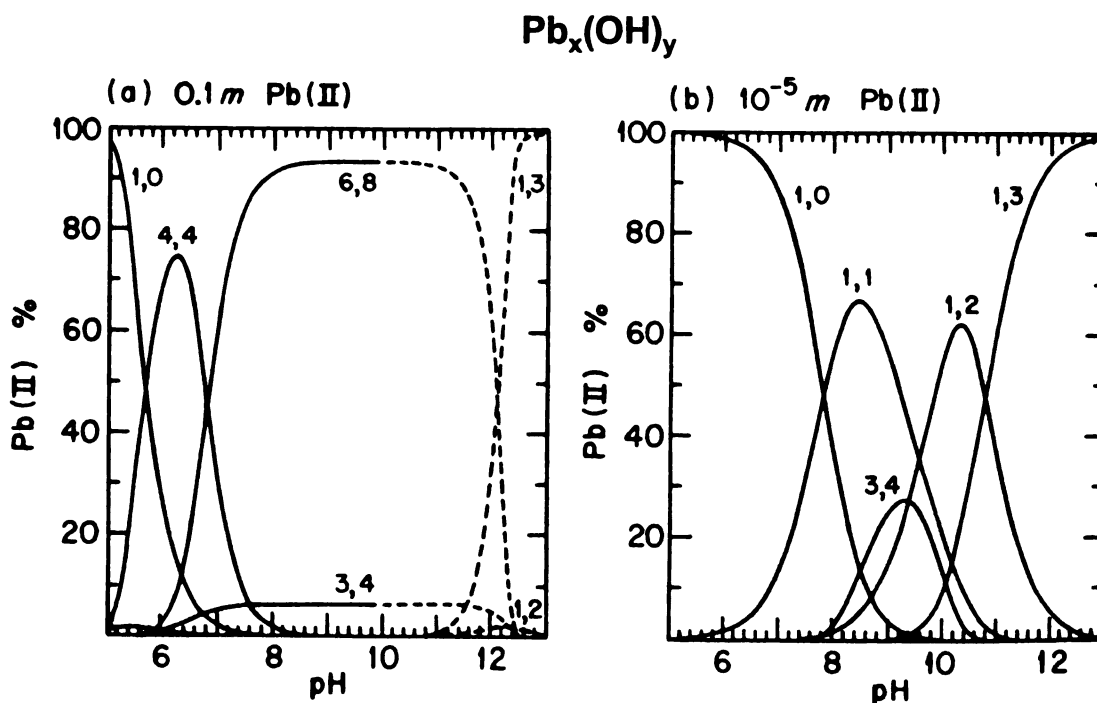
$$Pb_x(OH)_y$$

Figure 1.13. Distribution of hydrolysis products $Pb_x(OH)_y$ in aqueous solution at (a) high and (b) low concentration.[105]

1.5 Research objectives

Porous materials are of interest to material chemists due to their expansive applicability. Applications of porous materials include use as ion-exchangers, heterogeneous catalysts, gas adsorbents, and environmental remediation agents. As introduced before, the formation routes can be electrostatic or hydrogen-bonding interactions between the surfactant micelles and inorganic silica precursors. The electrostatic interactions often yield mesostructures with long-range hexagonal morphology. Mesostructures prepared through a hydrogen bonding interaction pathway have a short range ordered wormhole morphology. The 3D wormhole structure has been

30

shown to have greater accessibility to ligands present in the pores in comparison with 2D hexagonal structure.[97,106]

The overall goal of this work is to design and synthesize functionalized mesostructured materials (i.e. mesostructured silica) for potential use in environmental remediation. The functional moiety could be a conventional organic moiety introduced by organosilanes, hetero-atoms in the silicate framework, or the less commonly used surfactant. Hydrogen bonding supramolecular assembly between neutral alkylamine surfactant and a nonionic silica source will be utilized in order to have a better accessible wormhole structure morphology. The key objective is to improve the accessibility of the effective functional sites within the mesostructure silicas. Specifically, this objective will be achieved by:

1. Design and preparation of surfactant containing mesophase silicas where the surfactant is chemically stable inside the mesopores and can be utilized as the binding sites for heavy metals.

2. Design alternative synthesis routes to improve the mesostructure and the amine accessibility for the amine functionalized mesostructured silica materials.

3. Preparation of mesostructured aluminosilicate with high percentage of framework incorporated Al sites for better ion exchange capacity.

4. Examination of the lead adsorption capacity on the surfactant containing mesophase silicas, amine functionalized mesostructured silicas with improved amine accessibility and the mesostructured aluminosilicate material with high percentage of framework incorporated Al sites.

1.6 Reference

(1)   Sing, K. S. W.; Everett, D. H.; Haul, R. A. W.; Moscou, L.; Pierotti, R. A.;
        Rouquerol, J.; Siemieniewska, T. *Pure and Applied Chemistry* **1985**, *57*, 603-19.

(2)   Beck, J. S.; Vartuli, J. C.; Roth, W. J.; Leonowicz, M. E.; Kresge, C. T.; Schmitt,
        K. D.; Chu, C. T. W.; Olson, D. H.; Sheppard, E. W.; et al. *J. Am. Chem. Soc.*
        1992, *114*, 10834-43.

(3)   Kresge, C. T.; Leonowicz, M. E.; Roth, W. J.; Vartuli, J. C.; Beck, J. S. *Nature*
        1992, *359*, 710-12.

(4)   Beck, J. S.; Vartuli, J. C.; Kennedy, G. J.; Kresge, C. T.; Roth, W. J.; Schramm, S.
        E. *Chem. Mater.* **1994**, *6*, 1816-21.

(5)   Vartuli, J. C.; Schmitt, K. D.; Kresge, C. T.; Roth, W. J.; Leonowicz, M. E.;
        McCullen, S. B.; Hellring, S. D.; Beck, J. S.; Schlenker, J. L.; Olson, D. H.;
        Sheppard, E. W. *Chem. Mater.* **1994**, *6*, 2317-2326.

(6)   Hoffmann, F.; Cornelius, M.; Morell, J.; Froba, M. *Angew. Chem. Int. Ed.* **2006**,
        45, 3216-51.

(7)   Zhao, D.; Feng, J.; Huo, Q.; Melosh, N.; Frederickson, G. H.; Chmelka, B. F.;
        Stucky, G. D. *Science* **1998**, *279*, 548-552.

(8)   Zhao, X. S.; Lu, G. Q. *J. Phys. Chem. B* **1998**, *102*, 1556-1561.

(9)   Tanev, P. T.; Pinnavaia, T. J. *Science* **1995**, *267*, 865-7.

(10)   Bagshaw, S. A.; Prouzet, E.; Pinnavaia, T. J. *Science* **1995**, *269*, 1242-4.

(11)   Schmidt-Winkel, P.; Lukens, W. W., Jr.; Yang, P.; Margolese, D. I.; Lettow, J. S.;
        Ying, J. Y.; Stucky, G. D. *Chem. Mater.* **2000**, *12*, 686-696.

(12)   Mercier, L.; Pinnavaia, T. J. *Adv. Mater.* **1997**, *9*, 500-503.

(13)   Fryxell, G. E.; Liu, J.; Hauser, T. A.; Nie, Z.; Ferris, K. F.; Mattigod, S.; Gong, M.; Hallen, R. T. *Chem. Mater.* **1999**, *11*, 2148-2154.

(14)   Feng, X.; Fryxell, G. E.; Wang, L. Q.; Kim, A. Y.; Liu, J.; Kemner, K. M. *Science* **1997**, *276*, 923-926.

(15)   Takahashi, H.; Inagaki, S.; Kajino, T.; Usuki, A.; Li, B. In *Eur. Pat. Appl.*; (Kabushiki Kaisha Toyota Chuo Kenkyusho, Japan). Ep, 1999.

(16)   Han, Y.-J.; Watson, J. T.; Stucky, G. D.; Butler, A. *J. Mol. Catal. B: Enzym.* **2002**, *17*, 1-8.

(17)   Lei, C.; Shin, Y.; Liu, J.; Ackerman, E. J. *J. Am. Chem. Soc.* **2002**, *124*, 11242-11243.

(18)   Fan, J.; Lei, J.; Wang, L.; Yu, C.; Tu, B.; Zhao, D. *Chem. Commun.* **2003**, 2140-2141.

(19)   Lin, V. S. Y.; Motesharei, K.; Dancil, K.-P. S.; Sailor, M. J.; Ghadiri, M. R. *Science* **1997**, *278*, 840-843.

(20)   Dai, S.; Burleigh, M. C.; Shin, Y.; Morrow, C. C.; Barnes, C. E.; Xue, Z. *Angew. Chem. Int. Ed.* **1999**, *38*, 1235-1239.

(21)   McKittrick, M. W.; Jones, C. W. *Chem. Mater.* **2003**, *15*, 1132-1139.

(22)   Hicks, J. C.; Dabestani, R.; Buchanan, A. C., III; Jones, C. W. *Chem. Mater.* **2006**, *18*, 5022-5032.

(23)   Hicks, J. C.; Jones, C. W. *Langmuir* **2006**, *22*, 2676-2681.

(24)   Stein, A.; Melde, B. J.; Schroden, R. C. *Adv. Mater.* **2000**, *12*, 1403-1419.

(25)   Sims, S. D.; Burkett, S. L.; Mann, S. *Materials Research Society Symposium Proceedings* **1996**, *431*, 77-82.

(26)   Burkett, S. L.; Sims, S. D.; Mann, S. *Chem. Commun.* **1996**, 1367-1368.

(27) Fowler, C. E.; Burkett, S. L.; Mann, S. *Chem. Commun.* **1997**, 1769-1770.

(28) Lim, M. H.; Blanford, C. F.; Stein, A. *J. Am. Chem. Soc.* **1997**, *119*, 4090-4091.

(29) Brunel, D. *Microporous and Mesoporous Mater.* **1999**, *27*, 329-344.

(30) Mukherjee, P.; Laha, S.; Mandal, D.; Kumar, R. *Stud. Surf. Sci. Catal.* **2000**, *129*, 283-286.

(31) Lim, M. H.; Blanford, C. F.; Stein, A. *Chem. Mater.* **1998**, *10*, 467-470.

(32) Hall, S. R.; Fowler, C. E.; Mann, S.; Lebeau, B. *Chem. Commun.* **1999**, 201-202.

(33) Ganschow, M.; Wark, M.; Wohrle, D.; Schulz-Ekloff, G. *Angew. Chem., Int. Ed.* **2000**, *39*, 161-163.

(34) Huo, Q.; Margolese, D. I.; Stucky, G. D. *Chem. Mater.* **1996**, *8*, 1147-60.

(35) Melero, J. A.; Stucky, G. D.; van Grieken, R.; Morales, G. *J. Mater. Chem.* **2002**, *12*, 1664-1670.

(36) Yoshitake, H.; Yokoi, T.; Tatsumi, T. *Chem. Lett.* **2002**, 586-587.

(37) Chong, A. S. M.; Zhao, X. S. *J. Phys. Chem. B* **2003**, *107*, 12650-12657.

(38) Kang, T.; Park, Y.; Yi, J. *Ind. Eng. Chem. Res.* **2004**, *43*, 1478-1484.

(39) Yang, C.-M.; Zibrowius, B.; Schueth, F. *Chem. Commun.* **2003**, 1772-1773.

(40) Macquarrie, D. J. *Chem. Commun.* **1996**, 1961-1962.

(41) Macquarrie, D. J.; Jackson, D. B.; Mdoe, J. E. G.; Clark, J. H. *New J. Chem.* **1999**, *23*, 539-544.

(42) Brown, J.; Mercier, L.; Pinnavaia, T. J. *Chem. Commun.* **1999**, 69-70.

(43)   Mercier, L.; Bell, V. *Environ. Conscious Mater.: Ecomater., Proc. Int. Symp.* **2000**, 599-606.

(44)   Mercier, L.; Pinnavaia, T. J. *Chem. Mater.* **2000**, *12*, 188-196.

(45)   Mori, Y.; Pinnavaia, T. J. *Chem. Mater.* **2001**, *13*, 2173-2178.

(46)   Brown, J.; Richer, R.; Mercier, L. *Microporous and Mesoporous Mater.* **2000**, *37*, 41-48.

(47)   Park, B.-G.; Jo, N.-J.; Cho, W.-J.; Ha, C.-S. *Polymer International* **2002**, *51*, 1225-1230.

(48)   Blin, J. L.; Gerardin, C.; Rodehuser, L.; Selve, C.; Stebe, M. J. *Stud. Surf. Sci. Catal.* **2005**, *156*, 221-228.

(49)   Pauly, T. R.; Petkov, V.; Liu, Y.; Billinge, S. J. L.; Pinnavaia, T. J. *J. Am. Chem. Soc.* **2002**, *124*, 97-103.

(50)   Shah, J.; Kim, S.-S.; Pinnavaia, T. J. *Chem. Commun.* **2004**, 572-573.

(51)   Wei, Q.; Nie, Z.; Hao, Y.; Chen, Z.; Zou, J.; Wang, W. *Mater. Lett.* **2005**, *59*, 3611-3615.

(52)   Bois, L.; Bonhomme, A.; Ribes, A.; Pais, B.; Raffin, G.; Tessier, F. *Colloids Surf., A* **2003**, *221*, 221-230.

(53)   Hermans, S.; Sadasivan, S.; Judkins, C. M. G.; Johnson, B. F. G.; Mann, S.; Khushalani, D. *Adv. Mater.* **2003**, *15*, 1853-1857.

(54)   Yokoi, T.; Yoshitake, H.; Tatsumi, T. *J. Mater. Chem.* **2004**, *14*, 951-957.

(55)   Rosenholm, J. M.; Linden, M. *Chem. Mater.* **2007**, *19*, 5023-5034.

(56)   Radu, D. R.; Lai, C.-Y.; Huang, J.; Shu, X.; Lin, V. S. Y. *Chem. Commun.* **2005**, 1264-1266.

(57) Wang, X.; Chan, J. C. C.; Tseng, Y.-H.; Cheng, S. *Microporous Mesoporous Mater.* **2006**, *95*, 57-65.

(58) Wang, X.; Lin, K. S. K.; Chan, J. C. C.; Cheng, S. *J. Phys. Chem. B* **2005**, *109*, 1763-1769.

(59) Che, S.; Garcia-Bennett, A. E.; Yokoi, T.; Sakamoto, K.; Kunieda, H.; Terasaki, O.; Tatsumi, T. *Nat. Mater.* **2003**, *2*, 801-805.

(60) Yokoi, T.; Yoshitake, H.; Tatsumi, T. *Chem. Mater.* **2003**, *15*, 4536-4538.

(61) Yokoi, T.; Yoshitake, H.; Yamada, T.; Kubota, Y.; Tatsumi, T. *J. Mater. Chem.* **2006**, *16*, 1125-1135.

(62) Voss, R.; Thomas, A.; Antonietti, M.; Ozin, G. A. *J. Mater. Chem.* **2005**, *15*, 4010-4014.

(63) Chong, A. S. M.; Zhao, X. S.; Kustedjo, A. T.; Qiao, S. Z. *Microporous and Mesoporous Mater.* **2004**, *72*, 33-42.

(64) Mehdi, A.; Reye, C.; Brandes, S.; Guilard, R.; Corriu, R. J. P. *New J. Chem.* **2005**, *29*, 965-968.

(65) Alauzun, J.; Mehdi, A.; Reye, C.; Corriu, R. *New J. Chem.* **2007**, *31*, 911-915.

(66) Karakassides, M. A.; Fournaris, K. G.; Travlos, A.; Petridis, D. *Adv. Mater.* **1998**, *10*, 483-486.

(67) Zhang, W. Z.; Pauly, T. R.; Pinnavaia, T. J. *Chem. Mater.* **1997**, *9*, 2491-2498.

(68) Patterson, J.; Passino, R. *Metal Speciation, Separation, and Recovery*; Lewis: Chelsea, 1987.

(69) Ahmed, S.; Chughtai, S.; Keane, M. A. *Sep. Purif. Technol.* **1998**, *13*, 57-64.

(70) Gray, N. F. *Drinking water quality*; Wiley: New York, 1994.

(71)   Zuane, J. D. *Handbook of drinking water quality*; Van Nostrand Reinhold: New York, 1990.

(72)   Bailey, S. E.; Olin, T. J.; Bricka, R. M.; Adrian, D. D. *Water Res.* **1999**, *33*, 2469-2479.

(73)   Mercier, L.; Pinnavaia, T. J. *Environ. Sci. Technol.* **1998**, *32*, 2749-2754.

(74)   Fryxell, G. E.; Liu, J.; Hauser, T. A.; Nie, Z.; Ferris, K. F.; Mattigod, S.; Gong, M.; Hallen, R. T. *Chem. Mater.* **1999**, *11*, 2148-2154.

(75)   Liu, A. M.; Hidajat, K.; Kawi, S.; Zhao, D. Y. *Chem. Commun.* **2000**, 1145-1146.

(76)   Lee, B.; Kim, Y.; Lee, H.; Yi, J. *Microporous and Mesoporous Mater.* **2001**, *50*, 77-90.

(77)   Nooney, R. I.; Kalyanaraman, M.; Kennedy, G.; Maginn, E. J. *Langmuir* **2001**, *17*, 528-533.

(78)   Markowitz, M. A.; Klaehn, J.; Hendel, R. A.; Qadriq, S. B.; Golledge, S. L.; Castner, D. G.; Gaber, B. P. *J. Phys. Chem. B* **2000**, *104*, 10820-10826.

(79)   Lin, Y.; Fryxell, G. E.; Wu, H.; Engelhard, M. *Environ. Sci. Technol.* **2001**, *35*, 3962-3966.

(80)   Antochshuk, V.; Jaroniec, M. *Chem. Commun.* **2002**, 258-259.

(81)   Bibby, A.; Mercier, L. *Chem. Mater.* **2002**, *14*, 1591-1597.

(82)   Birnbaum, J. C.; Busche, B.; Lin, Y.; Shaw, W. J.; Fryxell, G. E. *Chem. Commun.* **2002**, 1374-1375.

(83)   Etienne, M.; Sayen, S.; Lebeau, B.; Walcarius, A. *Stud. Surf. Sci. Catal.* **2002**, *141*, 615-622.

(84)   Yoshitake, H.; Yokoi, T.; Tatsumi, T. *Chem. Mater.* **2002**, *14*, 4603-4610.

(85)   Antochshuk, V.; Olkhovyk, O.; Jaroniec, M.; Park, I.-S.; Ryoo, R. *Langmuir* **2003**, *19*, 3031-3034.

(86)   Lam, K. F.; Ho, K. Y.; Yeung, K. L.; McKay, G. *Mater. Res. Soc. Symp. Proc.* **2003**, *788*, 383-389.

(87)   Lam, K. F.; Ho, K. Y.; Yeung, K. L.; McKay, G. *Stud. Surf. Sci. Catal.* **2004**, *154C*, 2981-2986.

(88)   Walcarius, A.; Delacote, C. *Chem. Mater.* **2003**, *15*, 4181-4192.

(89)   Yokoi, T.; Tatsumi, T.; Yoshitake, H. *Stud. Surf. Sci. Catal.* **2003**, *146*, 531-534.

(90)   Yokoi, T.; Tatsumi, T.; Yoshitake, H. *Bull. Chem. Soc. Jpn.* **2003**, *76*, 2225-2232.

(91)   Yoshitake, H.; Yokoi, T.; Tatsumi, T. *Chem. Mater.* **2003**, *15*, 1713-1721.

(92)   Zhang, L.; Zhang, W.; Shi, J.; Hua, Z.; Li, Y.; Yan, J. *Chem. Commun.* **2003**, 210-211.

(93)   Walcarius, A.; Etienne, M.; Lebeau, B. *Chem. Mater.* **2003**, *15*, 2161-2173.

(94)   Kang, T.; Park, Y.; Park, J. C.; Cho, Y. S.; Yi, J. *Stud. Surf. Sci. Catal.* **2003**, *146*, 527-530.

(95)   Kang, T.; Park, Y.; Choi, K.; Lee, J. S.; Yi, J. *J. Mater. Chem.* **2004**, *14*, 1043-1049.

(96)   Olkhovyk, O.; Antochshuk, V.; Jaroniec, M. *Colloids Surf., A* **2004**, *236*, 69-72.

(97)   Kim, Y.; Lee, B.; Yi, J. *Sep. Sci. Technol.* **2004**, *39*, 1427-1442.

(98)   Yokoi, T.; Tatsumi, T.; Yoshitake, H. *J. Colloid Interface Sci.* **2004**, *274*, 451-457.

(99)   Lesaint, C.; Frebault, F.; Delacote, C.; Lebeau, B.; Marichal, C.; Walcarius, A.; Patarin, J. *Stud. Surf. Sci. Catal.* **2005**, *156*, 925-932.

(100) Walcarius, A.; Delacote, C. *Anal. Chim. Acta* **2005**, *547*, 3-13.

(101) Luan, Z.; Fournier, J. A.; Wooten, J. B.; Miser, D. E.; Chang, M. J. *Stud. Surf. Sci. Catal.* **2005**, *156*, 897-906.

(102) Olkhovyk, O.; Jaroniec, M. *Adsorption* **2005**, *11*, 205-214.

(103) Zhang, L.; Yu, C.; Zhao, W.; Hua, Z.; Chen, H.; Li, L.; Shi, J. *J. Non-Cryst. Solids* **2007**, *353*, 4055-4061.

(104) Yang, H.; Xu, R.; Xue, X.; Li, F.; Li, G. *J. Hazard. Mater.* **2008**, *152*, 690-698.

(105) Charles F. Baes, J.; R.E.Mesmer *The hydrolysis of cations*; Wiley: New York, 1976.

(106) Pauly, T. R.; Liu, Y.; Pinnavaia, T. J.; Billinge, S. J. L.; Rieker, T. P. *J. Am. Chem. Soc.* **1999**, *121*, 8835-8842.

Chapter 2

Removal of lead species from aqueous solution by surfactant-containing mesophase silica materials

2.1 Introduction

Until the discovery of the cooperative assembly of surfactant micelles with silicates by Mobil scientists in 1992, which led to the synthesis of MCM-41 and the M41S family of mesoporous materials,[1] the surfactant component were almost exclusively used as surface and interface modifiers. This discovery sparked more than a decade of extensive research on surfactant-directed assembly, a process in which surfactant is used to direct and assemble inorganic building blocks into mesoscopically ordered structures. Organic components, either on the silicate surface or as part of the silicate walls, have been incorporated into the siliceous frameworks to further modify the physical and chemical properties of mesoporous silicates. These mesoporous inorganic or inorganic-organic hybrid materials have been considered for a wide range of applications in the areas of catalysis,[2-5] environmental remediation,[6-9] optically active materials,[10,11] polymerization science,[12-14] fixation of biological active species,[15] and drug delivery.[16-18]

Up to now researches have mainly focused on the application of surfactant-free mesoporous inorganic or organofunctionalized derivatives. Except for a few studies, little attention has been paid to the properties and applications of as-made periodic mesophase silica materials in which the structure-directing surfactant functions as an organic modifier of properties. Sugi et al.[19] found that as-made, surfactant containing MCM-41 silica exhibits high catalytic activity for the Knoevenagel condensation, being attributable to basic $(SiO)_3SiO^-$ sites which occur in large amounts in as-made silica mesophases in

order to balance the charge of the cetyltrimetylammmounium (CTA) surfactant in the pores. The surfactant-retained mesophase materials also have potential as adsorbents of organic pollutants. The sorption of hydrophobic organic molecules (e.g. chlorophenol) from aqueous solution into as-made MCM-41 mesophases was first reported in 1998.[20] Later on, the as-made surfactant containing MCM-41 mesophase materials were utilized by different groups to remove trichloroethylene and tetracholoroethylene,[21] chlorinated phenol,[22] benzene,[23] toluene and naphthalene[24], and organic dyes.[25,26] Miyake et al. used mesophase MCM-41 microspheres synthesized from tetrabutylorthosilicate (TBOS) to separate phenol from aniline in the column study.[27,28] Other surfactant-containing mesophase materials, such as HMS, MCM-48, MCM-50 and FSM-16 systems were also investigated for the removal of organic compounds from aqueous solution.[22,23,29] As in micelles, nonpolar molecules can be dissolved in the hydrophobic core of the mesostructure-intercalated surfactant, where the hydrocarbon tails effectively act as a solvent. The carton in Figure 2.1 shows the possible positions for the hydrophobic organic molecules in the silica-surfactant mesophase materials.
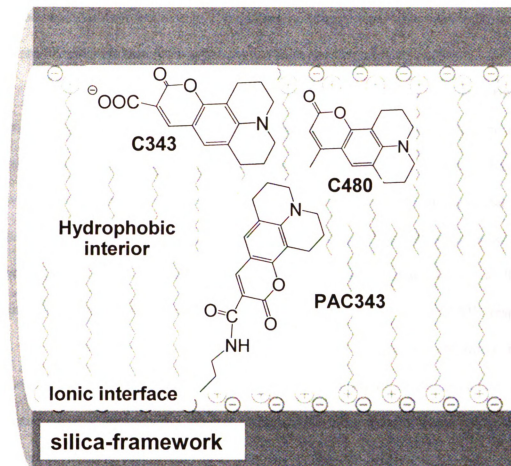
Figure 2.1. Schematic illustration of the location of hydrophobic organic molecules in the surfactant-containing mesophase silica, reproduced from reference 25. C343, C480 and PAC343 stands for hydrophobic organic molecules coumarin dye 343, coumarin dye 480 and propylamide coumarin dye 343.

Recently, the as-made materials have been used as adsorbents for heavy metal ion in aqueous solution. The Sayari group successfully used as-made MCM-41 with a co-intercalated co-surfactant to expand the pore size of MCM-41 to adsorb Co^{2+}, Ni^{2+}, Cu^{2+} ions from aqueous solution using the nitrogen binding site on the intercalated co-surfactant N,N-dimethyl alkylamine.[30] This was the first example using a surfactant-containing mesophase silica as an adsorbent for heavy metals. Choi et al. later on observed that the as-made surfactant containing MCM-41 and HMS silica materials are

good adsorbents for Pb^{2+} from aqueous solution, while the calcined pure siliceous materials after surfactant removal did not show any trapping capacities.[31]

The surfactant component of the as-made mesostructure is the primary factor controlling the performance of as-made mesophase silica materials for the removal of metal ions from solution. Amine surfactants are good choices since they have nitrogen with lone electron pairs, therefore having good affinity with heavy metal to form a complex. The work reported by the Sayari and Choi groups of as-made surfactant-containing mesophase silica materials used tertiary and primary amines as the binding sites in the case of co-intercalated surfactant expanded MCM-41 and HMS, respectively.

An important issue regarding the use of surfactant-containing mesophase materials as metal ion adsorbents is the concern for leaching of the surfactant. Zhao et al. observed slow alkylammonium ion surfactant leaching from as-made MCM-41 material under conditions that mimic ground water.[21] Similar behavior has been reported for organic-exchanged smectites[32] and surfactant modified zeolites,[33] though with a relatively faster leaching rate. The lower leaching rate for the mesophase may be related to the structure location of the surfactant in the mesoporous materials (i.e., interior to the Si framework). The interaction between the surfactant and silicate moiety during the synthesis process can be electrostatic or hydrogen bonding. No stable interaction, such as covalent bond, is formed between the surfactant head group and the silica moiety. Therefore, stabilizing the surfactant inside the mesoporous silica materials remains a challenge.

In this work, alkylamine surfactants containing different numbers of amine groups were chosen as the templating agents for the silica framework, as well as serving as

adsorption sites for heavy metals. The trapping capacity was compared for surfactants containing different amine groups in order to investigate the adsorption mechanism. Also, an epoxide functional group that can react with the surfactant amine head group was also introduced into the mesostructured silica framework. Covalent bond formation between the surfactant and the silicate framework was expected to immobilize surfactant inside the framework pores. The resultant mesophases were characterized by XRD, N_2 adsorption-desorption isotherms, TEM and TGA analysis, Pb^{2+} adsorption experiments were also carried out.

2.2 Experimental methods

2.2.1   Reagents

Tallow mono-, di-, tri- and tetraamine with the structures shown in Figure 2.2 were obtained as free samples from Tomah[3] Product, Inc. Dodecylamine (DDA), tetraethyl orthosilicate (TEOS), (3-Glycidyloxypropyl) trimethoxysilane (Epoxide organosilane), lead atomic absorption standard solution (~1000 ppm), and lead nitrate (99.999% purity) were purchased from Aldrich. The structure of the epoxide organosilane is provided in Figure 2.3. Ethanol was purchased in-house. All the reagents were used without further purification. Water used in the synthesis was double-exchanged to remove cations and anions via a Millipore filter apparatus.

tallow monoamine (N₁)

tallow diamine (N₂)

tallow triamine (N₃)

tallow tetraamine (N₄)
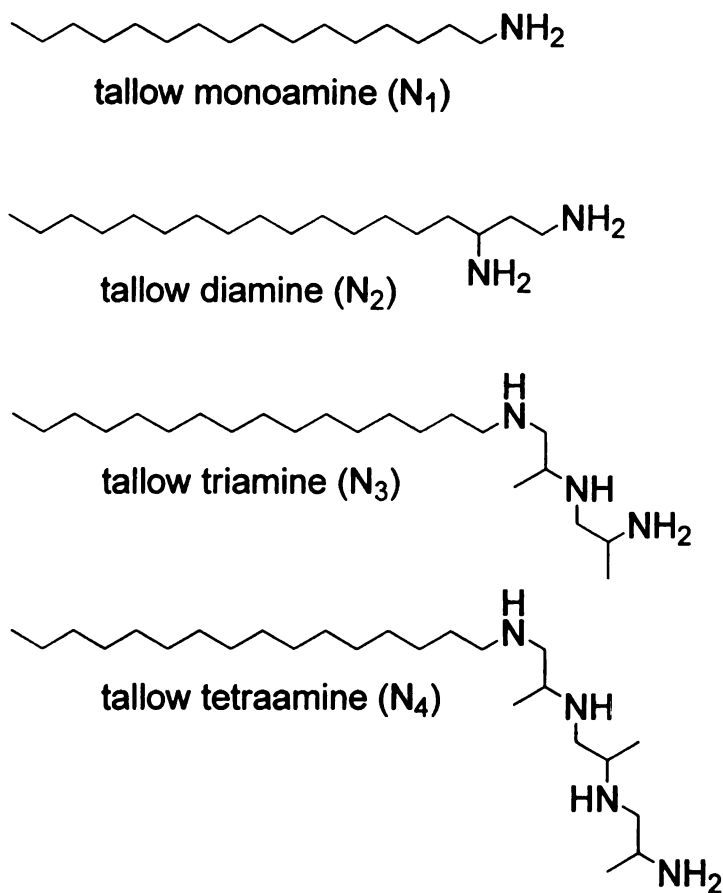
Figure 2.2. Chemical structure of Tallow amine surfactant series
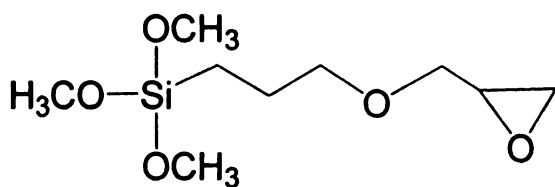
Figure 2.3. Chemical structure of (3-Glycidyloxypropyl) trimethoxysilane

2.2.2 Materials synthesis

2.2.2.1 Tallow amine surfactant intercalated mesophase silicas

Desired amount of tallow amine surfactant was dissolved in a plastic bottle with

162 g H_2O and 46 g EtOH. After obtaining a homogeneous surfactant solution, TEOS

was added and the mixture was aged at 60°C for 24 hr. The products were recovered by filtration and air-dried. The total molar ratio of reagents was Tallow surfactant: TEOS: H_2O: EtOH = 0.25: 1: 180: 20. The products were denoted Tallow N1, N2, N3, N4 respectively, corresponding to the tallow amine, diamine, triamine and tetraamine used as surfactants.

2.2.2.2 Epoxide functionalized surfactant intercalated mesophase silicas

Desired amount of dodecylamine surfactant was dissolved in an aqueous solution containing 25 wt % ethanol in a plastic bottle. After obtaining a homogeneous surfactant solution, a mixture of TEOS and epoxide organosilane was introduced while stirring. The mixture was aged at 60°C for 24 hr. The products were recovered by filtration and air-dried. The total molar ratio of reagents was DDA: Epoxide organosilane: TEOS: H_2O: EtOH = 0.25: x: (1-x): 180: 20, where x is the fraction of silicon centers containing the epoxide organofunctional groups. The non-covalently-bonded surfactant was removed by solvent extraction at a solid to solvent (EtOH) ratio of 1 g to 50 mL. The extraction was repeated once, and the solid was rinsed with ethanol. The final products were obtained by filtration and air-dried at 80°C. The extracted products were denoted x HMS-epoxide-E, where x represents the percentage of epoxide functionalized silicon centers and E indicates that physically adsorbed surfactant was removed by ethanol extraction. To further study the structural properties of the materials, some of the as made materials were also calcined at 600°C for 4 hr. to remove all the surfactant and organic moieties. The calcined products were denoted as x HMS-epoxide-C, where x represents the mole fraction of epoxide functionalized silicon centers and C indicates the material was calcined.

2.2.3 Pb^{2+} trapping experiments

2.2.3.1 Pb^{2+} isotherms for tallow amine surfactant intercalated mesophase silicas

For the tallow amine surfactant-containing samples, 0.1 gram of the dry silica was dispersed in 100 mL water for 24h at room temperature to pre-wet the samples. Then 100 mL of Pb^{2+} solution with the desired concentration was added and the solution was kept stirring another 24h. When the reaction was complete after the 24 hr period, the mixture was filtered and the filtrate was collected for the atomic absorption analysis. The ratio of silica to initial Pb^{2+} solution was 0.1g to 200 mL and the initial lead nitrate concentration was from 5 to 300 ppm. The difference between the initial and equilibrium lead concentrations indicates the amount of lead that was trapped on the solid adsorbents. The lead trapping isotherms were plotted using the equilibrium concentration as the x axis and the adsorbed Pb^{2+} on the adsorbents as the y axis.

2.2.3.2 Pb^{2+} trapping experiments for epoxide functionalized amine surfactant intercalated mesophase silicas

The Pb^{2+} adsorption experiments were carried out by stirring 0.05 g of epoxide functionalized amine surfactant intercalated silica in 100 mL of lead nitrate (Pb(NO$_3$)$_2$) solution at 25°C. The initial Pb^{2+} concentration for these experiments was 116 ppm in all cases. The mixtures were stirred for 24 hours and then filtered through a 0.25 μm filter paper to collect the final filtrate solution.

The amount of Pb^{2+} in the filtrate after the adsorption experiments was analyzed by cold vapor atomic absorption spectroscopy (AAS). The difference between the initial

and equilibrium lead concentrations indicates the amount of Pb^{2+} that was trapped on the solid adsorbents.

2.2.4 Characterization

X-ray diffraction (XRD) patterns were obtained on a Rigaku Rotaflex 200B diffractometer equipped with Cu K_α X-ray radiation and a curved crystal graphite monochromator operating at 45 kV and 100 mA.

N_2 adsorption-desorption isotherms were obtained at −196 °C on a Micromeretics Tristar 3000 sorptometer using standard procedures. Samples were outgassed at 150 °C and 10^{-6} Torr for a minimum of 12 hr prior to analysis. Surface areas were calculated from the linear part of a BET plot of the nitrogen adsorption data according to IUPAC recommendations. The Barrett-Joyner-Halenda (BJH) method was used to obtain the pore size distribution from the adsorption branch of the isotherms.

Transmission electron microscopy (TEM) images were taken on a JEOL 2200FS microscope with filed emission electron source and an accelerating voltage of 200 keV. Sample grids of mesoporous silicas were prepared by sonicating the powdered sample in EtOH for 10 min and evaporating 2 drops of the suspension onto a holey carbon-coated film supported on 300 mesh copper grids.

The TGA curves were recorded in air on a Cahn TGA System 121 thermogravimeter using a heating rate of 5 °C/min.

Equilibrium concentrations of Pb^{2+} in solution were measured on a cold vapor atomic absorption spectroscopy Varian SpectrAA-200 using lead cathode with maximum working current of 10 mA.

2.3 Results and discussion

2.3.1 Tallow amine surfactant intercalated mesophase silica

Tallow amine surfactants have an average of 16 alkyl carbon atoms in the hydrophobic chain and hydrophilic head groups containing various nitrogen numbers. Due to the similarity between tallow amine surfactants and dodecylamine, which is used as the surfactant template for the assembly of HMS silica mesophases, wormhole mesostructures were expected for the mesophases synthesized using tallow amine surfactants as structure directing templates. The X-ray powder diffraction patterns of the surfactant-containing Tallow N1, N2 N3 and N4 materials and their surfactant-free forms obtained from calcinaiton at 600°C for 4 hours all showed a single reflection at a two theta value around 1.5-2.0 degree or a d-spacing of 4-6 nm (Figure 2.4), indicating wormhole structures was successfully made. The intensities of the XRD patterns for the as-made surfactant containing mesophase materials are weaker than those for the calcined derivatives. This is because there are two phases in the as-made materials, the surfactant phase and the silicate phase, resulting in contrast matching of the XRD patterns.
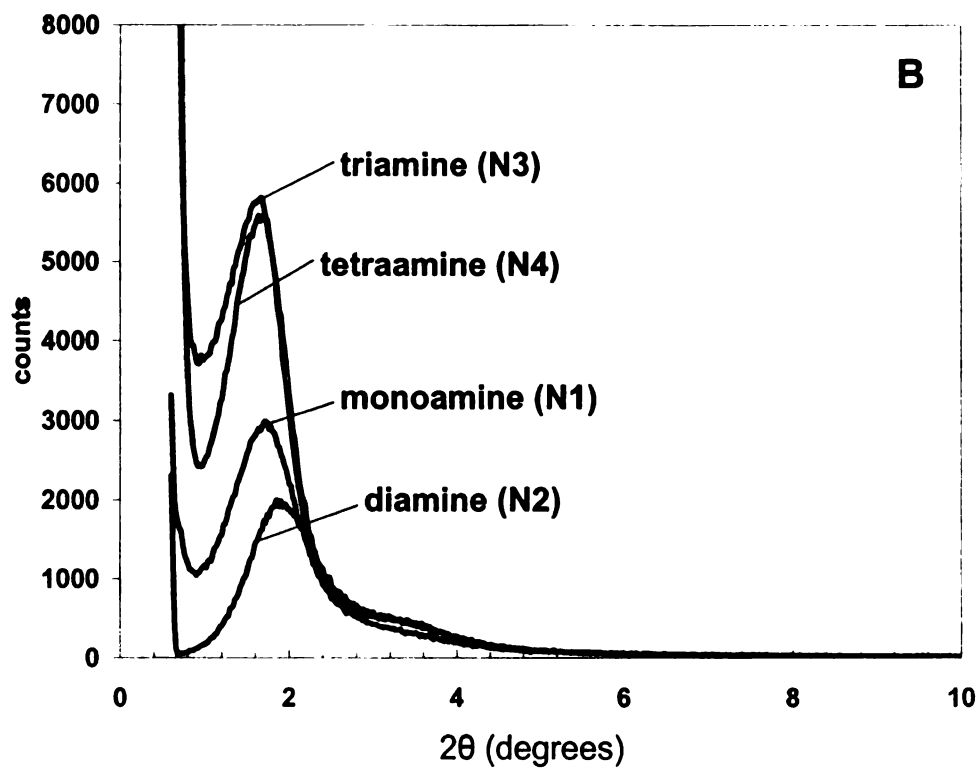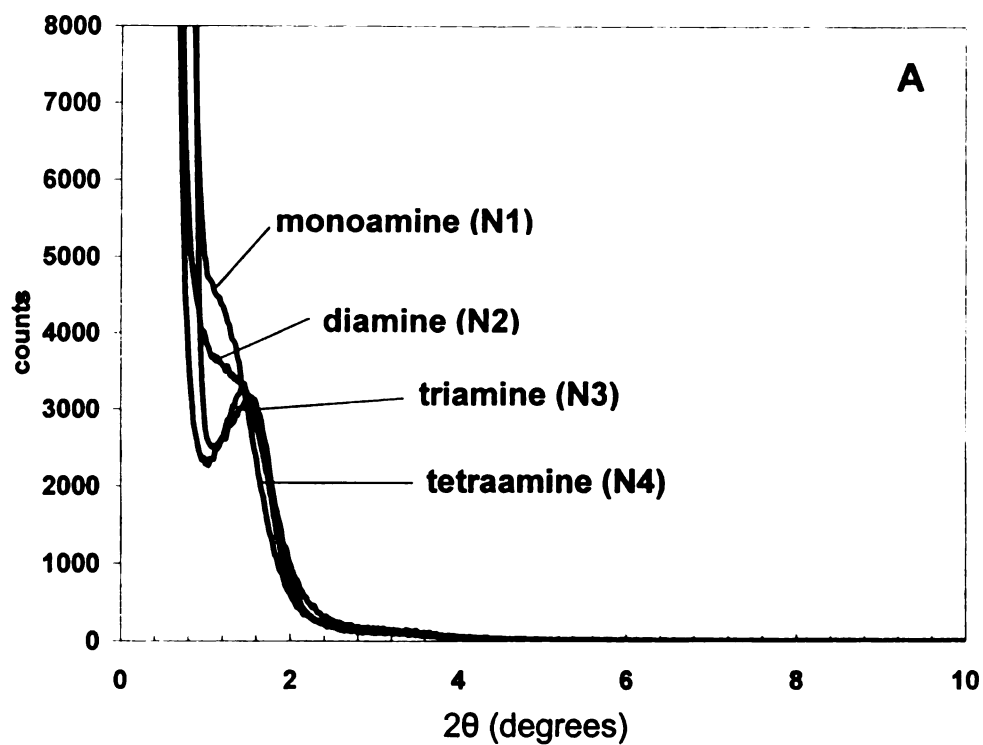
Figure 2.4. X-ray powder diffraction of (A) as-made tallow amine surfactant intercalated

mesophase silicas and (B) the counterparts after calcination at 600°C for 4 hours.

The N_2 adsorption-desorption isotherms and the BJH pore size distributions for the calcined Tallow-N1, N2, N3 and N4 were studied in order to further understand the structure and porosity properties of the surfactant containing mesophase materials. As shown in Figure 2.5, the N_2 filling steps at relative pressure between 0.4 and 0.6 indicated the existence of mesoporosity in the calcined Tallow amine materials. The pore size decreases upon increasing the number of nitrogen atoms in the surfactant head group, from 3.8 nm for the silica synthesized by using tallow monamine (N1) as surfactant to 3.0 nm for the material synthesized with tallow tetraamine surfactant (N4). It is well known that the interaction between the surfactant micelle and the silica moiety involves hydrogen bonding. Increasing the number of nitrogen atoms in the head group of the surfactants increases the hydrogen bonding interaction with the inorganic silica moiety. The pore size decreases with the tighter interaction. The BET surface area remained relatively consistent while increasing the nitrogen numbers in the surfactants. The detailed physical properties are summarized in Table 2.1.

Pb^{2+} adsorption performance was investigated on the as-made surfactant containing mesophase materials. The trapping isotherm patterns are summarized in Figure 2.6. The monoamine surfactant containing mesophase material reached a saturation plateau at an equilibrium concentration of 25 ppm. The maximum lead trapping capacity of the monoamine surfactant containing mesophase (N1) was about 0.2 mmol g^{-1}. The diamine, triamine and tetraamine surfactant containing mesophase all share a similar isotherm pattern and have the same maximum trapping capacity of 1.2 mmol g^{-1}. The trapping isotherm saturation plateau of diamine (N2) and triamine (N3) surfactant containing mesophases was reached around equilibrium concentration of 40

51

ppm, while the saturation plateau of tetraamine surfactant containing mesophase (N4) was reached around equilibrium concentration of 80 ppm. The monoamine surfactant containing mesophase behaves differently from the multiamine surfactant containing mesophases. This might be due to the chelating complex formation between the multiamine surfactant and the Pb^{2+} cation. The monoamine surfactant only has one nitrogen atom in one surfactant molecule; therefore the formation constant of lead complex would be relatively low. Because of the certain geometry of the multi nitrogens in a multiamine surfactant molecule, only certain amount of the lead cations can accept the long pair of electrons on the nitrogen. Therefore, there is no significant difference between the lead adsorption isotherms among the diamine, triamine and tetraamine surfactant containing mesophase materials.

The tallow amine series surfactants were not just utilized as the structure direct agents, but as the binding sites for heavy metal (e.g. Pb^{2+}) as well. The surfactant containing mesophase materials showed excellent trapping performance, having a maximum trapping capacity varied from 0.2 to 1.2 mmol g^{-1}.

During the trapping experiments, however, foaming was noticed while filtering the adsorbents from the equilibrium filtrate. This suggests the leaking of the surfactant from the mesophase materials. The mesophase materials could not have good potential uses in the heavy metal removal application unless the surfactant can be somehow "fixed" inside the mesopores and will not be leaching out.
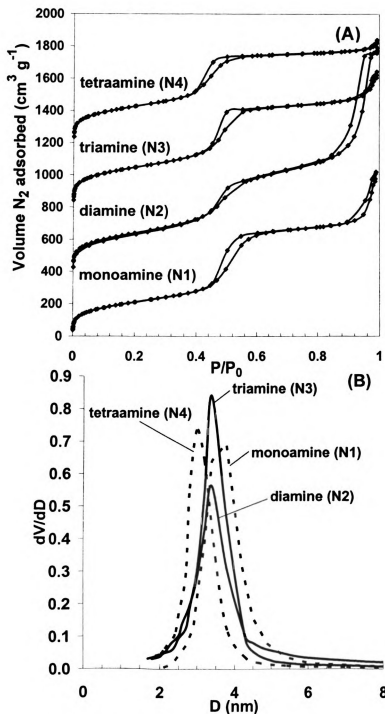
Figure 2.5. (A) N_2 adsorption-desorption isotherms and (B) BJH framework pore size distributions calculated from the N_2 adsorption branch of the calcined mesostructured silica materials synthesized with tallow amine surfactants as templates. The isotherms are offsite vertically by 400 cm^3 g^{-1} for clarity.

Table 2.1. Physical properties of tallow amine templated mesostructured silicas after calcination at 600°C for 4 hours

Calcined silica	d_{100} spacing (nm)	Pore size[a] (nm)	BET surface area ($m^2 \, g^{-1}$)	Total pore volume[b] ($cm^3 \, g^{-1}$)
Monoamine (N1)	4.9	3.8	746	1.58
Diamine (N2)	4.6	3.4	860	2.15
Triamine (N3)	5.2	3.4	866	1.18
Tetraamine (N4)	5.2	3.0	809	0.99

[a] Pore size diameter was determined by the BJH model from the adsorption branches of the isotherms. [b] Total pore volume was determined at $P/P_0=0.98$.
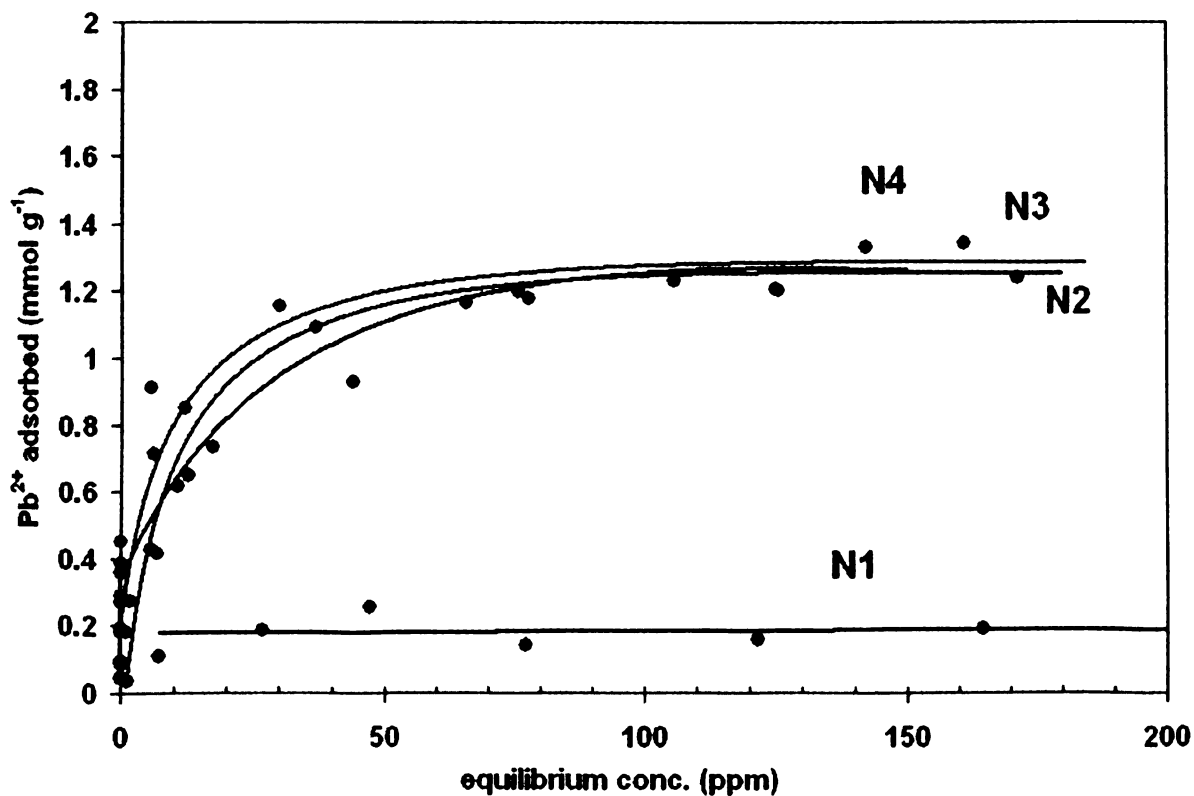
Figure 2.6. The Pb^{2+} trapping isotherms for tallow amine surfactant containing mesophase silicas.

2.3.2 Epoxide functionalized dodecylamine containing mesostructured silicas

An epoxide moiety was introduced into the dodecylamine surfactant containing mesophase materials in order to link the dodecylamine surfactant inside the mesopores through covalent binding. The head group of a dodecylamine surfactant molecule is a primary amine which contains two active hydrogens. When the epoxide organosilane was introduced to the surfactant solution, the active hydrogen on the dodecylamine molecule will open the epoxy ring to form C-N covalent bonds. The epoxy ring will be opened and a covalent bond will be formed between the nitrogen on the surfactant molecule and the less substituted carbon on the epoxy ring. If more epoxide is available, the active hydrogen on the secondary amine formed in the first step reaction will react with another epoxy ring to form another covalent bond between the less substituted carbon on the second epoxy ring and the nitrogen on the surfactant molecule. The overall reaction is described in Figure 2.7A. The reaction stoichiometry used to form the organofunctionalized surfactant-containing mesophase was DDA: Epoxide organosilane: TEOS: H_2O: EtOH = 0.25: x: (1-x): 180: 20, where x is the fraction of silicon center linked with epoxide organofunctional groups and x equals to 0.05, 0.10, 0.25 and 0.50. When x equals to 0.05 or 0.10, only a part of the dodecylamine surfactant molecules are able to form covalent bonds with epoxy rings, while the remaining non-covalent-bonded surfactants will be removed after solvent extraction with ethanol. Partially surfactant filled pores were expected for the extracted materials x-HMS-epoxide-E with x=0.05 or 0.10. Figure 2.7B illustrates the as-made surfactant containing mesophase products, the ethanol extracted products containing covalently bonded partial surfactant, and the calcined products which have no surfactant or organic epoxide groups in the pores. If the

x value (epoxide moiety) is higher than 0.25, all of the surfactant was expected to form covalent bonds with the epoxy rings linked to the framework. Thus, no surfactant can be removed by the solvent extraction.

(A)
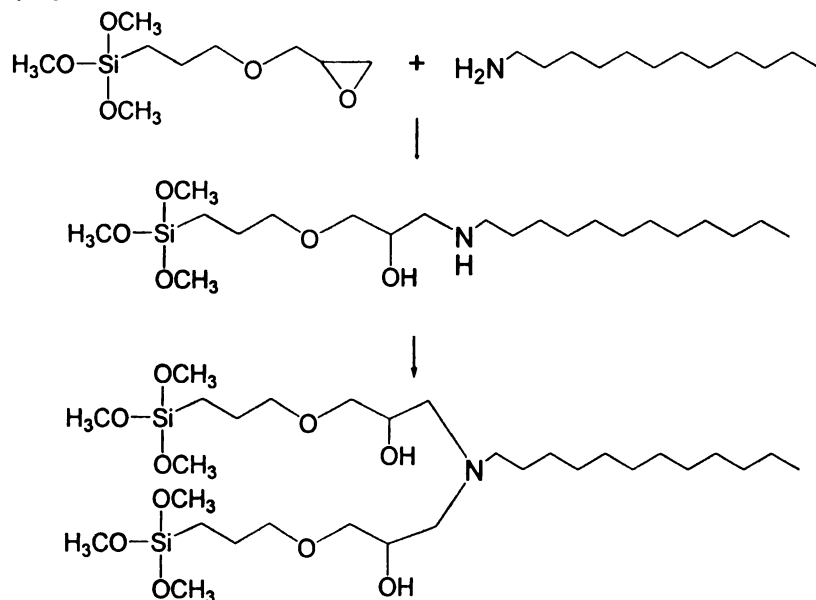
(B)

As-made
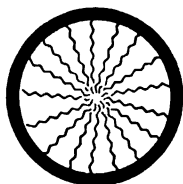
extracted
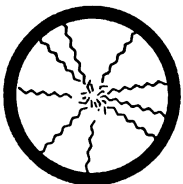
calcined
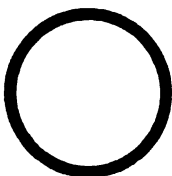
Figure 2.7. (A) The formation of the covalent bonds between the epoxide functional moiety and the dodecylamine surfactant and (B) a schematic illustration of the mesostructured silicas after different synthesis steps.

Figure 2.8 shows the X-ray powder diffraction patterns of the extracted epoxide functionalized surfactant-containing mesophase materials x HMS-epoxide-E. In all cases, a single diffraction peak was observed at low angle, indicating the formation of a wormhole mesostructure. The center of the single diffraction peak moves to higher two theta value, indicating a smaller d_{100} spacing, with increasing epoxide moiety loading. The intensity of the XRD patterns decreases with increasing epoxide loading. With increasing the epoxide loading, more dodecylamine surfactant was kept inside the mesopores through the formation of covalent bonds. Stronger hydrogen bonding interaction between the surfactant micelles and the silicate moiety resulted in a smaller unit cell size. The intercalation of more surfactant will cause the XRD intensity to decrease due to increased phase contract matching.

N_2 adsorption desorption isotherms and pore size distributions obtained from the adsorption isotherm branch for the x HMS-epoxide-E silicas are shown in Figure 2.9A and 2.9B, respectively. Increasing the epoxide functionality from 0 to 0.05 and 0.10 causes the step in the adsorption-desorption isotherms to move from higher to lower relative pressure, indicating a decrease of the pore size. The decrease in the pore size is also clearly shown in the pore size distributions in Figure 2.9B. Extracted HMS-E silica without an epoxide functionality has an average pore size of 2.3 nm, while the 0.05-HMS-epoxide-E and 0.10-HMS-epoxide-E have a pore size of 1.8 nm and 1.6 nm, respectively. In the case of HMS-E, there is only hydrogen bonding interaction between the head group of the surfactant micelles and the silicate framework. The interaction is relatively weak and loose. When the desired amount of epoxide was introduced into the silicate framework, at least equal amounts of the dodecylamine surfactant molecule will

form covalent bonds with the less substituted carbon on the epoxy ring by ring opening reaction. Therefore, the interaction between the surfactant micelle and the silicate framework became stronger and caused the pore size of the final product to shrink. The more epoxide introduced into the framework, the smaller the pore size of the final mesostructure. Figures 2.10A and 2.10B show the TEM images of 0.05-HMS-epoxide-E at low and high magnifications. The wormhole structure can be clearly observed. When the epoxide functionality is increased to 0.10, the wormhole mesostructure was maintained according to the TEM images (Fig. 2.10C, D). There is no significant difference between the TEM images of 0.05- and 0.10-HMS-epoxide-E materials.

x-HMS-epoxide-E derivatives with x=0.25 an 0.50 both showed no porosity based on the N_2 adsorption desorption isotherms (Fig. 2.9). At these epoxy loadings, all of the dodecylamine surfactants were expected to form covalent bonds with the functionalized silicate framework, so that free surfactant can be removed by solvent extraction. The absence of porosity for the x=0.25 and 0.50 HMS-epoxide-E derivatives was confirmed by the TEM images (Fig. 2.11). Solid spherical particles with diameter of few hundred nanometers were observed for the 0.25-HMS-epoxide-E material (Fig 2.11A, B), while the 0.50-HMS-epoxide-E material showed no regular shape for the poreless particles (Fig. 2.11C, D). When the epoxide functionality was increased to 0.50, it is hard to fully crosslink all the organosilane into the silica framework. Therefore some uneven contrast was observed in the TEM images of the 0.50-HMS-epoxide-E product.
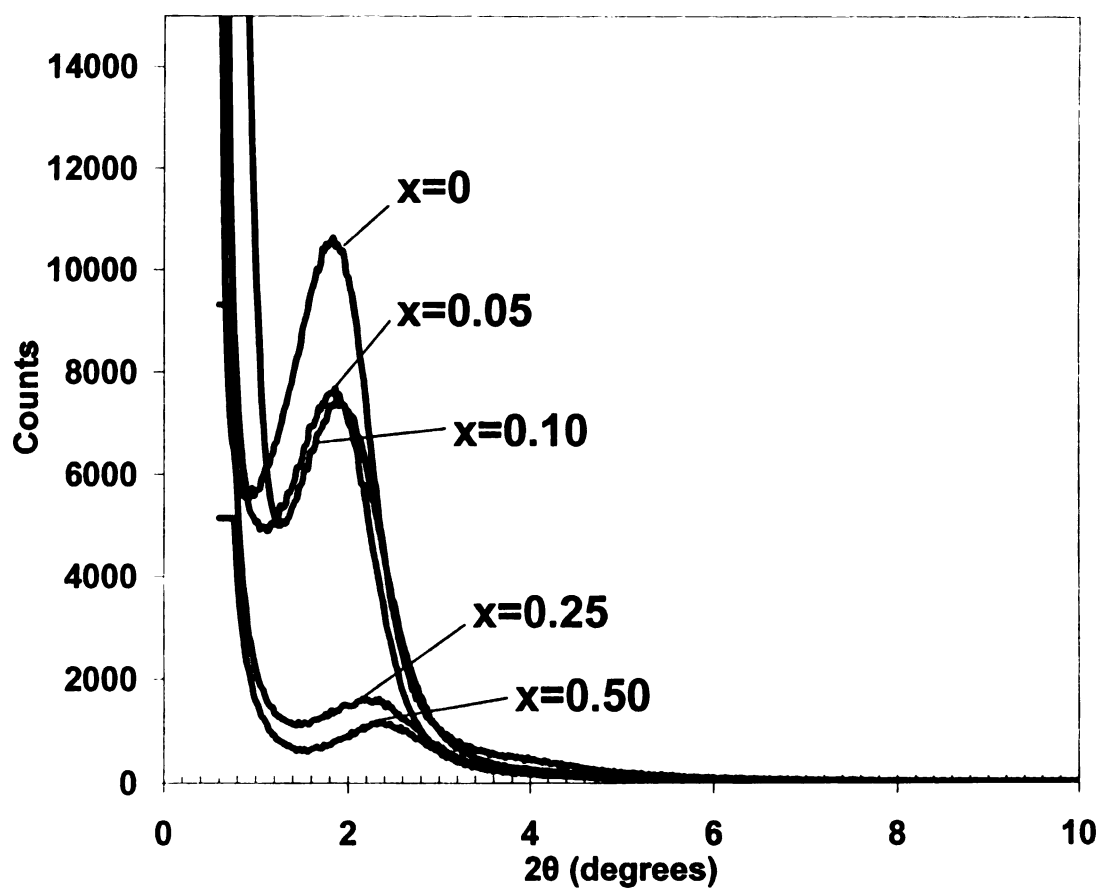
Figure 2.8. X-ray powder diffraction patterns of epoxide functionalized mesostructured silicas made with dodecylamine as the surfactant and subsequent solvent extraction, x-HMS-epoxide-E, where x represents the fraction of silicon centers with an epoxide functional moiety.
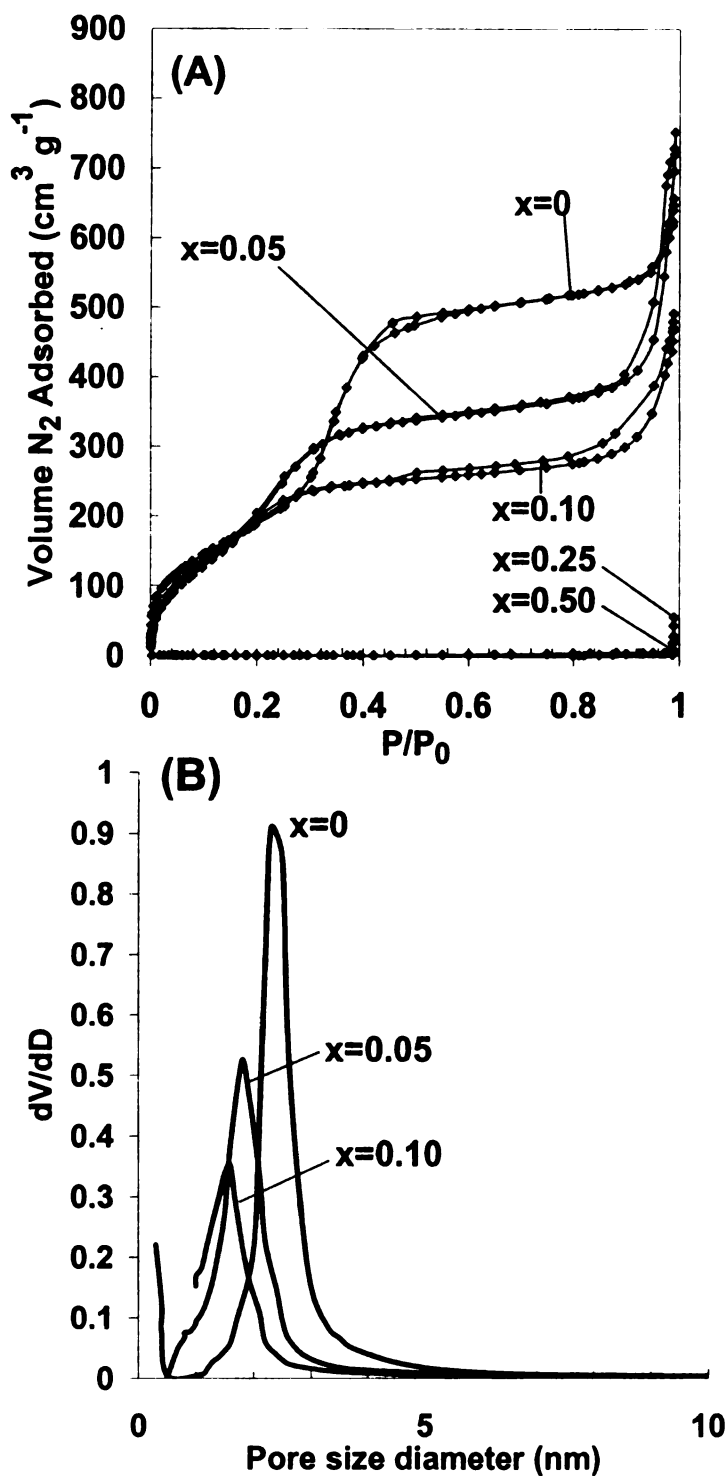
Figure 2.9. (A) N_2 adsorption-desorption isotherms and (B) pore size distributions determined from the N_2 adsorption isotherm branch for x-HMS-epoxide-E silicas templated by dodecylamine after extraction with ethanol, where x is the fraction of framework silicon atoms linked to epoxy groups.

60
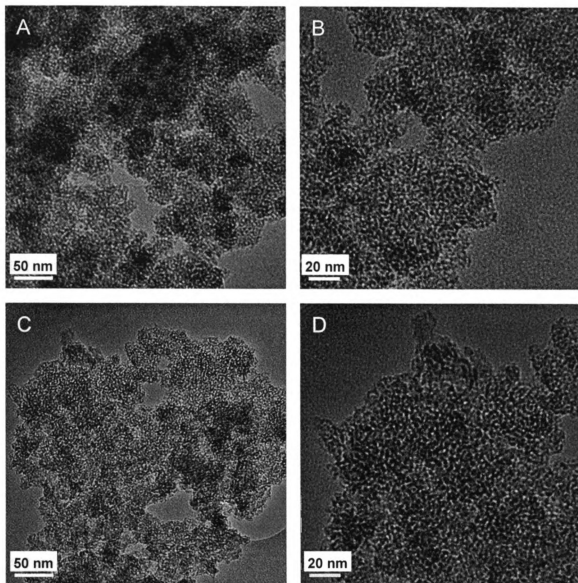
Figure 2.10. TEM images for epoxide functionalized, surfactant-containing mesophase silicas made with dodecylamine as surfactant, denoted x-HMS-Epoxide-E, where the theoretical epoxy loading is x=0.05 (A, B) and 0.10 (C, D).
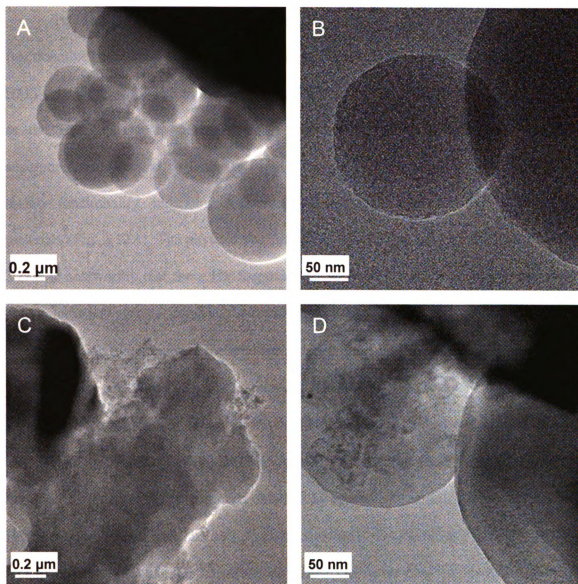
Figure 2.11. TEM images for epoxide functionalized, surfactant-containing mesophase silicas made with dodecylamine as surfactant, denoted x-HMS-Epoxide-E, where the theoretical epoxy loading is x=0.25 (A, B) and 0.50 (C, D).

To further understand the structure and porosity properties of the epoxide functionalized surfactant containing mesophase materials, calcined derivatives denoted x-HMS-epoxide-C were also investigated. HMS-epoxide-C materials share a similar trend as the HMS-epoxide-E materials. N_2 adsorption-desorption isotherms showed the adsorption steps moved to lower relative pressure with increasing degree of epoxide moiety functionality, indicating a decrease on the pore size of x HMS-epoxide-C materials (Fig. 2.12A). The physical properties of each product are summarized in Table 2.2. It is noteworthy that the x HMS-epoxide-C materials always have larger pore size, pore volume and surface area than the counterparts x HMS-epoxide-E materials. Take the x=0.10 epoxide functionalized material for instance, the 0.10-HMS-epoxide-C derivative has a pore size of 2.2 nm, total pore volume of 1.32 cm^3 g^{-1}, and surface area of 1374 m^2 g^{-1} while the corresponding values for the 0.10-HMS-epoxide-E are 1.6 nm, 0.76 cm^3 g^{-1}, and 758 m^2 g^{-1}. 0.25- and 0.50-HMS-epoxide-C also showed some porosity, which is totally different from the counterparts obtained by solvent extraction. For example, 0.25-HMS-epoxide-C has a pore size of 1.3 nm, pore volume of 0.76 cm^3 g^{-1}, and BET surface area of 1128 m^2 g^{-1} while the 0.25-HMS-epoxide-E derivative does not have any porosity at all. This is because during the calcination process, the bonded epoxy and surfactant were from the framework pores. The previously partially "stuffed" pores were open again, causing the pore size, pore volume and surface area to increase.
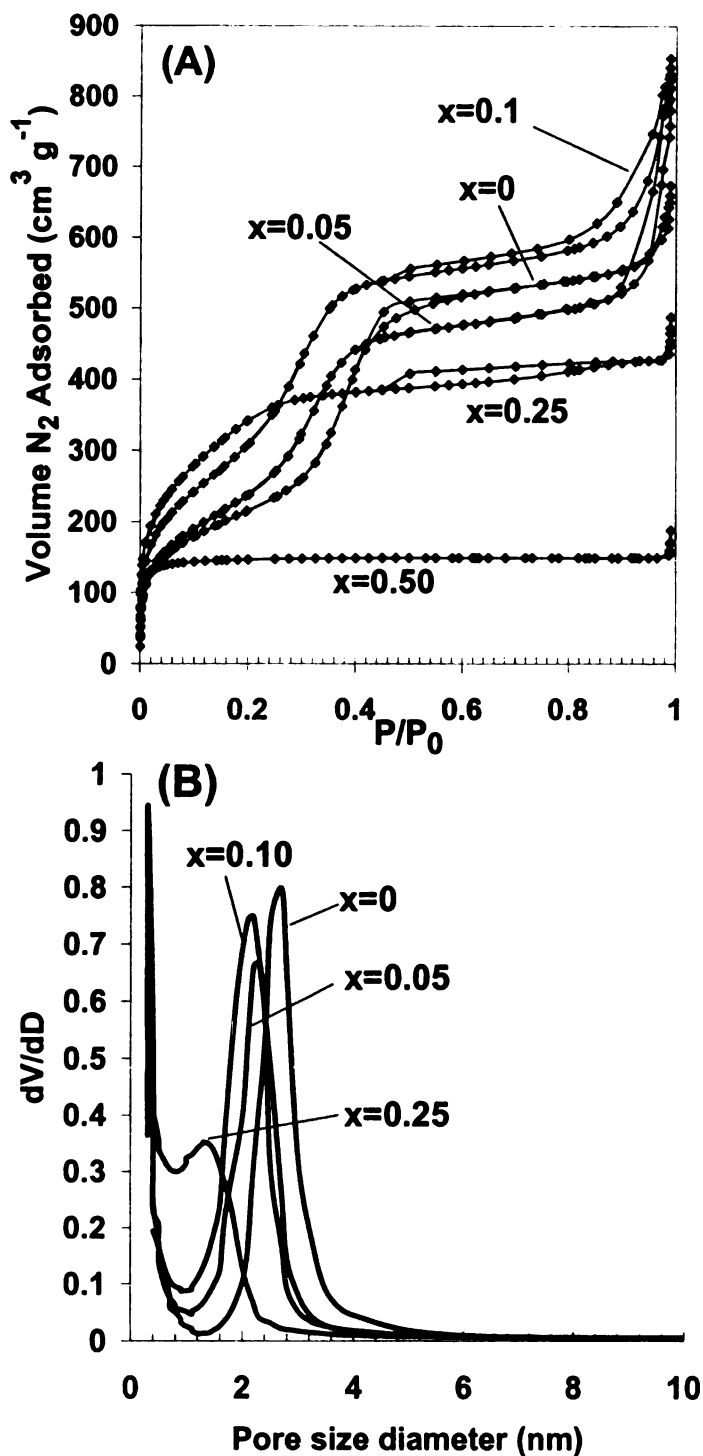
Figure 2.12. (A) N_2 adsorption-desorption isotherms and (B) pore size distributions determined from the N_2 adsorption isotherm branch for x-HMS-epoxide-C silicas templated by dodecylamine after calcination, where x is the fraction of framework silicon atoms linked to epoxy groups.

Table 2.2. Physical properties of epoxide functionalized mesostructure silica materials after solvent extraction x-HMS-epoxide-E and calcination x-HMS-epoxide-C.

materials	d_{100} spacing (nm)	Pore size[a] (nm)	S_{BET} ($m^2 g^{-1}$)	V_{total}[b] ($cm^3 g^{-1}$)
HMS-E	4.80	2.3	862	1.02
0.05-HMS-epoxide-E	4.75	1.8	972	1.18
0.10-HMS-epoxide-E	4.60	1.6	758	0.76
0.25-HMS-epoxide-E	3.77	N/A	0.11	0.09
0.50-HMS-epoxide-E	3.71	N/A	0.04	0.03
HMS-C	4.85	2.7	840	1.04
0.05-HMS-epoxide-C	4.85	2.3	1048	1.28
0.10HMS-epoxide-C	4.41	2.2	1374	1.32
0.25-HMS-epoxide-C	3.87	1.3	1128	0.76
0.50-HMS-epoxide-C	3.68	N/A	437	0.29

[a] Pore size diameter was determined by the BJH model from the adsorption branches of the isotherms. [b] Total pore volume was determined at P/P_0=0.98.

Through the formation of a covalent bond between the surfactant and the epoxide organic moiety in the silica framework, the surfactant was successfully retained inside the framework pores of HMS-epoxide-E materials. Thermal gravimetric analysis was carried out on the 0.50-HMS-epoxide-E material before and after the water extraction treatment. The TGA profile of 0.50-HMS-epoxide-E material after water extraction overlapped with the one without water extraction treatment, indicating that the surfactants inside the framework pores are stable and will not leach out (Fig. 2.13). It was also noted that foaming phenomenon was not observed during Pb^{2+} trapping experiments, further proving that the surfactants are covalently bonded to the silicate framework and are not leached.

The N contents of the adsorbents were determined by CHN elemental analysis. The results were listed in Table 2.3. Because all the nitrogen sources are from the dodecylamine surfactant, the N content indicates the amount of surfactant covalently bonded to the framework. The N content is proportional to the degree of epoxide functionality from x=0.05 to 0.25. When the epoxide functionality increases from x=0.25 to 0.50, the N content did not double. When there is x=0.25 epoxide organic moiety in the framework, the ratio of epoxide organosilane to dodecylamine is 1 to 1 and all of the surfactant can covalently bind to the epoxide (Figure 2.7A). When increasing the epoxide moiety to x=0.50, similar amount of surfactant was expected to be covalently bonded to the framework but with ratio of epoxy ring to dodecylamine 2 to 1.

A single point Pb^{2+} trapping experiment was carried out on the HMS-epoxide-E materials. The initial Pb^{2+} solution concentration was 116 ppm in all the cases. 0.05-HMS-epoxide-E mesophase material reduced the Pb^{2+} concentration to 48 ppm and had

trapping capacity of 0.33 mmol g^{-1}. The ratio of N to adsorbed Pb^{2+} on the 0.05-HMS-epoxide-E material is 1.5. The nitrogen usage efficiency is relatively high in this case. Upon increasing the degree of epoxide functionality, the N content increases as well. The trapping capacity of HMS-epoxide-E material, however, decreased with the increasing nitrogen content. It might because with the increasing surfactant molecules formed covalent bonds and stayed inside the pores, the environment became more hydrophobic in the framework pores. Therefore, it is hard for the hydrophilic lead cation to penetrate to the nitrogen binding site, causing the overall trapping capacity to decrease. Only a moderate degree of epoxide functionality provides a sufficient amount of surfactant inside the framework pores while at the same time maintaining a hydrophilic mesopore environment.
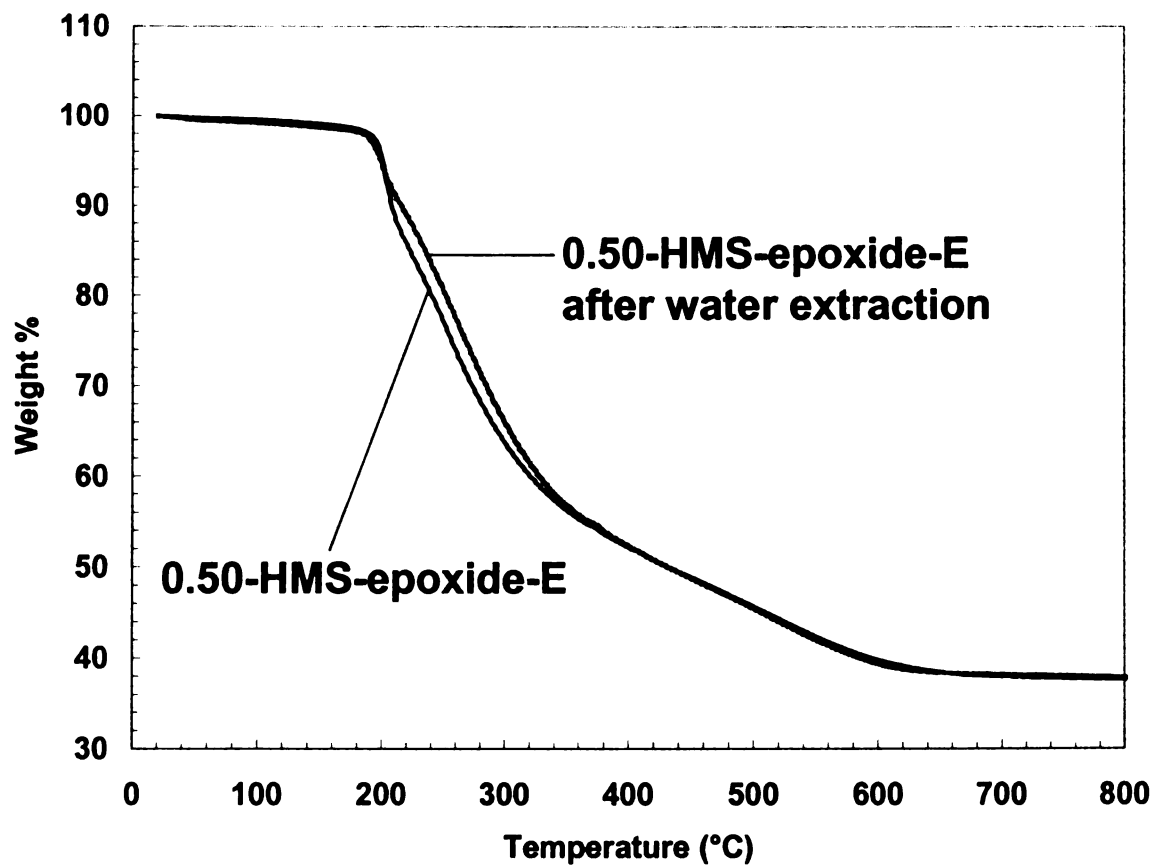
Figure 2.13. Thermal gravimetric analysis (TGA) profiles of 0.50-HMS-epoxide-E before and after water extraction.

Table 2.3. Pb^{2+} trapping performance of epoxide functionalized, dodecylamine-containing mesostructured silica materials, denoted x-HMS-epoxide-E.

x-HMS-epoxide-E x=	Equilibrium Pb^{2+} conc. [a] (ppm)	N density [b] (mmol g^{-1})	Pb^{2+} adsorbed (mmol g^{-1})	N : Pb^{2+} ratio
0.05	48	0.50	0.33	1.5:1
0.10	69	0.81	0.23	3.5:1
0.25	102	2.02	0.07	29:1
0.50	114	2.25	0.01	225:1

[a] 1 g of the silica adsorbent was dispersed in 1000 mL lead nitrate solution containing 116 ppm Pb^{2+}. [b] Nitrogen content was calculated from the CHN elemental analysis carried out in-house.

2.4 Conclusion

Most of the applications of the mesostructured silicas have focused on the functionalized surfactant-free mesoporous materials. For the purpose of heavy metal removal, different organic groups have been grafted into the surfactant-free silicate framework in order to achieve specific affinity with various heavy metals. In this work, an attempt was made to utilize the surfactant for the removal of heavy metal ions from solution.

The tallow amine surfactant intercalated mesophase silicas showed good affinity towards heavy metal Pb^{2+}. The tallow monoamine surfactant intercalated mesophase (N1) exhibited a maximum trapping capacity of 0.2 mmol of Pb^{2+} per gram of adsorbent, while the tallow diamine, triamine and tetraamine surfactant derivatives had a similar maximum Pb^{2+} trapping capacity of 1.2 mmol g^{-1}. The multiamine surfactant intercalated mesophases have a higher trapping capacity compared to the monoamine derivative, suggesting the chelating effect between the amine binding sites and the lead cations. The leaching rate of the surfactant in the as-made mesophase materials was described as being very low.[21] However, it remained a concern that the surfactant was not irreversibly bound inside the mesopores.

By introducing the epoxide organic moiety into the silica material synthesis process using the dodecylamine as the structure directly agents, the surfactant can be chemically stabilized inside the mesopores through the formation of covalent bonds between the amine head groups on the surfactant and the carbon on the epoxide ring. The epoxide functionalized, surfactant-containing mesophase silica HMS-epoxide-E was successfully synthesized. The surfactant was covalently connected to the silicate

framework and would not leach out during the adsorption applications. A wormhole structure was observed for the surfactant containing mesophases with moderate functionality of the epoxide moiety (i.e., x=0.05 and 0.10), while further increases in epoxide loading resulted little or no porosity of the final products due to the surfactant fully stuffing the mesopores. 0.05-HMS-epoxide-E has a 0.33 mmol g^{-1} Pb^{2+} trapping capacity and a high accessibility of the nitrogen. The Pb^{2+} trapping capacity of the mesophase materials decreased while increasing degree of epoxide functionality. The reduction in binding capacity with increased epoxide functionality may be due to a more hydrophobic pore environment. Therefore, the hydrophilic Pb^{2+} species is difficult to penetrate the interface between the surfactant and the silicate, where the nitrogen binding sites were located. It is suggested that introducing moderate epoxide functionality into the silica framework keeps the surfactant containing mesophase materials porous and less hydrophobic. This provides good heavy metal trapping capacity and higher availability of the surfactant binding site.

2.5 References

(1)   Beck, J. S.; Vartuli, J. C.; Roth, W. J.; Leonowicz, M. E.; Kresge, C. T.; Schmitt,
        K. D.; Chu, C. T. W.; Olson, D. H.; Sheppard, E. W.; et al. *J. Am. Chem. Soc.*
        1992, *114*, 10834-43.

(2)   Van Rhijn, W. M.; De Vos, D. E.; Sels, B. F.; Bossaert, W. D.; Jacobs, P. A.
        Chem. Commun. **1998**, 317-318.

(3)   Bossaert, W. D.; De Vos, D. E.; Van Rhijn, W. M.; Bullen, J.; Grobet, P. J.;
        Jacobs, P. A. *J. Catal.* **1999**, *182*, 156-164.

(4)   Yu, W.; Zhang, Z.; Wang, H.; Ge, Z.; Pinnavaia, T. J. *Microporous Mesoporous
        Mater.* **2007**, *104*, 151-158.

(5)   Cao, W.; Zhang, H.; Yuan, Y. *Catal. Lett.* **2003**, *91*, 243-246.

(6)   Mercier, L.; Pinnavaia, T. J. *Adv. Mater.* **1997**, *9*, 500-503.

(7)   Lesaint, C.; Frebault, F.; Delacote, C.; Lebeau, B.; Marichal, C.; Walcarius, A.;
        Patarin, J. *Stud. Surf. Sci. Catal.* **2005**, *156*, 925-932.

(8)   Yoshitake, H.; Yokoi, T.; Tatsumi, T. *Chem. Mater.* **2003**, *15*, 1713-1721.

(9)   Bibby, A.; Mercier, L. *Chem. Mater.* **2002**, *14*, 1591-1597.

(10)   Nguyen, T.-Q.; Wu, J.; Doan, V.; Schwartz, B. J.; Tolbert, S. H. *Science* **2000**,
        288, 652-656.

(11)   Ganschow, M.; Wark, M.; Wohrle, D.; Schulz-Ekloff, G. *Angew. Chem., Int. Ed.*
        2000, *39*, 161-163.

(12)   Kageyama, K.; Tamazawa, J.-I.; Aida, T. *Science* **1999**, *285*, 2113-2115.

(13)   Zhou, W.; Thomas, J. M.; Shephard, D. S.; Johnson, B. F. G.; Ozkaya, D.;
        Maschmeyer, T.; Bell, R. G.; Ge, Q. *Science* **1998**, *280*, 705-708.

(14)   Wu, C. G.; Bein, T. *Science* **1994**, *264*, 1757-9.

(15)   Zhang, X.; Guan, R.-F.; Wu, D.-Q.; Chan, K.-Y. *J. Mater. Sci.: Mater. Med.* **2007**, *18*, 877-882.

(16)   Czuryszkiewicz, T.; Ahvenlammi, J.; Kortesuo, P.; Ahola, M.; Kleitz, F.; Jokinen, M.; Linden, M.; Rosenholm, J. B. *J. Non-Cryst. Solids* **2002**, *306*, 1-10.

(17)   Arcos, D.; Ragel, C. V.; Vallet-Regi, M. *Biomaterials* **2001**, *22*, 701-708.

(18)   Vallet-Regi, M.; Ramila, A.; del Real, R. P.; Perez-Pariente, J. *Chem. Mater.* **2001**, *13*, 308-311.

(19)   Kubota, Y.; Nishizaki, Y.; Sugi, Y. *Chem. Lett.* **2000**, 998-999.

(20)   Denoyel, R.; Rey, E. S. *Langmuir* **1998**, *14*, 7321-7323.

(21)   Zhao, H.; Nagy, K. L.; Waples, J. S.; Vance, G. F. *Environ. Sci. Technol.* **2000**, *34*, 4822-4827.

(22)   Abdel-Fattah, T. M.; Bishop, B. *J. Environ. Sci. Health., Part A* **2004**, *A39*, 2855-2866.

(23)   Vartuli, J. C.; Malek, A.; Roth, W. J.; Kresge, C. T.; McCullen, S. B. *Microporous Mesoporous Mater.* **2001**, *44-45*, 691-695.

(24)   Zhao, Y. X.; Ding, M. Y.; Chen, D. P. *Anal. Chim. Acta* **2005**, *542*, 193-198.

(25)   Yamaguchi, A.; Amino, Y.; Shima, K.; Suzuki, S.; Yamashita, T.; Teramae, N. *J. Phys. Chem. B* **2006**, *110*, 3910-3916.

(26)   Yamaguchi, A.; Watanabe, J.; Mahmoud, M. M.; Fujiwara, R.; Morita, K.; Yamashita, T.; Amino, Y.; Chen, Y.; Radhakrishnan, L.; Teramae, N. *Anal. Chim. Acta* **2006**, *556*, 157-163.

(27)   Miyake, Y.; Yumoto, T.; Kitamura, H.; Sugimoto, T. *Phys. Chem. Chem. Phys.* **2002**, *4*, 2680-2684.

(28)   Miyake, Y.; Hanaeda, M.; Asada, M. *Ind. Eng. Chem. Res.* **2007**, *46*, 8152-8157.

(29)   Hashizume, H. *J. Environ. Sci. Health, Part A: Toxic/Hazard. Subst. Environ. Eng.* **2004**, *A39*, 2615-2625.

(30)   Sayari, A.; Hamoudi, S.; Yang, Y. *Chem. Mater.* **2005**, *17*, 212-216.

(31)   Choi, H. S.; Lee, D. G.; Cho, G. J.; Lee, C. Y.; Chung, J. S.; Yoo, I.-k.; Shin, E. W. *Hwahak Konghak* **2006**, *44*, 172-178.

(32)   Xu, S.; Boyd, S. A. *Environ. Sci. Technol.* **1995**, *29*, 312-20.

(33)   Li, Z.; Roy, S. J.; Zou, Y.; Bowman, R. S. *Environ. Sci. Technol.* **1998**, *32*, 2628-2632.

Chapter 3

Synthesis of mesostructure silicas with more accessible amino groups and their application as lead (Pb^{2+}) adsorbents

3.1 Introduction

Lead poisoning remains one of the most prevalent diseases of environmental origin in the United States today, particularly affecting young children. The U.S. Centers for Disease Control and Prevention currently estimates that 2.2 % of all U.S. children aged 1-5 years (434,000 children) have elevated blood lead levels.[1] Effective approaches to remove the toxic metals from contaminated water have involved the use of solid adsorbents, such as activated carbon, ion exchange resin, functionalized silica-based materials including silica gels, clays and mesoporous silicas. The advantages of functionalized mesoporous silicas for environmental remediation are their high surface areas, well-defined pore size, and the ability to covalently link organic groups to the framework to allow for selective adsorption of specific toxic heavy elements.

There are generally two methods to prepare mesostructured silicas with organic groups, namely grafting and direct assembly.[2] The grafting of functional groups to the pore walls of mesoporous molecular sieves can be achieved by the covalent fixation of hydrolysable moieties (of the type R_3SiL, where R = Cl or OCH_3 and L = functional organic group) to the surface Si-OH groups lining the pores of the mesostructures. Due to the limited number and random distribution of silanol groups on the surface of silicas, organofunctionalized mesostructured silicas from grafting method often end up having a low and uncontrollable loading of organic groups on the surface. The direct assembly method, on the other hand, uses the co-condensation of tetraethyl orthosilicate (TEOS)

75

and functionalized trialkoxysilane R_3SiL during the mesostructure synthesis process to give a better distribution of the organic groups through out the framework and a higher organic group loading. Therefore, the direct assembly pathway is considered superior to the grafting method.[3]

Many organic groups, such as vinyl, amino, thiol, imidazole etc., have been incorporated into the framework of mesostructured silicas by direct assembly pathway.[4-11] Among all the organic groups been incorporated into the framework, mercaptopropyl and aminopropyl are most popular due to their high affinity towards heavy metals in the application of environmental remediation. Mercaptopropyl group has been incorporated into different mesostructures, such as SBA-15, MCM-41 and HMS, trough co-condensation pathway then applied extensively as adsorbents for heavy metal ions like $Hg(II)$[4,12-14]. Amine functionalized mesostructured silica showed good trapping capacity for heavy metal ions because of the acid-base interaction between the lone pair on the nitrogen and metal cation.[9,14,15]. However the co-condensation reaction of aminopropyl organosilane with TEOS often suffers from the strong disruption of the mesostructure, particularly at organosilane levels above 20 mol %.[16]

Macquarrie et al. found that the amine containing silanes consistently give lower surface area than other kinds of organosilanes when incorporated into HMS silica mateirals.[17] A low pore volume and surface area were reported for amino functionalized SBA-15 silicas, as well.[18,19] Tatsumi et al. also revealed that not all the incorporated amino moieties were present on the surface; some of them were in the walls of the MCM-41 mesostructure framework.[9] It was suggested that the aminopropyl group of the amino organosilane binds to the Si atom of the same aminosilane molecule or to a neighboring

silicon and forms a penta-coordinate intermediate (as shown in Figure 3.1) that is very reactive with nucleophiles such as the hydroxyl groups formed after the hydrolysis of alkoxy groups on the organosilane or TEOS. It is also possible that the penta-coordinate intermediate is very reactive with water, leading to uncontrolled levels of polymerization (Figure 3.2).[20] Therefore, the direct co-condensation of APTES and TEOS will suffer the lost of mesostructure, and the accessibility of the amino groups will be low.
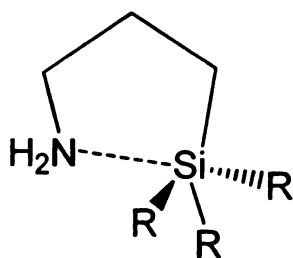
Figure 3.1. Penta-coordinate intermediate formed by the aminopropyl organosilane
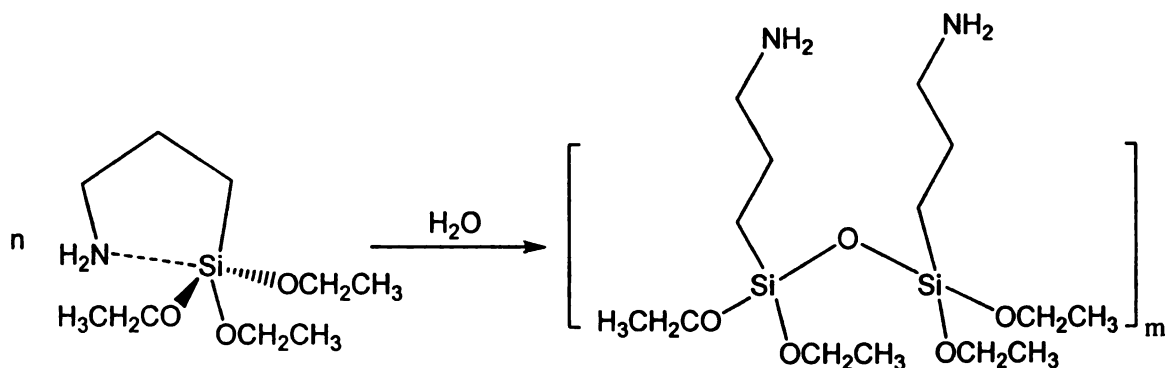
Figure 3.2. Uncontrolled polymerization of aminopropyl organosilane

Chong et al. studied the effect of different organosilanes on the formation of the mesostructured silica.[21] They found that the amine organosilane had the largest disruptive effects on the formation of the mesostructures. The co-condensation method requires that the organic group to be sufficiently hydrophobic to enter the core of the micelle and not too bulky to avoid its penetration. It was suggested that the amine group was very hydrophilic and this affected the mesostructure formation the most.[22] Rosenholm et al.

also showed that increasing the content of amine groups in the SBA-15 framework, the actually accessible amine groups dropped, indicating that most of the amines were buried in the wall of the silica framework, resulting in a disruptive effect on the formation of the mesostructure.[16] In the case of a HMS mesostructured silica framework, the introduction of aminopropyl compromised the wormhole framework, as verified by the absence of a diffraction peak at low angle in the X-ray pattern and a low surface area, as obtained from the nitrogen isothems.[23] Figure 3.3 demonstrates the possible positions of a hydrophilic aminopropyl moiety and a hydrophobic organic moiety (such as the mercaptopropyl group) within a silicate framework which was synthesized with a dodecylamine surfactant.

Due to the hydrophilicity of the amine functionalized organic moiety and the hydrogen bonding interaction between the amine organosilane and the silicate framework, it remained a challenge to synthesize accessible amine groups through co-condensation methods. Tatsumi proposed the incorporation of amine functional group into the silica framework through the use of an anionic surfactant during the co-condensation process.[24,25] The electrostatic interaction between the positively charged protonated amino groups in APTES and the negatively charged head groups in the anionic surfactant is a driving force for the self-assembly of the mesostructured organosilica. The amino functionalized material synthesized via the use of an anionic surfactant showed higher accessibility for the aminopropyl moiety in contrast to the MCM-41 derivative synthesized with a cationic surfactant.[26]
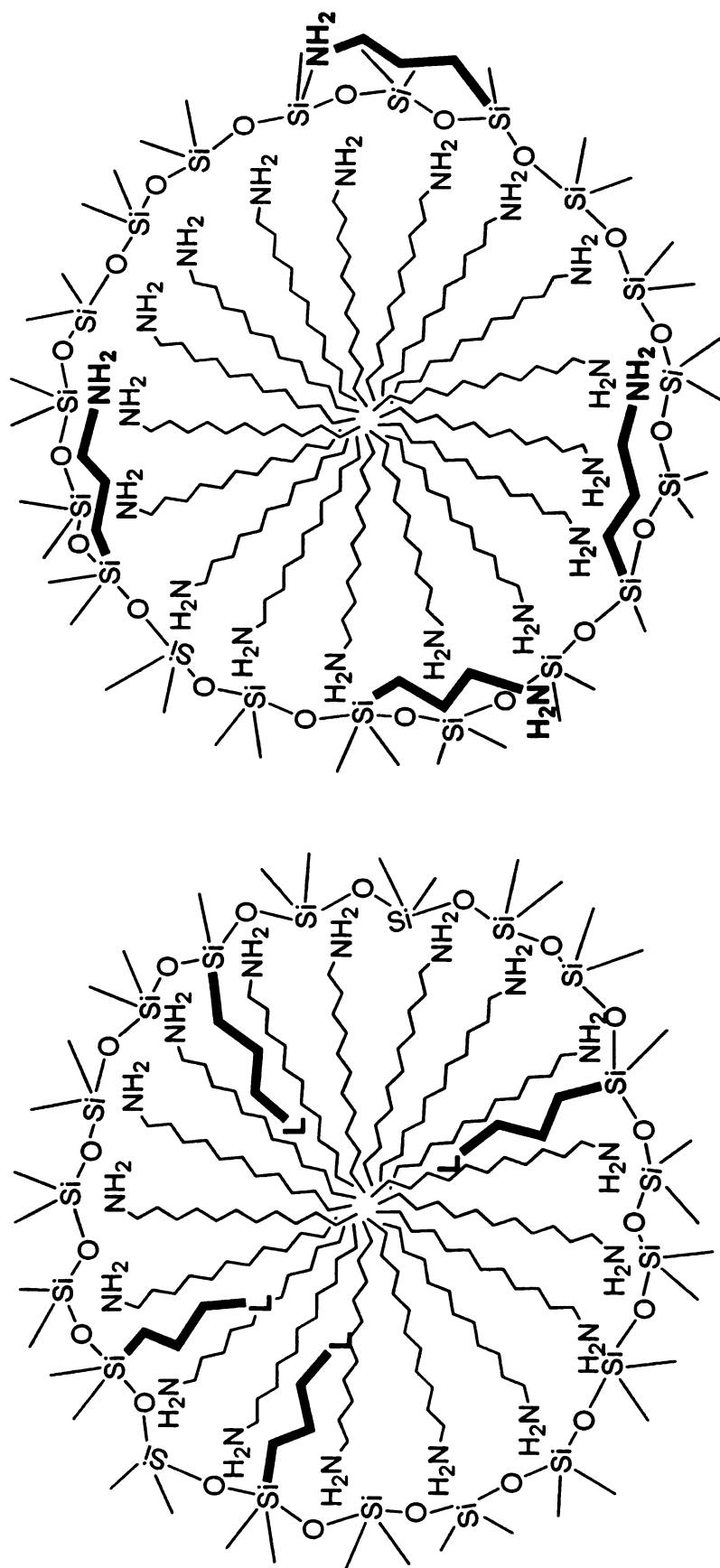
Figure 3.3. The possible positions for a hydrophobic mercaptopropyl organic moiety L group (left image) and a hydrophilic aminopropyl group in an as-made silicate mesostructure templated by dodecylamine as a surfactant.

In addition to the assistance provided by an electrostatic interaction between the positively charged amine moiety and the anionic surfactant, more chemistry can be utilized to improve the availability of the amine functional groups in the silicate framework. If the organosilane incorporated into the silica framework is hydrophobic, it will have a less disruptive effect on the formation of the mesostructure. Furthermore, if the hydrophobic group can be later converted into an amino group, a highly ordered mesostructure and better accessibility of the amine groups can be achieved.

In the present work, alternative approaches were used for the co-condensation of TEOS and organosilanes with hydrophobic groups, which later can be converted into amine groups in order to make them more accessible. First, 3-*tert*-butyloxycarbonylaminopropyltriethoxysilane (NH*t*BocTES) was introduced through co-condensation with tetraethyl orthosilicate (TEOS) with a dodecylamine surfactant under neutral pH conditions. The NH*t*Boc group is more hydrophobic compared to an amine group, so it is more likely to orient towards the core of the surfactant micelle, thus forming a better mesostructures. The amine group will be recovered by the subsequent deprotection of the *t*Boc group. Using the deprotection of carbamate groups, which are commonly used as protecting agents for amino groups in synthetic chemistry, earlier workers successfully incorporated amine groups into bulk silica[27] and a SBA-15 mesostructured silica[28] systems. The amine groups were recovered upon the removal of the protecting Boc group by either acidic hydrolysis or thermal treatment. However, the synthesis condition for SBA-15 is acidic at the very beginning, so the protecting groups may already be removed partially prior to mesostructure assembly. This work will use

dodecylamine surfactant under neutral pH condition in order to keep the Boc protected amine groups intact during mesostructure synthesis via the co-condensation method.

Secondly, an amine-functionalized mesostructured silica will be synthesized via the co-condensation of tetraethyl orthosilicate (TEOS) and 4-(Triethoxysilyl)butyronitrile (CNTES) with surfactant dodecylamine under neutral pH conditions. A nitrile group is much more hydrophobic compared to an amine group, and could point towards the core of the surfactant micelle to form more accessible organic groups. It has been successfully incorporated into the mesostructure by co-condensation method. A CN-functionalized MCM-41 showed much higher pore volume and surface area than the amine containing functionalized counterparts.[29] CN functionalized SBA-15 also showed good mesostructure orderness.[6,30,31] It was suggested that the disruptive effects on the formation of a mesostructure was much smaller for a nitrile organosilane than an amino organosilane.[21] Moreover, the amine group can be formed through a reduction process after the nitrile been successfully incorporated into the mesostructure framework.

More accessible amine groups were expected to be obtained by these two novel alternative amine incorporation routes. The resultant materials will be tested for the lead trapping capacities in the comparison with the HMS-NH$_2$ obtained by conventional direct co-condensation of TEOS and the amine organosilane APTES.

3.2 Experimental methods

3.2.1 Reagents

Dodecylamine (DDA), tetraethyl orthosilicate (TEOS), aminopropyltriethoxysilane (APTES), 4-(Triethoxysilyl)butyronitrile (CNTES), concentrated HCl solution, CH_2Cl_2, Et_3N, lead atomic absorption standard solution (~1000 ppm), and 99.999% lead nitrate were purchased from Aldrich. 3-*tert*-butyloxycarbonylaminopropyltriethoxysilane (NH*t*BocTES) (shown in Figure 3.4) was purchased from Gelest. Ethanol was purchased in-house. All the reagents were used without further purification. Water used in the synthesis was double-exchanged to remove cations and anions via a Millipore filter apparatus.
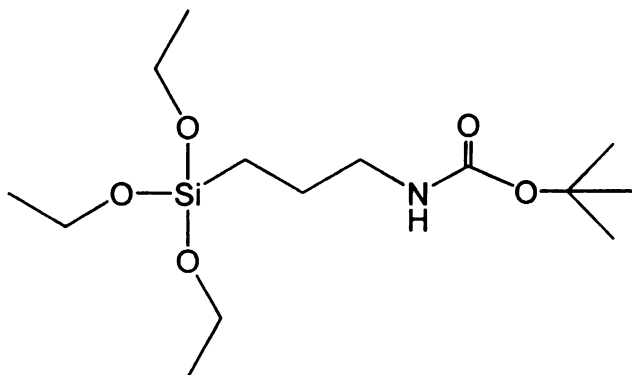
Figure 3.4. Chemical structure of butyloxycarbonylaminopropyltriethoxysilane (NH*t*BocTES).

3.2.2 Material synthesis

3.2.2.1 Synthesis of HMS-NHtBoc and HMS-NH2 (Boc) materials

*t*Boc protected amine functionalized mesostructured HMS organosilica was synthesized from tetraethyl orthosilicate (TEOS) and 3-*tert*-butyloxycarbonylaminopropyltriethoxysilane (NH*t*BocTES) using the direct assembly

82

method in the presence of dodecylamine (DDA) as the surfactant. In a typical co-condensation reaction, the desired amount of DDA was dissolve in ethanol and water co-solvent to get homogeneous solution. The mixture of TEOS and NHtBocTES was added to the surfactant solution, followed by aging the mixture at 60 °C for 24 hr. The products were recovered by filtration and dried in an 80 °C oven overnight. The surfactant template was removed by solvent extraction using a solid to ethanol ratio of 1 g to 50 mL. The extraction step was repeated and the final products were dried in the 80°C oven to remove any excess ethanol. The overall molar composition of the reaction mixture was x: (1-x): 0.25: 20: 180 NHtBocTES: TEOS: DDA: EtOH: H$_2$O, where x represents the mole fraction of silicon centers containing the Boc protected amine group. The expected molecular formula for the organosilica products was $(SiO_2)_{1-x}(SiO_{1.5}C_3H_6NHtBoc)_x$, where x equals to 0.10 and 0.20. The final products were denoted x HMS-NHtBoc, where x represents the mol fraction of silicon centers containing the Boc protected amine groups.

For the recovered amine functionalized HMS silica materials, 1.5 g of HMS-NHtBoc was dispersed in 40 mL 6 M HCl solution in a round bottle flask. The mixture was heated at 100°C overnight. The solid was filtered, washed with water, and dried in an 80°C oven completely. The dry solid was introduced in 30 mL of Et$_3$N/CH$_2$Cl$_2$ mixture (1:5 volume ratio of Et$_3$N to CH$_2$Cl$_2$) to deprotonate the amine groups. The final product was recovered by filtration and was dried in an oven overnight. It was denoted x HMS-NH$_2$ (Boc), where x represents the mol fraction of silicon centers containing the re-generated amine groups.

3.2.2.2 Synthesis of HMS-CN and HMS-NH2 (CN) materials

A nitrile functionalized mesostructured HMS organosilica was synthesized from tetraethyl orthosilicate (TEOS) and 4-(Triethoxysilyl)butyronitrile (CNTES) using the direct assembly method in the presence of dodecylamine (DDA) as the surfactant. The methods used for the synthesis were analogous to those provided in section 3.2.2.1 for the synthesis of HMS-NHtBoc. The resultant material was denoted x HMS-CN, where x = 10% or 20%, denoting the percentage of framework silicon centers that are organo-functionalized.

For the amine functionalized HMS silica materials, CN-HMS was dispersed in THF solution containing lithium aluminum hydride (LAH) as the reducing agents. The reaction was run at room temperature under N_2 protection for 4 hr followed by a HCl solution work-up. A Et_3N/CH_2Cl_2 mixture was used to remove the acidic proton on the protonated amine group. The final product was denoted x HMS-NH$_2$ (CN) indicating the amine groups were obtained by reduction of the nitrile groups, where x equals to 10 or 20 mol%.

A conventional direct co-condensation of TEOS and aminopropyl (APTES) was also carried out at x equals to 20mol % for comparison purposes. The product was denoted 20 % HMS-NH$_2$ (conv.).

3.2.3 Pb^{2+} trapping experiments

The adsorption experiment was carried out for metal lead by stirring 0.1 g of functionalized silica material in 100 mL of lead nitrate ($Pb(NO_3)_2$) solution at 25°C. The initial concentration for these experiments was 100 ppm in all cases. Mixtures were

stirred for 24 hours and then filtered through a 0.25 μm filter paper to collect the final filtrate solution.

The amount of lead in the filtrate after adsorption experiments was analyzed by cold vapor atomic absorption spectroscopy (AAS). And the difference between the initial and equilibrium lead concentrations indicates the amount of lead that was trapped on the solid adsorbents.

3.2.4 Characterization

X-ray diffraction (XRD) patterns were obtained on a Rigaku Rotaflex 200B diffractometer equipped with Cu K_α X-ray radiation and a curved crystal graphite monochromator operating at 45 kV and 100 mA.

N_2 adsorption-desorption isotherms were obtained at $- 196$ °C on a Micromeretics Tristar 3000 sorptometer using standard procedures. Samples were outgassed at 150 °C and 10^{-6} Torr for a minimum of 12 hr. prior to analysis. Surface areas were calculated from the linear part of a BET plot of the nitrogen adsorption data according to IUPAC recommendations. The Barrett-Joyner-Halenda (BJH) method was used to obtain the pore size distribution from the adsorption branch of the isotherms.

^{29}Si MAS NMR and ^{13}C CP MAS NMR spectra were recorded on a Varian 400 solid state NMR spectrometer with a Zirconia rotor at a spinning frequency of 4 kHz. ^{29}Si MAS NMR spectra were obtained at 79.5 MHz under single-pulse mode and a pulse delay of 400 seconds. ^{13}C CP MAS NMR spectra were recorded at 100.5 MHz under cross polarization mode with a pulse delay of 2 seconds and contact time of 1.3 ms.

Fourier transform infrared spectroscopy was used to identify the functional groups in the samples. Spectra were recorded with a Mattson Galaxy series 3000 equipment between 400 and 4000 cm^{-1} using KBr pellets.

Transmission electron microscopy (TEM) images were taken on a JEOL 2200FS microscope with filed emission electron source and an accelerating voltage of 200 keV. Sample grids of mesoporous silicas were prepared by sonicating the powdered sample in EtOH for 10 min and evaporating 2 drops of the suspension onto a holey carbon-coated film supported on 300 mesh copper grids.

Equilibrium concentrations of Pb^{2+} in solution were measured on a cold vapor atomic absorption spectroscopy Varian SpectrAA-200 using lead cathode with maximum working current of 10 mA.

3.3 Results and discussion

3.3.1 Synthesis of mesostructure HMS-NHtBoc and HMS-NH2 (Boc) materials

The butyloxycarbonyl-protected amine group (–NH/Boc) has hydrophobic properties and can be converted into amino groups through Boc group deprotection.[27,28] Also the Boc group is relatively large and has a size similar to a silica tetrahedron. Therefore, it is less likely to be buried in the walls of the silica framework and to form a better mesostructure by direct assembly method in comparison with the direct co-condensation of TEOS and APTES. Accordingly, 10 and 20 mol % of butyloxycarbonylaminopropyltriethoxysilane (NH/BocTES) was incorporated into the mesostructured silica by co-condensation reaction with TEOS in the presence of dodecylamine as surfactant at a reaction temperature of 60 °C. The resulting mesostructure was expected to survive the Boc deprotection process.

As is evident from the TEM images (Fig.3.5A), a wormhole mesostructure was successfully synthesized by the co-condensation of a Boc protected amine moiety and TEOS. The product after Boc deprotection still retained the wormhole structure according to Figure 3.5B. The pore size in the recovered amine functionalized mesostructured HMS silica appeared somewhat larger than that of the Boc protected amine functionalized derivative based on the TEM images. The accurate pore sizes will be determined from the N2 adsorption-desorption data.
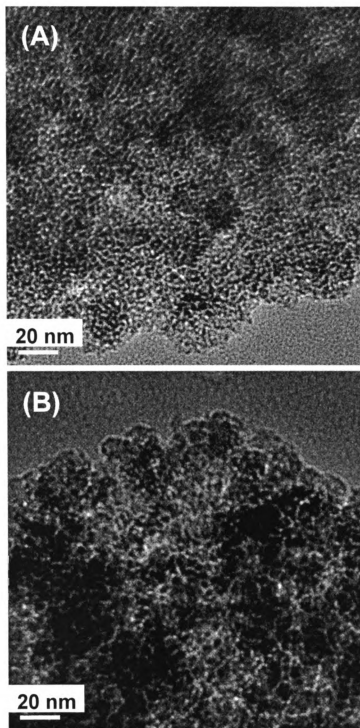
Figure 3.5. Transmission electron microscopy (TEM) images of (A) Boc-protected amine functionalized mesostructured silica, 20% HMS-NH*t*Boc and (B) the recovered amine functionalized mesostructured material after Boc deprotection, 20% HMS-NH$_2$ (Boc).

Figure 3.6 provides the powder XRD patterns for the NH*t*Boc functionalized HMS silicas and the amine derivatives after the removal of the protecting groups. The products containing 10 mol or 20 mol % NH*t*Boc groups showed a single X-ray diffraction at 2θ around $2.0°$, indicating the presence of a wormhole framework (Fig. 3.6). After the Boc group deprotection process, the HMS-NH$_2$ (Boc) materials also showed a single diffraction at low angle without any broadening of the peaks, suggesting that the wormhole mesostructure was well maintained. The d spacing of the functionalized mesostructure silica calculated from the 2θ values remained the same, 4.4 nm for 10mol % functionality and 4.7 nm for 20 mol % functionality samples, prior to and upon the removal of the *t*Boc protecting groups, indicating that the deprotection process did not affect the overall framework order. The XRD patterns agree with the observation in the TEM images.

Figure 3.7 reports the N$_2$ adsorption-desorption isotherms and Barrett-Joyner-Halenda (BJH) framework pore size distributions of the HMS-NH*t*Boc and HMS-NH$_2$ (Boc) mesostructured organosilicas. Table 3.1 lists the d spacing, surface area, average framework pore size and pore volume for each product. The 10 and 20% HMS-NH*t*Boc derivatives and the 20% HMS-NH$_2$ (CN) products showed steep N$_2$ uptake in the P/P$_0$ region of 0.2, suggesting the pore size for these three materials are more towards the micropore range. The 10% HMS-NH$_2$ (Boc) from showed steep N$_2$ uptake in the P/P$_0$ region of 0.3-0.4, suggesting the pore size of this material to be close to the mesopore range. The pore size for 10 and 20% HMS-NH*t*Boc materials are 1.2 and 1.5 nm, while values of 1.5 and 1.8 nm are obtained for 10 and 20% HMS-NH$_2$ (Boc), respectively. The pore size decreased from 1.5 nm to 1.2 nm, while increasing the NH*t*Boc loading from

10% to 20%. This is because the introduction of the hydrophobic NHtBoc groups will occupy space inside the mesopores, causing the pore size to decrease. HMS-NH$_2$ (Boc) materials have a pore size 0.3 nm larger than the HMS-NHtBoc materials for both 10 and 20 mol % amine loadings due to the removal of the bulky *tert*-Boc groups. As the functional group loading is increased, the surface area and pore volume decreases. This is a common result for directly assembled functionalized mesostructured materials, due to pore congestion by the organic moieties. Moreover, the total volume and BET surface area of HMS-NH$_2$ (Boc) were comparable to the counterparts before the Boc deprotection process. Take 20 % functionalized HMS materials, for example. The 20 % HMS-NHtBoc derivative has a pore volume of 0.97 cm^3 g^{-1} and a surface area of 573 m^2 g^{-1} while values for the 20% HMS-NH$_2$ (Boc) are 0.95 cm^3 g^{-1} and 567 m^2 g^{-1}, respectively.

The physical properties of the 20 mol % HMS-NH$_2$ (conv.) which was synthesized by the conventional direct co-condensation of TEOS and APTES directly are also listed in Table 3.1. This derivative showed no X-ray diffraction and a very broad pore size distribution. The pore volume and surface area were only 0.60 cm^3 g^{-1} and 99 m^2 g^{-1}. While for the 20mol % HMS-NH$_2$ (Boc) synthesized by the Boc protection pathway, the material showed d spacing of 4.7 nm, a pore size diameter of 1.2 nm, a BET surface area of 573 m^2 g^{-1} and a total pore volume of 0.97 cm^3 g^{-1}.
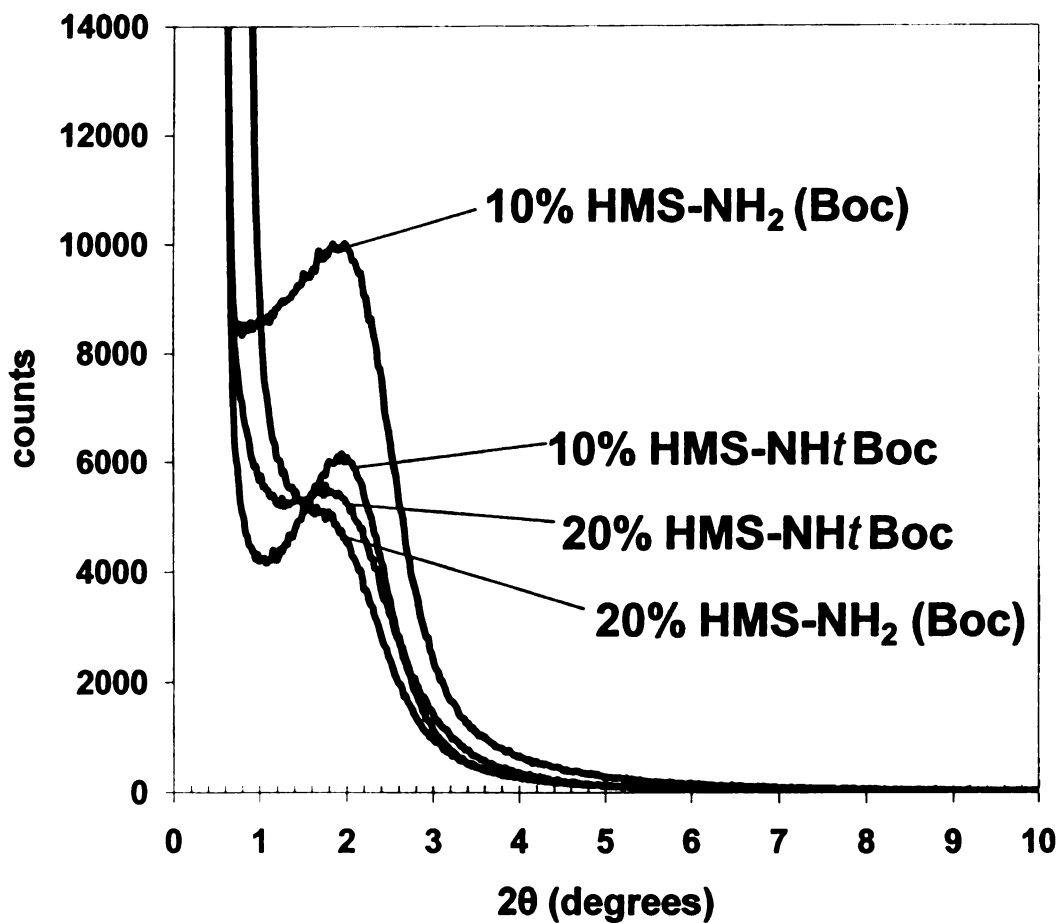
Figure 3.6. X-ray diffraction patterns of amino functionalized HMS mesostructured silicas before and after the deprotection of tBoc groups at different organosilane loadings of 10 mol % and 20 mol %.
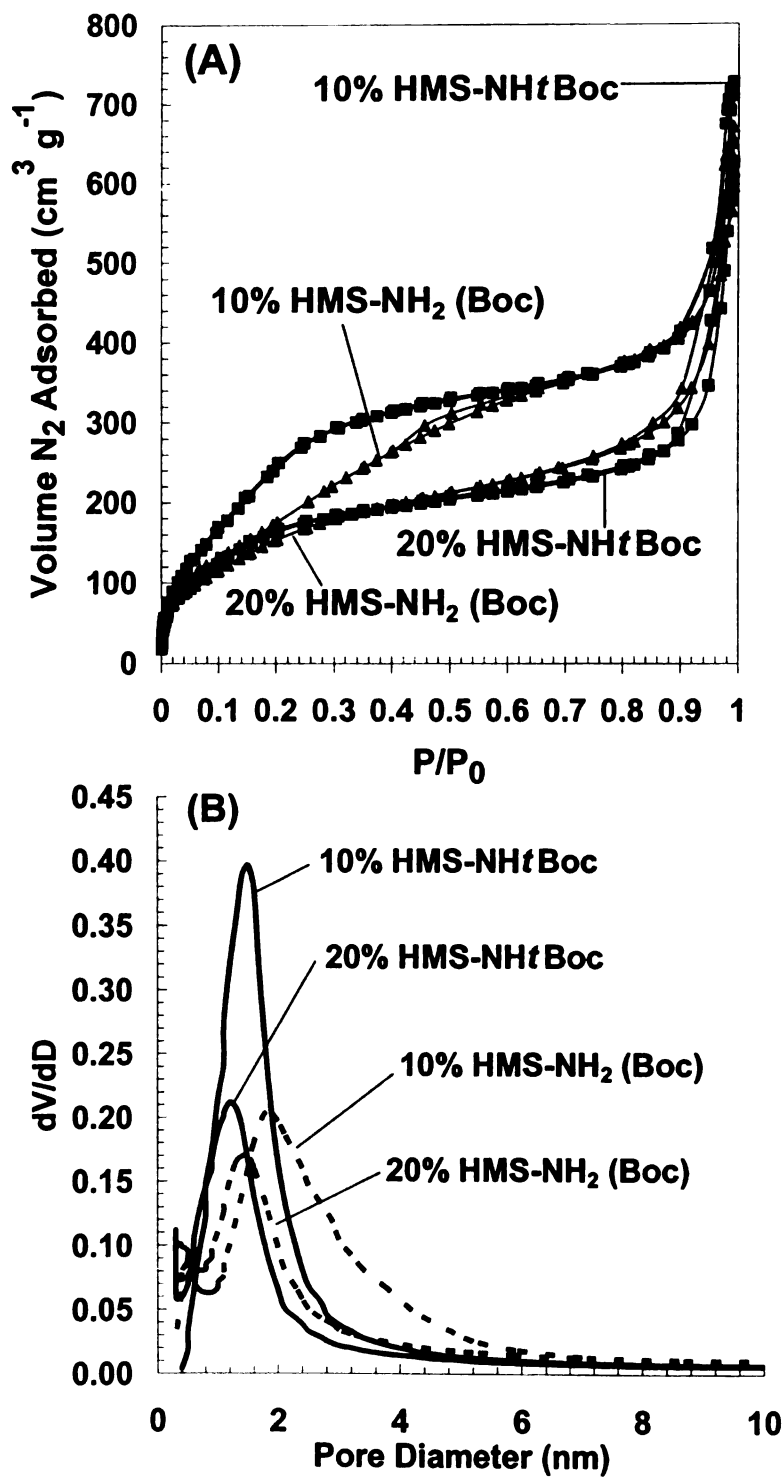
Figure 3.7. (A) N_2 adsorption-desorption isotherms and (B) BJH pore size distributions for mesoporous amino-functional HMS wormhole silicas (10 and 20 % NH_2 groups) before and after the deprotection of the tBoc groups.

Table 3.1. Physical properties of Boc protected amine functionalized mesostructured silica (HMS-NHtBoc), the recovered amine functionalized mesostructured silica (HMS-NH$_2$ (Boc)) and conventionally assembled amine functionalized silica (HMS-NH$_2$ (conv.)) synthesized with a dodecylamine porogen.

	d spacing (nm)	Pore size [a] (nm)	Total volume [b] (cm^3 g^{-1})	BET surface area (m^2 g^{-1})
10%HMS-NHtBoc	4.4	1.5	1.13	948
10%HMS-NH$_2$ (Boc)	4.4	1.8	1.04	713
20%HMS-NHtBoc	4.7	1.2	0.97	573
20%HMS-NH$_2$ (Boc)	4.7	1.5	0.95	567
20%HMS-NH$_2$ (conv.)	no peak	2.2	0.60	99

[a] Pore size diameter was determined from the BJH model and the adsorption branches of the isotherms. [b] Total pore volume was determined at P/P$_0$=0.98.

Figure 3.8 shows the complete conversion from –NHtBoc groups to –NH$_2$ groups, as judged by FT-IR spectroscopic study. In Figure 3.8A, the absorbance around 1700 cm^{-1} is from the carbon-oxygen stretching frequency for the –C=O in the Boc group. The absorbances around 2987 and 2950 cm^{-1} are the characteristic peaks for the C-H stretching modes in the t-Butyl groups of the Boc group, and the 1370 cm^{-1} absorbance is the C-H bending from the t-Butyl groups of the Boc groups. After Boc removal, the FT-IR spectrum of the amino functionalized mesostructured silica, denoted HMS-NH$_2$ (Boc), showed no absorbance characteristic from Boc groups, indicating that the removal of Boc group was successful and complete (Fig. 3.8B). The calcined mesostructured HMS silica is also shown in Fig. 3.8C for comparison. The spectrum in Fig. 3.8B is very similar to the spectrum in Fig. 3.8C except for absorbance around 2950 cm^{-1} indicating the alkane C-H stretching, and the 1540 cm^{-1} band indicating the N-H bending frequency.

The ^{13}C cross polarization MAS NMR spectrum for HMS-NHtBoc showed the presence of a carbonyl group (-C=O) around 154 ppm, methyl groups around 24 ppm and the tertiary carbon around 75 ppm from *tert*-Butyl groups, indicating that the –NHtBoc functional groups were successfully incorporated into the silica material (Fig. 3.9). After the deprotection of tBoc group, only the alkyl carbons from aminopropyl groups were observed, further proving that the removal of Boc is complete and the conversion to NH$_2$ is successful. The resonance at 54 ppm is attributed to the methylene carbon of an ethoxy group most likely originating from the ethanol used to remove the surfactant. The resonance from methyl carbon of the ethoxy groups which should be around 18 ppm was not distinguishable due to other peaks present in that region.
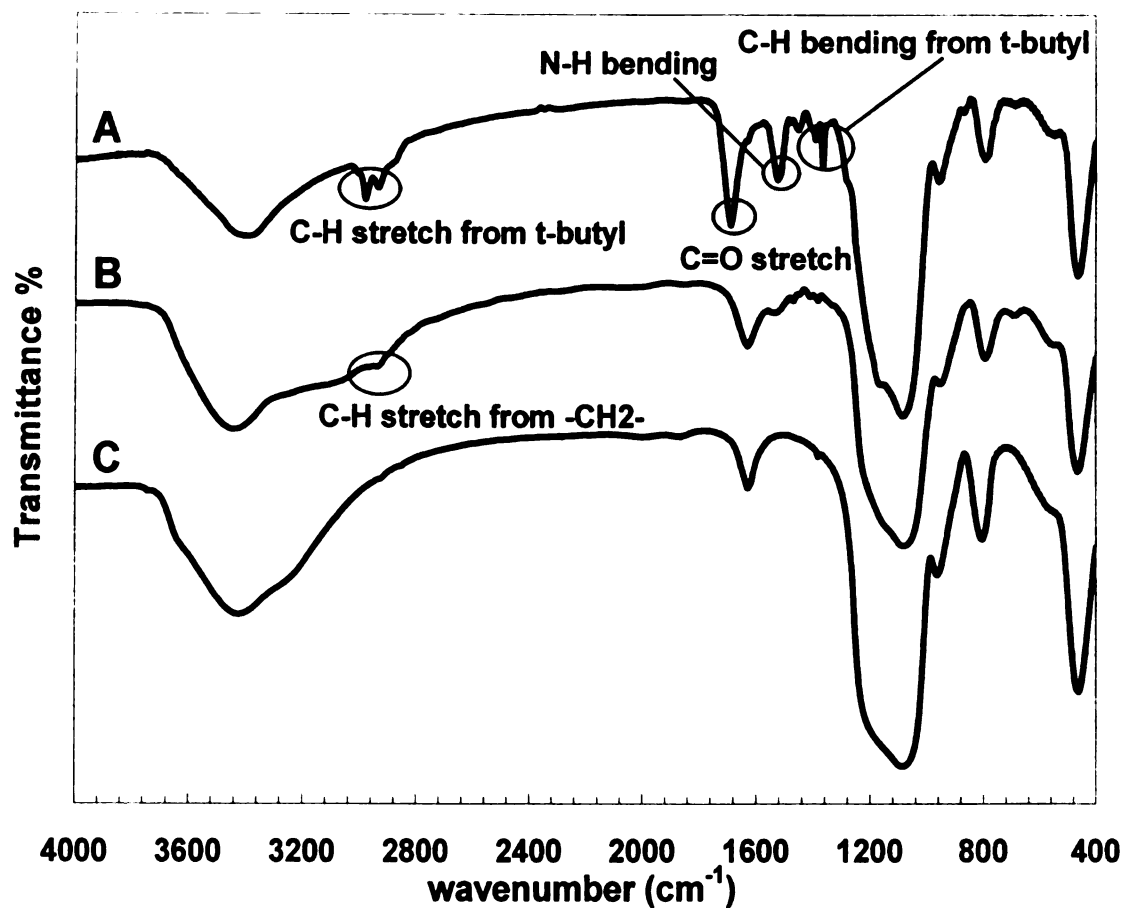
Figure 3.8. FT-IR spectra of (A) 20 mol % HMS-NH*t*Boc before the Boc group deprotection, (B) 20 mol % HMS-NH₂ (Boc) after the deprotection and (C) calcined HMS containing no organic groups.
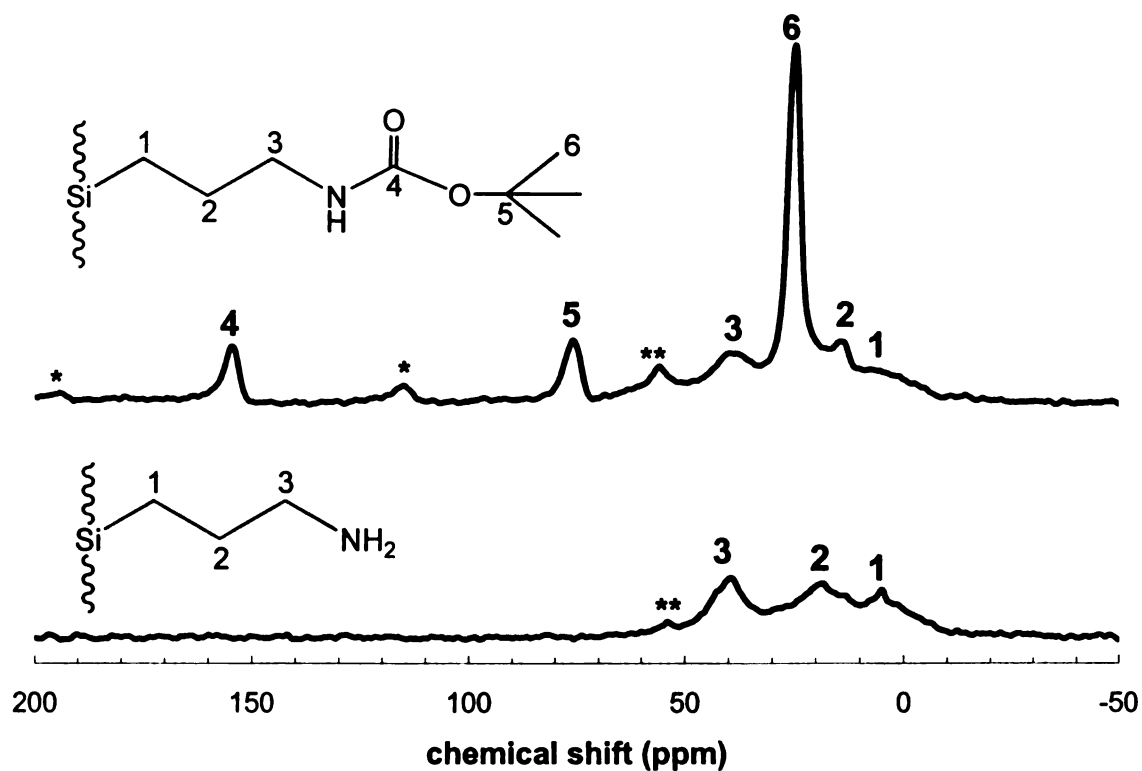
Figure 3.9. ^{13}C CP-MAS NMR spectra of the mesostructure organosilicas 20 mol % HMS-NH*t*Boc and 20 mol % HMS-NH₂ (Boc).

* Side bands in the MAS NMR spectra.

** These two peaks are attributed to residual either ethoxy groups from the solvent ethanol used for extraction of the surfactant.

The HMS-NHtBoc and HMS-NH$_2$ derivatives showed no significant difference on the ^{29}Si MAS NMR spectra, both having three peaks prior to and after the removal of the Boc groups (Figure 3.10). The one around -110 ppm is the Q^4 band which indicates the complete crosslink of SiO$_4$ units. The -100 ppm peak is Q^3, demonstrating the silica center with three oxygens bridging to another tetrahedral silica center and a silanol group. The T^3 band around -70 ppm indicates the silicon centers which have been functionalized by organic groups (existence of Si-C bond). The 20 mol % HMS-NHtBoc product showed 13% organo-functionalization based on the integral intensity of the area beneath the T^3 band. The relative intensity remained the same after the removal of tBoc group for the 20 mol % HMS-NH$_2$ (Boc) material. The similarity in ^{29}Si MAS NMR spectra for the HMS-NHtBoc and HMS-NH$_2$ materials suggested that the silica framework was not changed during the removal of Boc protecting groups.

As expected, the Boc-protected, amine-functionalized mesostructured HMS silica was successfully synthesized due to the hydrophobicity of the bulky tBoc groups. Moreover, the mesostructure was retained after the removal of Boc protecting groups and the amine functionalized mesostructured synthesized by this alternative route showed a better quality mesostructure in comparison with the derivative synthesized by the conventional co-condensation of TEOS and APTES. The accessibility of the recovered amine groups will be investigated by heavy metal ion trapping experiments and reported later this chapter.

The Boc protected amine moiety has only been incorporated previously into SBA-15 mesostructured silica system as reported in the literature.[28] This work was repeated at 20% organic moiety loading to obtain 20% SBA-NHtBoc and 20% SBA-NH$_2$ (Boc)

materials. Neither material showed characteristic peaks for the hexagonal arrayed mesostructure in the XRD patterns. This might because the synthesis conditions for SBA-15 co-condensation are very acidic, though not as strongly acidic as the acidic hydrolysis conditions used to deprotect the Boc groups. Nevertheless, the Boc protected amine organic groups do not appear to completely stable during the direct assembly process. Thus, it will have unprotected amine groups, same as the direct co-condensation of TEOS and APTES. Therefore, the Boc protecting groups may not function as expected in the SBA-15 system. The accessibility of the amine groups on the 20% SBA-NH$_2$ (Boc) materials will be studied in the lead trapping experiment described below.
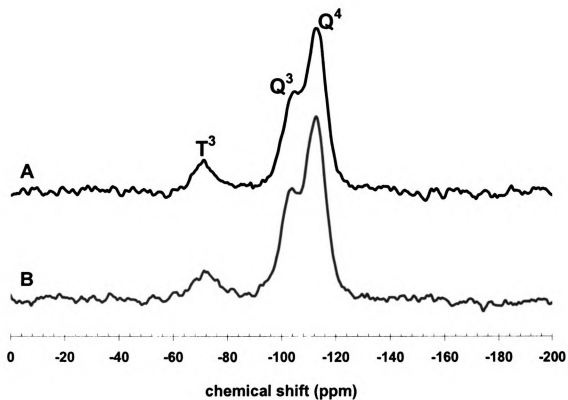
Figure 3.10. ^{29}Si MAS NMR spectra of (A) the mesostructured organosilica 20 mol % HMS-NHtBoc and (B) 20 mol % HMS-NH$_2$ (Boc).

3.3.2 Synthesis of mesostructured HMS-CN and HMS-NH₂ (CN) materials

The hydrophobic nitrile group has been previously incorporated into a silica mesostructure by the co-condensation method. CN-functionalized MCM-41 showed a much higher pore volume and surface area than the amine-containing functionalized counterparts.[29] CN-functionalized SBA-15 also showed good mesostructure order.[6,30,31] It was suggested that the disruptive effects on the formation of the mesostructure was much smaller for the nitrile organosilane than the amino organosilane.[21] Moreover, the CN group has the potential to be converted to an amine groups through reduction process after been successfully incorporated into the mesostructure framework. Accordingly, 4-(triethoxysilyl)butyronitrile (CNTES) was co-condensed with TEOS to make an organo-functionalized mesostructure silica, denoted HMS-CN. Then, lithium aluminum hydride (LAH) was used to reduce the nitrile group to an amine groups. This alternative route was chosen due to the difficulty to make amino-functionalized mesostructure by the direct assembly pathway.

X-Ray diffraction patterns were measured for 10 and 20 mol % HMS-CN mesostructure silicas and the counterparts obtained after the nitrile reduction to HMS-NH₂ (CN) materials. In all cases, a single reflection was observed and centered at 2θ of $2°$ (Fig. 3.11), indicating the successful formation of a wormhole HMS mesostructure with nitrile functionalization and a well retained mesostructure after nitrile reduction. However, the intensity of the reflection decreased after the nitrile reduction. The d spacing for 10% HMS-CN and HMS-NH₂ (CN) are both 4.5 nm, and the value for the 20 % functionality forms are both 4.2 nm. This indicates that the long term ordering of the mesostructures was maintained after the reduction from nitrile to amine groups.
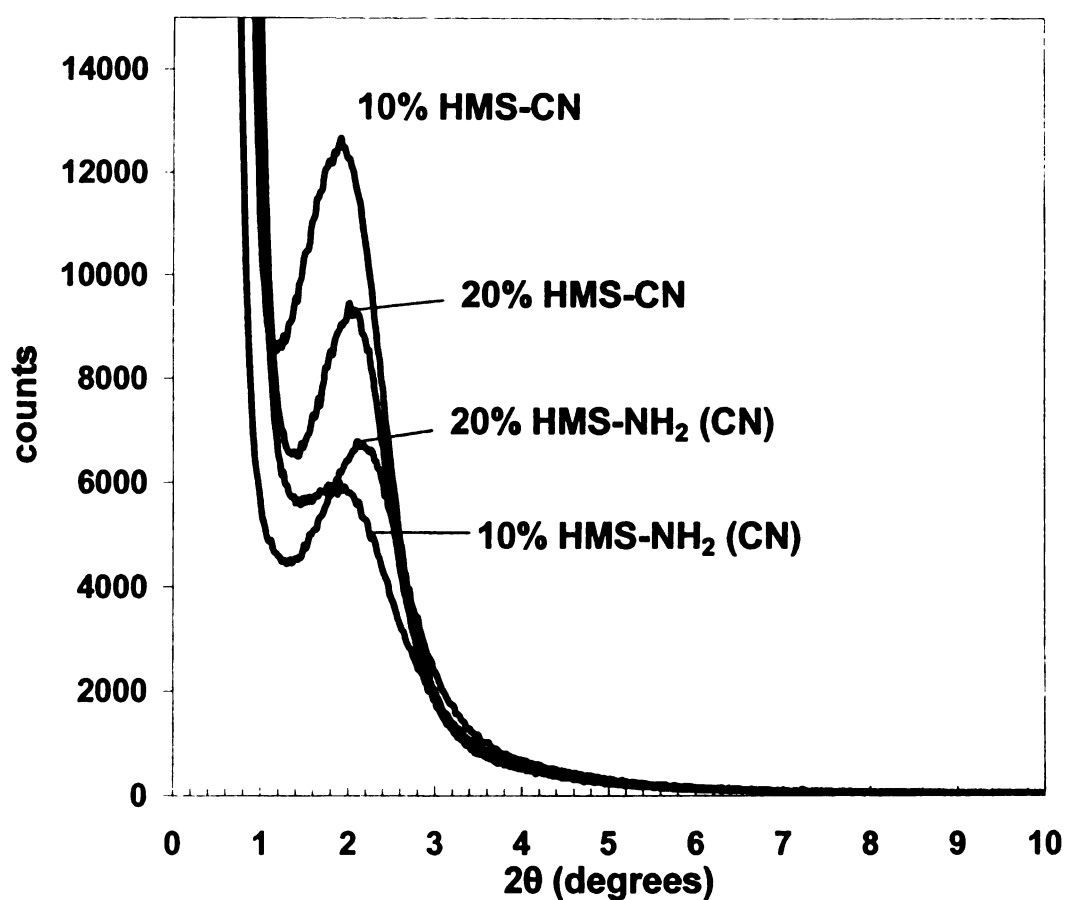
Figure 3.11. X-ray diffraction patterns of amino-functionalized HMS mesostructured silicas before and after the reduction of CN groups to NH_2 groups at different organosilane loadings of 10 mol % and 20 mol %.

The results of the N_2 adsorption-desorption isotherms and the pore size distributions obtained from the adsorption branch are shown in Figure 3.12. The physical properties of the organofunctionalized mesostructured silicas before and after the nitrile reduction are summarized in Table 3.2. The N_2 isotherms for the HMS-CN materials showed an obvious step in the region of relative pressure of 0.2-0.4, indicating that the mesostructure was successfully synthesized. The pore size of HMS-CN decreased from 2.0 nm to 1.6 nm upon increasing the nitrile loading from 10 to 20 mol %. The pore volume and surface area also decreased with increased nitrile loading. Interestingly, after the nitrile reduction process the mesostructure was retained. For instance, the 20 % HMS-NH_2 (CN) mesostructured silica showed pore size of 1.6 nm, a pore volume of 0.70 cm^3 g^{-1} and a surface are of 818 m^2 g^{-1}, which are compatible to the values for 20 % HMS-CN before the nitrile reduction process. The pore size did not change significantly after the nitrile reduction; this might be due to the fact that the total length of the organic group did not change much from butyronitrile to butyl amine conversion. The nitrogen content based on elemental analysis decreased only slightly after the nitrile reduction reaction, suggesting that the majority of the functional group is still incorporated in the silica framework. It is noteworthy that the 20 mol %HMS-NH_2 (conv.), which was made by the conventional co-condensation of TEOS and APTES directly, showed no X-ray diffraction, a broad pore size distribution, a pore volume of 0.60 cm^3 g^{-1} and a surface area of 99 m^2 g^{-1}. In contrast, the 20 mol % HMS-NH_2 (CN) synthesized by the nitrile reduction pathway showed a single X-ray reflection around $2\theta = 2.0°$ (4.2 nm), a narrow pore size distribution with a maximum peak of 1.6 nm, a total pore volume of 0.70 cm^3 g^{-1} and BET surface area of 818 $m^2 g^{-1}$.

The TEM images of functionalized HMS materials before and after the nitrile reduction both showed wormhole structure (Fig. 3.13). This further proves that the structure of functionalized material is retained after the reduction process. The TEM images of amine functionalized HMS silica after nitrile reduction showed less order for the wormhole structure compared with the counterpart before the reduction, which is in agreement with the reduced intensity for the X-ray diffraction pattern and the pore size distribution profile.
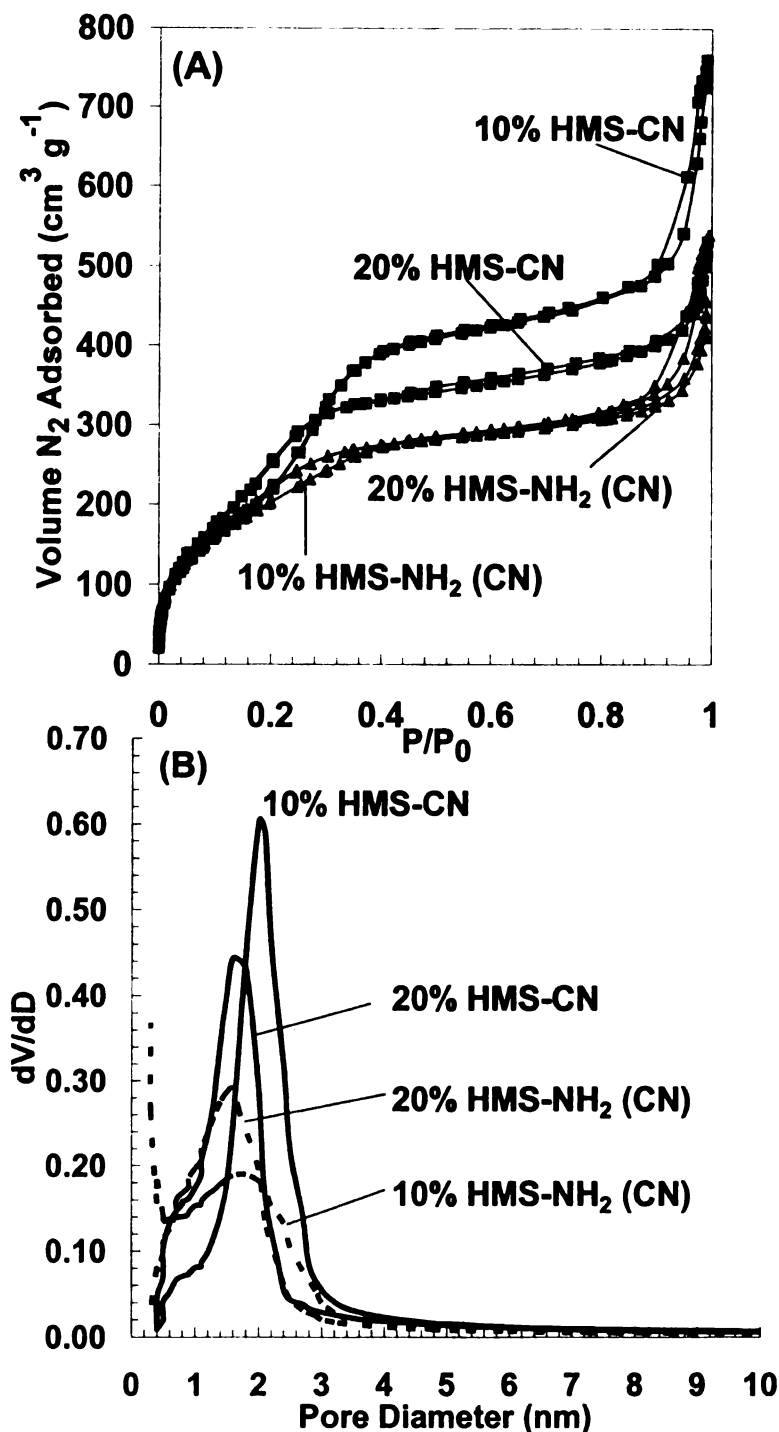
Figure 3.12. (A) N_2 adsorption-desorption isotherms for mesoporous AP-HMS amino-functional silicas (10 and 20 % AP groups) before and after the reduction of CN groups to amine groups. (B) provides the BJH framework pore size distributions obtained from the adsorption branches of the isotherms.

Table 3.2. Physical properties of HMS-CN, HMS-NH$_2$ (CN) and HMS-NH$_2$ (conv.) organosilicas assembled at 60 °C.

	d spacing (nm)	Pore size [a] (nm)	Total volume [b] ($cm^3 g^{-1}$)	BET surface area ($m^2 g^{-1}$)	N content [c] ($mmol g^{-1}$)
10%HMS-CN	4.5	2.0	1.16	1059	1.24
10%HMS-NH$_2$ (CN)	4.5	1.8	0.83	762	1.13
20%HMS-CN	4.2	1.6	0.82	1000	2.29
20%HMS-NH$_2$ (CN)	4.2	1.6	0.70	818	1.83
20%HMS-NH$_2$ (conv.)	no peak	2.2	0.60	99	2.45

[a] Pore diameter was determined by the BJH model from the adsorption branches of the isotherms. [b] Total pore volume was determined at $P/P_0=0.98$. [c] Nitrogen content was calculated from the CHN elemental analysis.

105
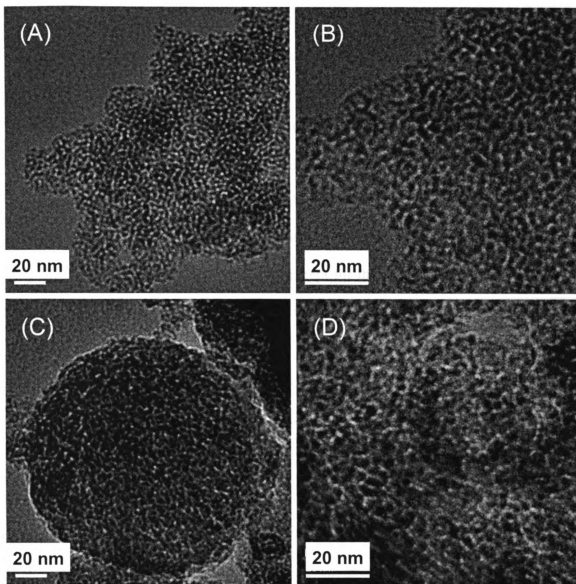
Figure 3.13. Transmission electron microscopy (TEM) images of (A, B) nitrile-functionalized mesostructure silica material, 10 % HMS-CN and (C, D) the recovered amine functionalized mesostructure silica material 10 % HMS-NH$_2$ (CN) at low and high magnification.

Figure 3.14 reports the FT-IR spectra before and after nitrile reduction. In Figure 3.14B, the absorbance around 2260 cm^{-1} is attributed to the carbon nitrogen stretching on the $-C\equiv N$ group. After the nitrile reduction process, the FT-IR spectrum of the amino functionalized mesostructured silica (Fig. 3.14C) shows a very weak absorbance from $-C\equiv N$ groups, indicating that the nitrile reduction process was successful and nearly complete. The pure calcined HMS silica is also shown (Fig. 3.14A) for comparison. The spectrum of the amino-functionalized mesostructured HMS-NH$_2$ (CN) (Fig. 3.14C) was very similar to the spectrum in Fig. 3.14A except for the absorbance around 2950 cm^{-1}, indicating the alkane C-H stretching from the butyl amine group still exists after the reduction.

^{13}C cross polarization MAS NMR spectroscopy was used to analyze the organic groups incorporated onto the silica framework (Fig. 3.15). For the ^{13}C CP MAS NMR spectrum of the 20 mol % HMS-CN sample, the resonance at 118 ppm was attributed to the carbon in -C$\equiv$N group. The small peaks at 160 ppm, 80 ppm, and 40 ppm are the side bands of the triple-bonded carbon resonance. After the reduction of the nitrile group, the C$\equiv$N carbon peak disappeared. The new peak at chemical shift of 38 ppm is attributed to the carbon adjacent to the newly formed amine group, indicating the successful conversion. For both ^{13}C CP NMR spectra, there are two peaks around 58 ppm and 18 ppm, respectively. These two peaks are attributed to carbon species due to either ethoxy groups from either incomplete hydrolysis of TEOS or, more likely, residual ethanol adsorbed in the surfactant removal process.

The complete conversion from nitrile to amine group was proven by the disappearances of the C≡N stretching at 2260 cm^{-1} in the FT-IR spectrum (Fig. 3.14) and the nitrile carbon resonance at 118 ppm in the ^{13}C CP MAS NMR spectrum (Fig. 3.15).
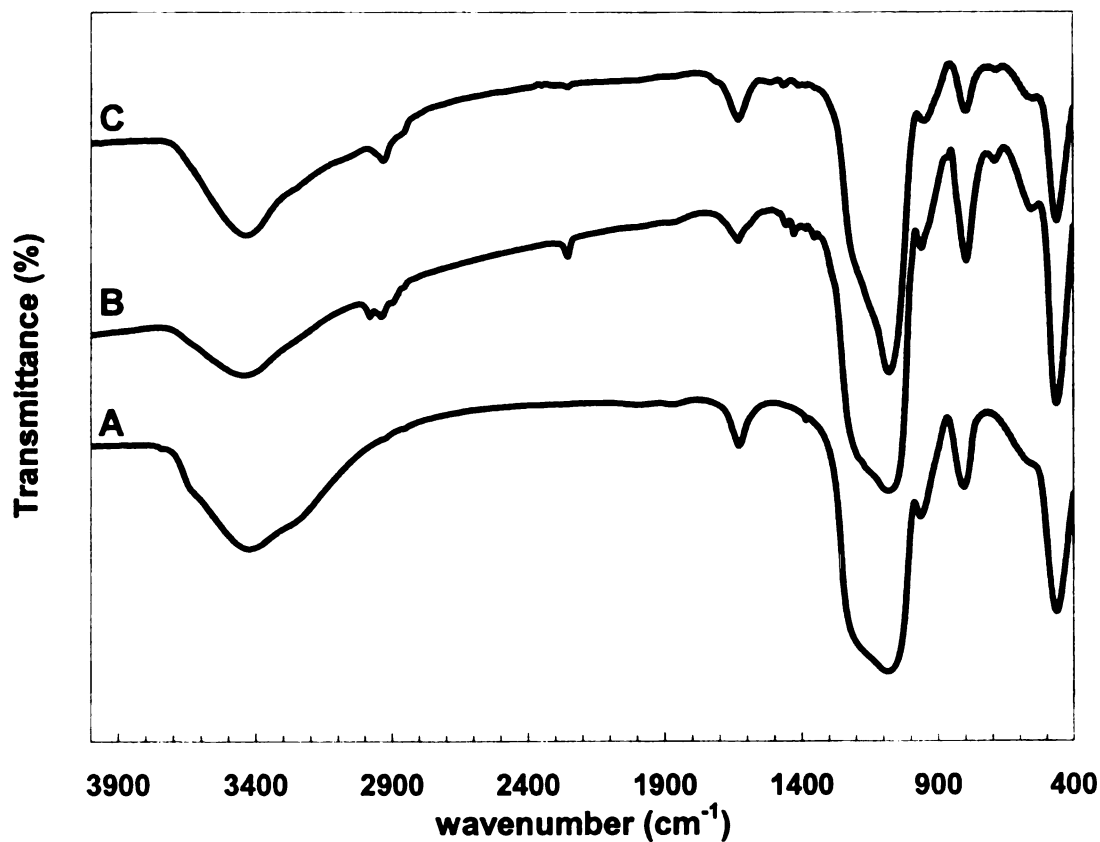
Figure 3.14. FT-IR spectra of (A) calcined mesostructured silica HMS, (B) 20 % HMS-CN, and (C) 20% HMS-NH$_2$ after CN reduction.
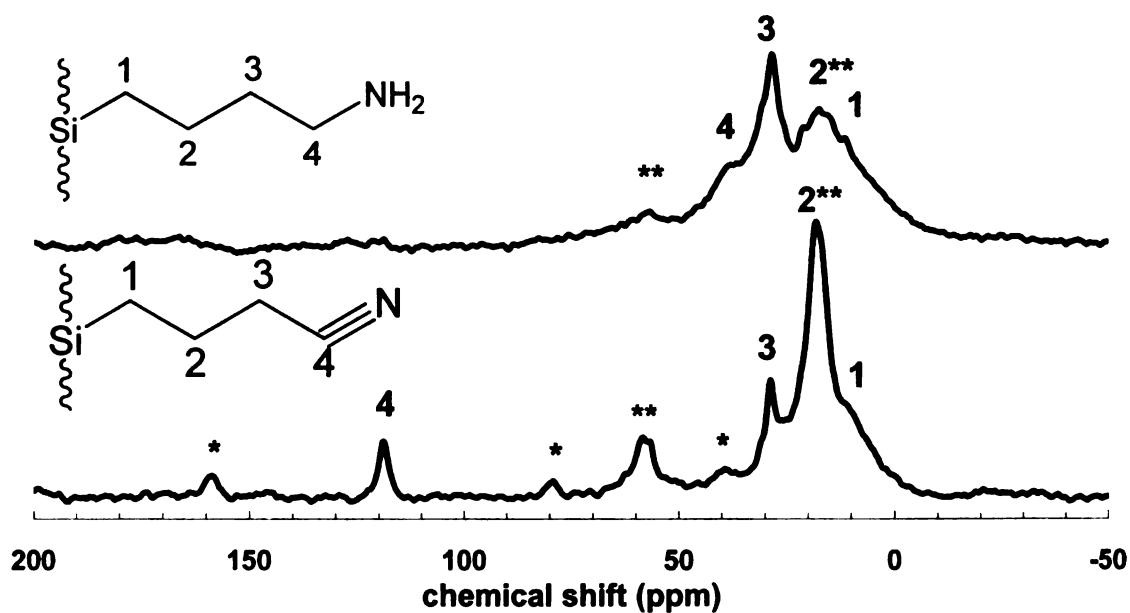
Figure 3.15. ^{13}C CP MAS NMR spectra of 20% HMS-CN and 20% HMS-NH$_2$ (CN) after the reduction of the nitrile group.

* Side bands in the MAS NMR spectra.

** These two peaks are attributed to residual ethanol.

3.3.3 Adsorption performance

Pb^{2+} adsorption on pure HMS silica material is negligible at the 100 ppm level, so the lead adsorption observed for the modified HMS samples should be exclusively attributed to the presence of organic functional groups anchored to the silica walls. The accessibility of the amine groups on the functionalized mesostructured HMS organosilicas synthesized by alternative routes, namely Boc protection and nitrile reduction, were investigated by the heavy metal ion (i.e. Pb^{2+}) adsorption performance. The HMS-NH$_2$ (conv.) material synthesized by conventional co-condensation of TEOS and APTES was also studied for comparison. The results are shown in Table 3.3.

The NHtBoc functionalized HMS mesostructured silica materials (10 mol and 20 mol % HMS-NHtBoc) showed no trapping capacities for lead at all. After the deprotection of tBoc groups, the amine groups were accessible by pointing towards the pore and the recovered amine-functionalized HMS silica materials showed good adsorption performance. The 10 mol % HMS-NH$_2$ (Boc) reduced the lead content from 100 ppm to 30 ppm, having a trapping capacity of 0.34 mmol g^{-1}. The 20 mol % HMS-NH$_2$ (Boc) reduced the lead content from 100 ppm to 0.85 ppm, having a trapping capacity of 0.48 mmol g^{-1}. The latter derivative did not double the capacity of the 10 mol % counterpart even though the nitrogen content was double that of 10 mol% HMS-NH$_2$ (Boc). This is because the equilibrium concentration after the adsorption by 20mol % HMS-NH$_2$ (Boc) was already 0.85 ppm, so the material was not saturated and did not show the maximum trapping capacity. Since the pure HMS silica material and NHtBoc functionalized HMS material showed no trapping capacities under the same experimental

condition, this further proves that the conversion from NHtBoc to NH$_2$ group was successful.

The HMS-CN mesostructured silica does not have significant trapping capacities. The counterpart obtained after nitrile reduction, HMS-NH$_2$ (CN), was studied for the trapping of heavy metal ions (i.e. Pb^{2+}). The trapping capacity increased slightly from 0.23 mmol g^{-1} for 10 % HMS-NH$_2$ (CN) to 0.26 mmol g^{-1} for 20 % HMS-NH$_2$ (CN), even though the nitrogen content in those materials increased significantly from 1.13 mmol g^{-1} to 1.83 mmol g^{-1}. The HMS-NH$_2$ (CN) organosilica showed a lower adsorption capacity compared with HMS-NH$_2$ (Boc), due to the lower nitrogen content in the adsorbent. This reduction in nitrogen content might be caused by the cleavage of organic moiety during the relative strong reduction condition.

Conventional 20% HMS-NH$_2$ (conv.) also was tested for the lead trapping experiment. This mesophase has a trapping capacity of 0.17 mmol g^{-1}, while the derivatives synthesized by the alternative routes have trapping capacities of 0.48 mmol g^{-1} for the Boc protection method and 0.26 mmol g^{-1} for the nitrile reduction method.

The nitrogen to adsorbed lead ratio was calculated for the studied materials to quantify the accessibility of the amino groups. The N/Pb ratio for 20% HMS-NH$_2$ (conv.) is 14, while the ratios for 20% HMS-NH$_2$ (Boc) and 20% HMS-NH$_2$ (CN) are 4.9 and 7.0, respectively. It is clear that the availability of nitrogen is improved by using the amine group protection and nitrile reduction method as alternative synthesis routes.

The Corriu group has made the effort on SBA-15 silica materials by using the Boc protection method.[28] A problem might arise for the SBA-15 system, because the synthesis conditions for SBA-15 are acidic, and the deprotection of Boc group is also acidic. Thus,

the amino group may be partially deprotected during the SBA-15 synthesis and the amine groups may not be accessible again. The HMS system, however, only requires neutral synthesis condition, allowing the NHtBoc moiety to remain intact during the co-condensation step. The 20 mol % SBA-15 (Boc) derivative was synthesized and then tested the adsorption performance. This sample showed a trapping capacity of 0.18 mmol g^{-1} with a nitrogen to adsorbed lead ratio of 11, which is similar to the value of 14 observed for 20mol % HMS-NH$_2$ (conv.).

Table 3.3 The lead trapping performance of amine functionalized HMS organosilicas synthesized by the alternative routes and the derivative synthesized by the conventional co-condensation of TEOS and APTES.

	final ppm (ppm)	adsorbed Pb^{2+} (mmol g^{-1})	N content (mmol g^{-1})	N: adsorbed Pb^{2+} ratio	N: total Pb^{2+} ratio
10%HMS-NH$_2$ (Boc)	30	0.34	1.24	3.7	2.6
20%HMS-NH$_2$ (Boc)	0.85	0.48	2.32	4.9	4.8
20%SBA-NH$_2$ (Boc)	63	0.18	1.98	11.0	4.1
10%HMS-NH$_2$ (CN)	53	0.23	1.13	5.0	2.3
20%HMS-NH$_2$ (CN)	46	0.26	1.83	7.0	3.8
20%HMS-NH$_2$ (conv.)	64	0.17	2.45	14.0	5.1

The initial $Pb(NO_3)_2$ concentration was 100 ppm, and 0.1 g of adsorbent was used per 100 mL of Pb^{2+} solution.

3.4 Conclusions

Among the various functional groups incorporated into the mesostructure silicas, the amine group is of greatest interest because of its potential applications in the area of heavy metal ion adsorption, enzyme trapping, and catalysis. Due to the hydrophilicity and hydrogen bonding interaction between the amine group and silica surface, it is hard to incorporate the amino-functional organosilane (APTES) through co-condensation with TEOS.

In the present work, mesoporous amine-functionalized HMS organosilicas have been successfully synthesized via alternative routes. A hydrophobic *t*Boc protected amine group and nitrile group have been successfully incorporated by direct assembly with TEOS in the presence of dodecylamine as a surfactant. The mesostructure obtained showed a much higher structural order in comparison to derivatives synthesized by the conventional direct co-condensation of TEOS and APTES. The amine groups were recovered later on inside the mesopores of organosilica framework. Acidic hydrolysis was used to remove the *t*Boc protecting group, while lithium aluminum hydride (LAH) was used to reduce the nitrile group back to amine group. The improved structures of the amine functionalized organosilica materials were well retained during the removal of *t*Boc groups and the reduction of nitrile groups.

Pb^{2+} trapping experiments were carried out on the resultant amine-functionalized mesostructured HMS organosilicas in order to investigate the accessibility of the amine groups. Both HMS-NH$_2$ (Boc) and HMS-NH$_2$ (CN) materials showed good trapping capacities towards lead species from aqueous solution, having lead trapping capacities of 0.23-0.48 mmol g^{-1}. The N/Pb ratio was calculated on the lead containing adsorbent to

quantify the availability of the amine groups. The amine functionalized mesostructured HMS organosilicas synthesized by the alternative routes showed a low N/Pb ratio of 3.7-7.0 in contrast to the N/Pb ratio of 14 for the derivative synthesized by the direct co-condensation of TEOS and APTES. It suggests that the amine groups obtained by the alternative routes were much less buried in the framework and the accessibility of the amine group is much higher. Therefore, the resultant materials can be served as good heavy metal ion adsorbents.

3.5 References

(1)   Centers for Disease Control and Prevention *Morbidity and Mortality Weekly Report* **2000**, *49*, 1133-1137

(2)   Hoffmann, F.; Cornelius, M.; Morell, J.; Froeba, M. *Angew. Chem. Int. Ed.* **2006**, *45*, 3216-3251.

(3)   Lim, M. H.; Stein, A. *Chem. Mater.* **1999**, *11*, 3285-3295.

(4)   Brown, J.; Mercier, L.; Pinnavaia, T. J. *Chem. Commun.* **1999**, 69-70.

(5)   Kang, T.; Park, Y.; Choi, K.; Lee, J. S.; Yi, J. *J. Mater. Chem.* **2004**, *14*, 1043-1049.

(6)   Yang, C.-m.; Wang, Y.; Zibrowius, B.; Schueth, F. *Phys. Chem. Chem. Phys.* **2004**, *6*, 2461-2467.

(7)   Zhang, X.; Zhang, F.; Chan, K.-Y. *Scripta Mater.* **2004**, *51*, 343-347.

(8)   Wang, Y.; Zibrowius, B.; Yang, C.-m.; Spliethoff, B.; Schueth, F. *Chem. Commun.* **2004**, 46-47.

(9)   Yokoi, T.; Yoshitake, H.; Tatsumi, T. *J. Mater. Chem.* **2004**, *14*, 951-957.

(10)   Mori, Y.; Pinnavaia, T. J. *Chem. Mater.* **2001**, *13*, 2173-2178.

(11)   Shah, J.; Kim, S.-S.; Pinnavaia, T. J. *Chem. Commun.* **2004**, 572-573.

(12)   Mercier, L.; Pinnavaia, T. J. *Adv. Mater.* **1997**, *9*, 500-503.

(13)   Lesaint, C.; Frebault, F.; Delacote, C.; Lebeau, B.; Marichal, C.; Walcarius, A.; Patarin, J. *Stud. Surf. Sci. Catal.* **2005**, *156*, 925-932.

(14)   Etienne, M.; Sayen, S.; Lebeau, B.; Walcarius, A. *Stud. Surf. Sci. Catal.* **2002**, *141*, 615-622.

(15) Yoshitake, H.; Yokoi, T.; Tatsumi, T. *Chem. Mater.* **2003**, *15*, 1713-1721.

(16) Rosenholm, J. M.; Linden, M. *Chem. Mater.* **2007**, *19*, 5023-5034.

(17) Macquarrie, D. J.; Jackson, D. B.; Mdoe, J. E. G.; Clark, J. H. *New J. Chem.* **1999**, *23*, 539-544.

(18) Wang, X.; Lin, K. S. K.; Chan, J. C. C.; Cheng, S. *J. Phys. Chem. B* **2005**, *109*, 1763-1769.

(19) Wang, X.; Chan, J. C. C.; Tseng, Y.-H.; Cheng, S. *Microporous Mesoporous Mater.* **2006**, *95*, 57-65.

(20) Kanan, S. M.; Tze, W. T. Y.; Tripp, C. P. *Langmuir* **2002**, *18*, 6623-6627.

(21) Chong, A. S. M.; Zhao, X. S.; Kustedjo, A. T.; Qiao, S. Z. *Microporous and Mesoporous Mater.* **2004**, *72*, 33-42.

(22) Kim, Y.; Lee, B.; Yi, J. *Sep. Sci. Technol.* **2004**, *39*, 1427-1442.

(23) Bois, L.; Bonhomme, A.; Ribes, A.; Pais, B.; Raffin, G.; Tessier, F. *Colloids Surf., A* **2003**, *221*, 221-230.

(24) Yokoi, T.; Yoshitake, H.; Tatsumi, T. *Chem. Mater.* **2003**, *15*, 4536-4538.

(25) Che, S.; Garcia-Bennett, A. E.; Yokoi, T.; Sakamoto, K.; Kunieda, H.; Terasaki, O.; Tatsumi, T. *Nat. Mater.* **2003**, *2*, 801-805.

(26) Yokoi, T.; Yoshitake, H.; Yamada, T.; Kubota, Y.; Tatsumi, T. *J. Mater. Chem.* **2006**, *16*, 1125-1135.

(27) Bass, J. D.; Katz, A. *Chem. Mater.* **2003**, *15*, 2757-2763.

(28) Mehdi, A.; Reye, C.; Brandes, S.; Guilard, R.; Corriu, R. J. P. *New J. Chem.* **2005**, *29*, 965-968.

(29)   Huh, S.; Wiench, J. W.; Yoo, J.-C.; Pruski, M.; Lin, V. S. Y. *Chem. Mater.* **2003**, *15*, 4247-4256.

(30)   Yang, C.-M.; Zibrowius, B.; Schueth, F. *Chem. Commun.* **2003**, 1772-1773.

(31)   Fiorilli, S.; Onida, B.; Bonelli, B.; Garrone, E. *J. Phys. Chem. B* **2005**, *109*, 16725-16729.

Chapter 4

Alumination of siliceous wormhole mesostructure and its application as heavy metal adsorbents

4.1 Introduction

Microporous aluminosilicate molecular sieves known as zeolites contain regular arrays of uniformly sized channels and admit molecules below a certain critical size into their internal space which makes them useful as heterogeneous catalysts and adsorbents. The discovery of M41S family of mesoporous materials with uniformly sized unidimensional pore structure has widened the applications because of its much higher surface area and larger pore size.[1,2] Ion-exchange, catalytic and adsorptive properties of such molecular sieve materials originate from acid sites which were modified by framework substitution. Modification is usually achieved by incorporation of hetero-atoms, particularly Al atoms, into the otherwise electrically neutral siliceous framework which consequently would have no acid sites.[3] Therefore, a lot of effort has been devoted into the insertion of aluminum sites to the pure mesostructured silicas. Typically aluminum is incorporated into the framework of the silicates by either direct assembly or by post-synthesis methods.

The direct assembly method often requires specialized synthesis conditions depending on the respective structures of the mesoporous materials, and suffers from an undesirable decease in the structure integrity.[4,5] Therefore it is difficult to directly prepare well ordered aluminosilicate mesostructured materials with low Si/Al ratio. Moreover, it was observed that when compared to zeolites, the concentration of the acid sites on the direct assembled mesostructured aluminosilicate materials is low even at high Al

loading.[6,7] It was suggested that the low acidity may be related to the mechanism of formation of the aluminosilicate and to the position occupied by 4-coordinate Al in the framework.[8] A large portion of the Al incorporated in the mesostructured aluminosilicate may be buried in the inorganic framework and is therefore less efficient at generating acid sites.

On the other hand, the incorporation of Al onto preformed mesostructures by post synthesis means is reported to be advantageous with respect to structure ordering and physical stability.[9] Previous studies have shown that aluminum can be incorporated into siliceous MCM-41 materials via post synthesis procedures by using various aluminum sources such as sublimated $AlCl_3$ aqueous solution,[10] $AlCl_3$ non-aqueous solution,[11,12] aluminum isoalkyoxide non-aqueous solution,[13-15] trimethylaluminum in non-aqueous solution,[16,17] aluminum isopropoxide in supercritical fluids,[18] aqueous aluminum chlorhydrate,[19-21], and aqueous sodium aluminate solution[9,22] etc. Alumination of SBA-15 by a post synthesis method has been investigated using different aqueous and nonaqueous aluminum sources.[23-26] The alumination of wormhole mesostructured silica has been explored by Robert Mokaya and William Jones by using $Al(OPr)_3$ in hexane solution as aluminum source.[13] All the references for the alumination of mesostructured silica materials by post synthesis/grafting methods are listed in Table 4.1.

Table 4.1. Summary of the literature work on the alumination of mesostructured silica materials by post synthesis/grafting methods

Author	Parent mesostructure	Al sources	Grafting condition	Application	Si/Al ratio	Al geometry
S. S. Jaenicke[9]	MCM-41	i) AlCl$_3$ in chloroform ii) Al(OPr)$_3$ in isopropoxide solution iii) NaAlO$_2$ solution iv) Al(NO$_3$)$_3$ solution	Reflux 2hr. followed by calcination 60°C stirred 3hr. followed by calcination	Cumene conversion	1.3-6.4 1.3-11.8 3.2 62.7	Td, Oh Td, Oh Td, Oh mainly Td
Michael Hunger[10]	MCM-41	Sublimated AlCl$_3$	sublimation in vacuum 36hr.	NM	NM	Td, Oh
Vasant R. Choudhary[11,12]	MCM-41	AlCl$_3$ in CCl$_4$	Reflux, 1.5hr.	benzylation benzoylation	4.8-16.7	Td, Oh
Robert Mokaya and William Jones[13,15,20]	MCM-41 MMS (wormhole)	Al(OPr)$_3$ in hexane	Rm. temp. 24hr. no stirring followed by calcination	Cumene conversion	6.1-38.5 11.2	Td, Oh
M. V. Landau[14]	MCM-41	Al(OBu)$_3$ in tolune and Et$_3$N	85°C stirred 6hr. followed by hydrolysis and calcination	Catalytic advantage	NM	Td, Oh
Reiner Anwander[16]	MCM-41	Al(CH$_3$)$_3$ in hexane	Rm. temp., stirred 20hr.	Lewis acidity	NM	Td, Oh
T. Sano[17]	MCM-41	Al(CH$_3$)$_3$ in toluene	Rm.temp.24hr, no stirring	Cumene conversion and stability	NM	Td, Oh
Robert Mokaya[18]	MCM-41	Al(OPr)$_3$ in supercritical fluid	40°C for CO$_2$, 110°C for Propane, 19hr followed by calcination	Improve hydrothermal stability	10.0	NM
Robert Mokaya and William Jones[19,21,27]	MCM-41	i) Aluminum chlorohydrate (Al$_{13}$$^{7+}$) ii) AlCl$_3$ iii) NaAlO$_2$	80°C, stirred 2hr. pH=3.3-3.5 followed by calcination	Cumene conversion	6.1-17.0 39.0 4.0	Td, Oh

Table 4.1 (cont'd)

Author	Parent mesostructure	Al sources	Grafting condition	Application	Si/Al ratio	Al geometry
Jacek Klinowsk[22]	MCM-41	NaAlO$_2$ solution	30-150°C for 3 or 12 hr. followed by calcination	NM	1.9-9.9	Mainly Td
Hsien-Ming Kao[23]	SBA-15	(NH$_4$)$_3$AlF$_6$ solution	Rm. temp. stirred 18 hr.	Cumene conversion	5.3-24.8	Td only
Larry Kevan[24]	SBA-15	i) AlCl$_3$ in dry EtOH ii) Al(OPr)$_3$ in hexane iii) NaAlO$_2$ solution	Rm. temp. stirred 12hr.followed by calcination	Ion exchange	21.3-40 8.5-37 20.8	Td, Oh Td, Oh Td only
Jimenez-Lopez, A.[25]	SBA-15	AlCl$_3$ in TMAOH solution	80°C 3hr. followed by calcination	Catalytic reactivity	5.5-49.0	Td, Oh
Juliette Blanchard[26]	SBA-15	AlCl$_3$ in TMAOH solution	80°C 2hr. followed by calcination	Cumene conversion	7.2-27	Td, Oh
Robert Mokaya[28]	MCM-41	Al(OPr)$_3$ in TMAOH solution	**with CTAB** Rm. temp. stirred 20hr, then autoclave 150°C 48hr. then calcination	NM	5.8-80	Td, Oh
S. Kawi[29]	MCM-41 Al-MCM41	Al(NO$_3$)$_3$ solution	Stirred at 50°C followed by calcination	Increase stability	10-∞	Td, Oh
Yuhan Sun[30,31]	Al-MSU-S	NaAlO$_2$ solution	**with CTAB** autoclave 110°C for 12 hr. then calcination	Cumene cracking	2.8 or 14	Td, Oh
T. Klimova[32]	SBA-16	i) AlCl$_3$ in dry EtOH ii) Al(OPr)$_3$ in hexane iii) NaAlO$_2$ solution	Rm. temp. stirred 12hr. followed by calcination	Catalytic activity	29.5 30.5 30.0	Td, Oh Td, Oh Td only

Rm. Temp.-room temperature
NM-not mentioned in the literature

122

Post synthesis methods usually generate two kinds of Al sites, 4-cordinate tetrahedron site and 6-cordinate octahedron site. Only the Td sites are incorporated into the framework and can generate acid sites. It is noteworthy that among all the literature studies, the aluminosilicates with mainly all tetrahedron Al sites were all synthesized by using aluminum aqueous solution as the aluminum sources.[9,22-24] However, the parent mesostructures that have been investigated are limited to only MCM-41 and SBA-15 silica materials. During the post synthesis/grafting process, the Al is first in contact with the outer surface of the host silica before penetrating into the internal pore channel system. Thus, the uniform distribution of Al into the internal pore channels may be hindered by the rather long and one dimensional pore channels of the mesoporous MCM-41 and SBA-15 silicas.[18] A wormhole mesostructure silica material, however, has three dimensional pore channel connections and a smaller domain size. Therefore it is considered to be easier to graft Al uniformly into the host silica.

In this present work the wormhole mesostructure HMS was utilized as the host silica material, and lithium aluminum hydride and sodium aluminate were used as the aluminum source for the post synthesis grafting. The efficiency of these methods for aluminum incorporation and their effect on the pore structure were investigated by a combination of characterization techniques including N_2 adsorption-desorption, powder X-ray diffraction, and [27]Al magic angle spinning solid state NMR. The ion exchange capacity of the aluminated HMS was evaluated by their performance on Pb^{2+} trapping experiments.

4.2 Experimental methods

4.2.1 Reagents

Dodecylamine (DDA), tetraethoxy orthosilicate (TEOS), lead atomic absorption standard solution (~1000 ppm), 1.0 M lithium aluminum hydride (LAH) in tetrahydrofuran solution, sodium aluminate (Na_2AlO_2), aluminum chloride ($AlCl_3$), sodium hydroxide (NaOH), and 99.999% lead nitrate were purchased from Aldrich. Ethanol was purchased in-house. All the reagents were used without further purification. Water used in the synthesis was double-exchanged to remove cations and anions via a Millipore filter apparatus.

4.2.2 Material synthesis

4.2.2.1 Alumination of mesoporous silica by LAH and water work-up

The parent mesoporous HMS material was synthesized by using dodecylamine (DDA) as the surfactant under neutral pH condition. The desired amount of DDA was dissolved in a plastic bottle with 162 g H_2O and 46 g EtOH. After obtaining a homogeneous surfactant solution, TEOS was added and the mixture was aged at 60°C for 24 hr. The products were recovered by filtration and air-dried followed by calcination at 600°C for 4 hr. The total molar ratio of reagents was DDA: TEOS: H_2O: EtOH = 0.25: 1: 180: 20.

A 0.5-g quantity of the calcined parent HMS mesostructured silica was added t the desired amount of 1M LAH in THF. The mixture was stirred under N_2 flow for 1 hr., followed by water work-up. Enough water was added in the work-up to consume all the LAH in the reaction flask. The product was filtered, washed with water exclusively and

then dried in air. The product was denoted HMS-LAH (x), where x represents the silica to aluminum ratio. The HMS-LAH (x) was then calcined at 600°C in air for 4hr. The final product was named HMS-LAH-C (x), where C represents the calcination process. Two ratios of silica to aluminum were carried out, namely 2.8 and 1.4, respectively.

4.2.2.2 Alumination of mesoporous silica by sodium aluminate

Two methods were investigated using sodium aluminate as the aluminum sources. Method I involves the preparation of fresh sodium aluminate by the reaction of $AlCl_3$ and NaOH. Method II involved the dissolution of purchased sodium aluminate in water directly.

Method I. ($AlCl_3$ + NaOH): a 0.5-g quantity of the calcined parent mesostructured silica was introduced into a desired amount of 0.1M $AlCl_3$ solution with stirring. Then, 0.1M NaOH solution was added drop wise to the mixture. The molar ratio of $AlCl_3$ to NaOH was 1 to 4. The mixture was mixed for 1hr. The product was recovered by filtration, washed by water and then dried in air completely. It was denoted HMS-Al-I. The HMS-Al-I was then calcined at 600°C in air for 4hr. The final product was named HMS-Al-I-C. The Si/Al ratio was 2.8.

Method II. ($NaAlO_2$): a 0.5-g quantity of the calcined parent mesostructure silica was introduced into the desired amount of 0.1M $NaAlO_2$ solution with stirring. The mixture was mixed for 1hr. The product was recovered by filtration, washed by water and then dried in air completely. It was named HMS-Al-II. The HMS-Al-II was then calcined at 600°C in air. The final product was named HMS-Al-II-C. The Si/Al ratio was 2.8.

4.2.3 Pb^{2+} trapping experiments

The Pb^{2+} adsorption experiment was carried out by stirring 0.05 g of aluminated silica material in 100 mL of lead nitrate (Pb(NO$_3$)$_2$) solution at 25°C. The initial concentration of Pb^{2+} for these experiments was 100 ppm in all cases. The mixtures were stirred for 24 hours and then filtered through a 0.25 μm filter paper to collect the final filtrate solution.

The amount of lead in the filtrate after the adsorption experiments was analyzed by cold vapor atomic absorption spectroscopy (AAS). The difference between the initial and equilibrium lead concentrations indicated the amount of lead that was trapped in the solid adsorbents.

4.2.4 Characterization

X-ray diffraction (XRD) patterns were obtained on a Rigaku Rotaflex 200B diffractometer equipped with Cu K$_\alpha$ X-ray radiation and a curved crystal graphite monochromator operating at 45 kV and 100 mA.

N$_2$ adsorption-desorption isotherms were obtained at −196 °C on a Micromeretics Tristar 3000 sorptometer using standard procedures. Samples were outgassed at 150 °C and 10^{-6} Torr for a minimum of 12 hr prior to analysis. Surface areas were calculated from the linear part of a BET plot of the nitrogen adsorption data according to IUPAC recommendations. The Barrett-Joyner-Halenda (BJH) method was used to obtain the pore size distribution from the adsorption branch of the isotherms.

MAS NMR spectra were recorded on a Varian 400 solid state NMR spectrometer with a zirconia rotor at a spinning frequency of 4 kHz. ^{27}Al MAS NMR spectra were recorded at 104.2 MHz under single-pulse mode and a pulse delay of 0.5 second.

Equilibrium concentrations of Pb^{2+} in solution were measured on a cold vapor atomic absorption spectroscopy Varian SpectrAA-200 using lead cathode with maximum working current of 10 mA.

4.3 Results and discussion

4.3.1 Aluminated HMS-LAH and HMS-LAH-C mesostructures

Aluminum was introduced into the silica framework by the in-situ hydrolysis of water work-up of lithium aluminum hydride (LAH). The product of LAH and water is H_2, $Al(OH)_3$ and LiOH, which can further react to produce $LiAlO_2$. Usually, for reduction reactions carried out by LAH, the excess LAH is worked up using acid to remove any precipitate of $Al(OH)_3$. A water work-up was used in this work to keep the aluminum in the framework of mesostructured HMS silica materials.

The X-ray diffraction patterns suggest the lost of mesostructure ordering upon LAH alumination in comparison with the pristine HMS mesostructure silica. A broad diffraction was observed for HMS-LAH materials, after calcination the HMS-LAH-C barely showed an undistinguishable peak (Fig. 4.1). Wide angle X-ray diffraction patterns show new peaks at 2θ of 20, 30, 36 and 64 degree for the HMS-LAH, and only a broad peak around 2θ of 66° for the calcined counterparts compared to pristine HMS which only shows a broad diffraction at a 2θ of 23° (Fig. 4.2). The introduction of aluminum into the mesostructured silica caused the lost of long range wormhole ordering for the material, as verified by the low angel X-ray diffraction patterns. The new wide-angle XRD peaks indicates the formation of aluminum hydroxide with some degree of crystallinity.[33] The crystalline structure, however, was not stable and vanished after the calcination.

Figure 4.3 reports the N_2 adsorption–desorption isotherms (Fig. 4.3A) and Barrett-Joyner-Halenda (BJH) framework pore size distributions (Fig. 4.3B) for aluminated HMS-LAH silicas and the counterparts after calcination. Table 4.2 summarizes the d spacing, pore size, total pore volume and BET surface area for each product. The isotherms for aluminated HMS materials before and after calcination all showed steps at a relative pressure of 0.35-0.45, indicating the presence of mesopores. The surface area and pore volume decrease upon increasing the Al content in the HMS-LAH. The calcined HMS-LAH-C showed a pore volume and surface area comparable to the counterpart before calcination, but with an increased pore size. For instance, the HMS-LAH (1.4) has a lower surface area (387 m^2 g^{-1}) and pore volume (0.76 cm^3 g^{-1}) compared with the pristine HMS (surface area of 941 m^2 g^{-1} and pore volume of 1.12 cm^3 g^{-1}). The HMS-LAH-C (1.4) has a surface area (256 m^2 g^{-1}) and pore volume (0.64 cm^3 g^{-1}) comparable to HMS-LAH, but the pore size increased from 2.4 nm (HMS-LAH) to 2.7 nm after calcination. The pore volume and surface area decreased upon increasing the Al content in the initial alumination synthesis mixture. The alumination reaction was only carried out at room temperature. Thus, the Al most likely is located on the surface rather than penetrated inside the walls of the inorganic silica framework. The additional layer of framework Al and the sorption of non-framework Al resulted in the decrease of pore volume and surface area.

The ^{27}Al MAS NMR spectra were recorded for HMS-LAH and HMS-LAH-C in order to identify the coordination geometry of the Al centers incorporated into the silica framework and follow the change in the environment of the Al after calcination. Generally, there are two types of Al sites in aluminated silica materials, tetrahedrally

coordinated (framework) Al sites with a chemical shift around 50 ppm and octahedrally coordinated (non-framework) Al sites with a resonance at a chemical shifts around 0 ppm.[30,33] The ^{27}Al MAS NMR spectrum of HMS-LAH shows two peaks (Fig. 4.4A). The resonance at 6.8 ppm, indicates the presence of Al in octahedral sites at 54% abundance. The resonance at 55 ppm indicates tetrahedral Al at 46 % abundance. After calcination, the ^{27}Al MAS NMR spectrum of HMS-LAH-C showed two peaks at the same chemical shifts (6.8 ppm and 55 ppm) (Fig. 4.4B). Interestingly, after calcination, more tetrahedral Al was incorporated into the framework while less non-framework octahedral Al remained in the pores. The abundances of tetrahedral Al and octahedral Al in the calcined form are 83% and 17%, respectively. The pore size was observed an increase by 0.3 nm from HMS-LAH to HMS-LAH-C. This suggests that calcination induced the condensation of hydroxyl groups, resulting in the more incorporation of tetrahedral Al into the framework at the expense of octahedral Al.

Figure 4.1. Low angle X-ray diffraction patterns of aluminated HMS made using LAH as the aluminum source before and after calcination at 600°C. The numbers in parenthesis provide the overall Si/Al used in the synthesis.
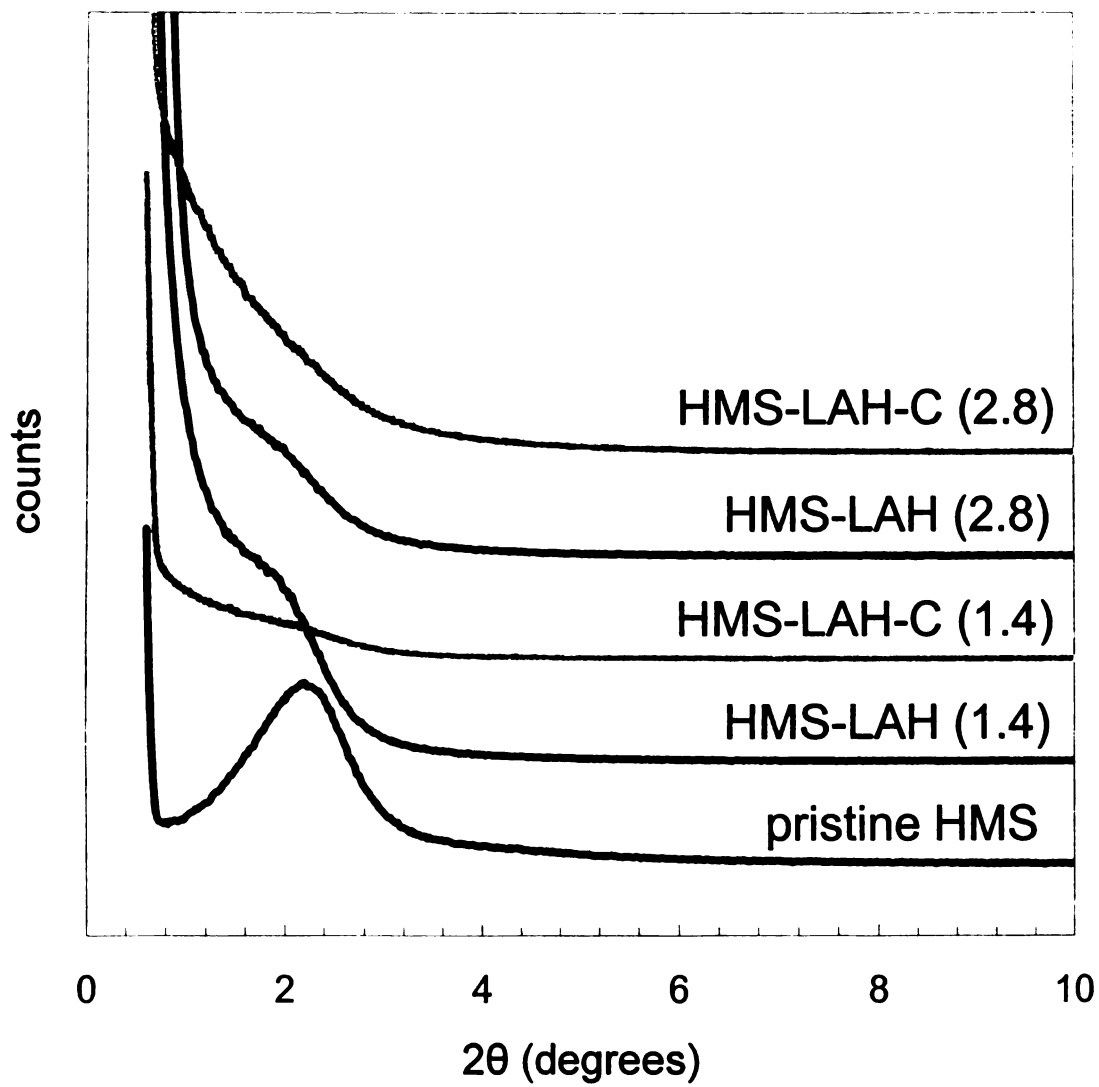
Figure 4.2. Wide angle X-ray diffraction patterns of aluminated HMS made using LAH as the aluminum source before and after calcination at 600°C. The numbers in parenthesis provide the overall Si/Al used in the synthesis.

Figure 4.3. (A) N_2 adsorption–desorption isotherms and (B) BJH framework pore size distributions for pristine HMS (●), HMS-LAH (■) and HMS-LAH-C (□).

Table 4.2. Physical properties of mesostructured silica aluminated by reaction with LAH.

	pore size [a] (nm)	S_{BET} ($m^2 \ g^{-1}$)	V_{tot} [b] ($cm^3 \ g^{-1}$)
Pristine HMS	2.4	941	1.12
HMS-LAH (2.8)	2.3	597	0.85
HMS-LAH-C (2.8)	2.7	426	0.81
HMS-LAH (1.4)	2.4	387	0.76
HMS-LAH-C (1.4)	2.7	256	0.64

[a] Pore size diameter was determined by the BJH model from the adsorption branches of the isotherms. [b] Total pore volume was determined at $P/P_0 = 0.98$.

Figure 4.4. ^{27}Al MAS NMR spectra of aluminated HMS-LAH (2.8), (A) before and (B) after calcination at 600°C for 4 hr.

4.3.2 Aluminated HMS-Al-I, HMS-Al-II, HMS-Al-I-C, and HMS-Al-II-C mesostructures

Sodium aluminate has been used as the aluminum source for the alumination fo mesostructured silica.[9,19,22,24,30-32] In this present work, two methods were used to incorporate sodi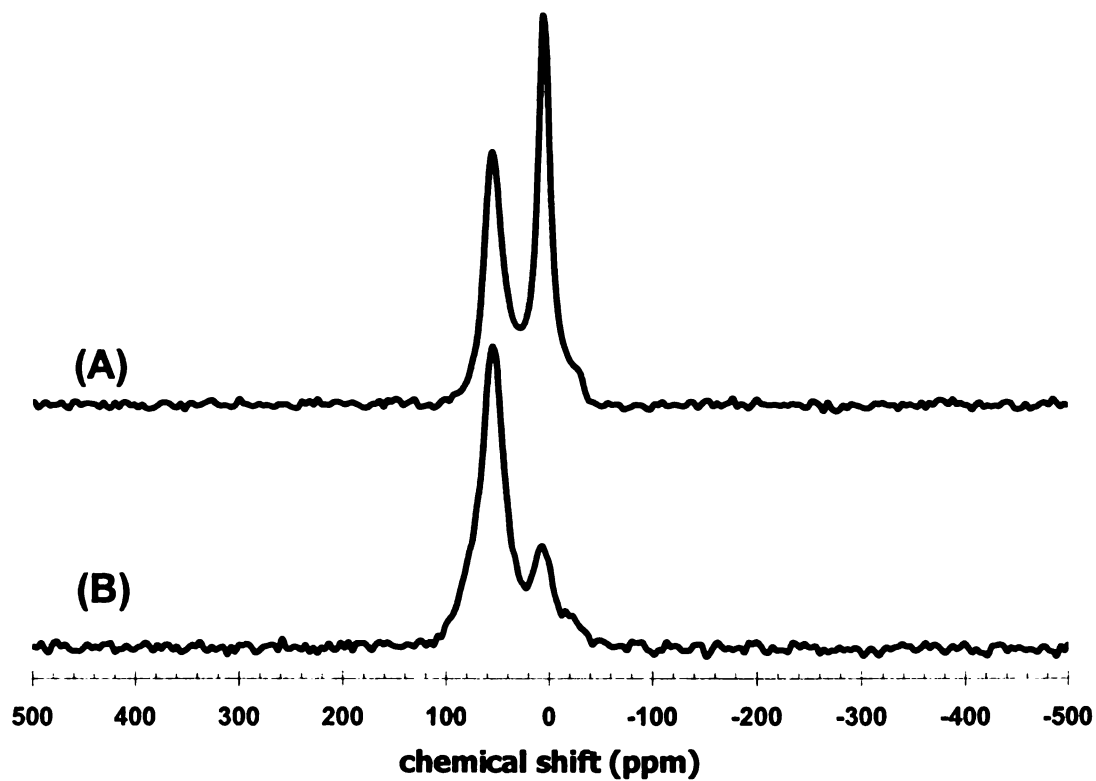um aluminate into the wormhole HMS mesostructure framework. Method I used $AlCl_3$ solution followed by addition of NaOH solution to make fresh $NaAlO_2$, while method II used a $NaAlO_2$ solution directly. The amount of NaOH used was four times as the amount of $AlCl_3$, thus the following reaction was expected:

$$AlCl_3 + 4NaOH \rightarrow NaAlO_2 + 2H_2O + 3NaCl$$
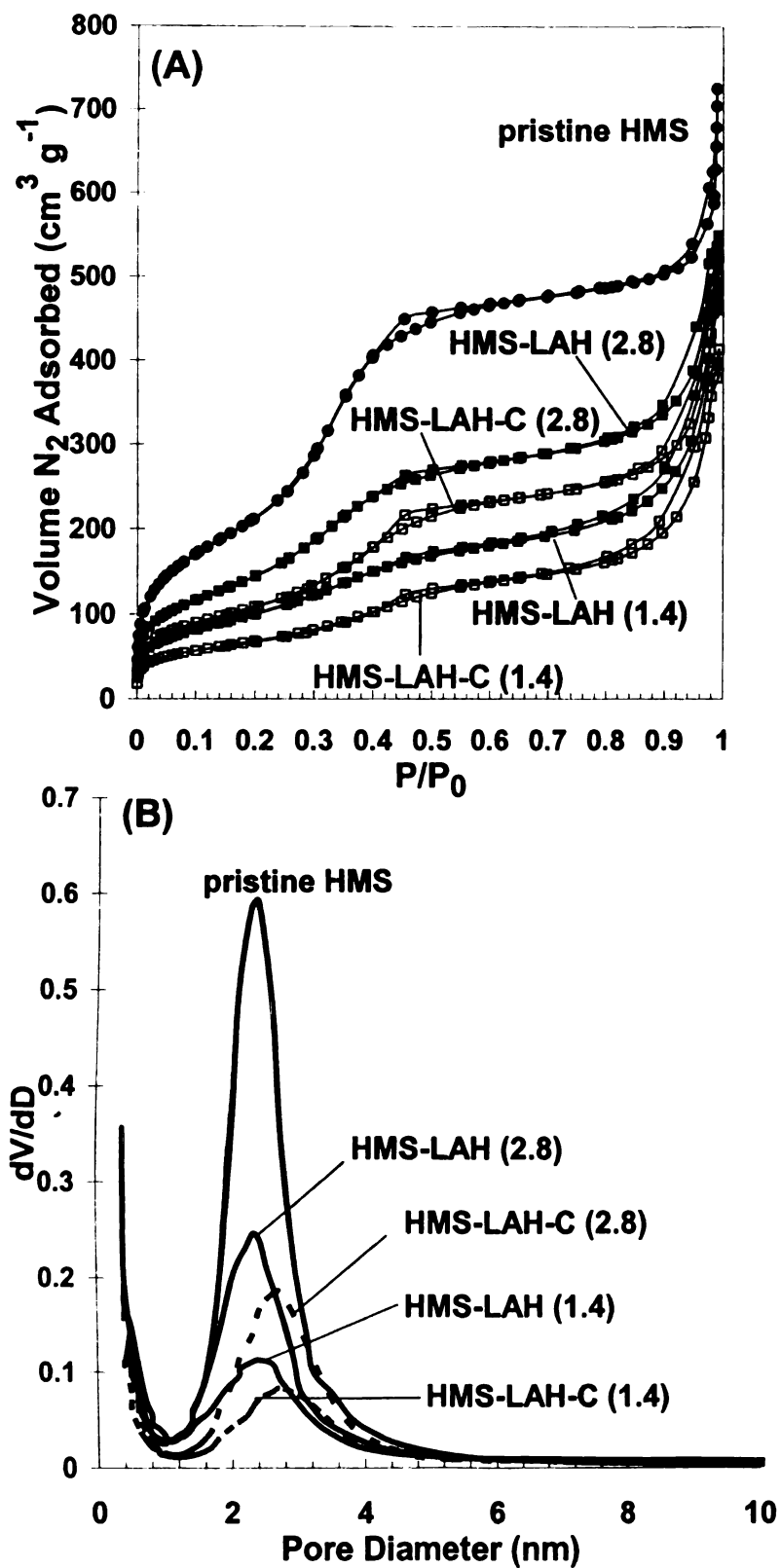
Therefore, method I and method II both used $NaAlO_2$ as the Al source for alumination. Only one Si/Al ratio (i.e. 2.8) was investigated.

The X-ray diffraction patterns of aluminated HMS materials by both methods before and after calcination showed no distinguishable diffraction peak at low angle, indicating the loss of mesostructure upon aluminum incorporation (Fig. 4.5). The X-ray patterns at wide angle (Fig. 4.6) showed no peak besides the Si-O short range ordering diffraction around 2θ of 23°, suggesting that all the aluminum is in the amorphous phase.

Figure 4.7 reports the N_2 adsorption–desorption isotherms (Fig. 4.7A) and Barrett-Joyner-Halenda (BJH) framework pore size distributions (Fig. 4.7B) for aluminated HMS-LAH silicas and the counterparts after calcination. Interestingly, the HMS-Al and HMS-Al-C prepared by both methods showed nearly identical results, respectively. The overlapping isotherms and pore size distributions for the aluminated mesostructure silica synthesized by method I and II suggests that the physical properties of the resulting materials have no obvious differences. The surface area and pore volume

135

decreased after the incorporation of aluminum compared to the HMS parent silica material. The pore size of HMS-Al materials (2.4 nm) did not change compared to the parent HMS silica materials, while the pore size after calcination increased to 2.5-2.6 nm for HMS-Al-C materials. This might be due to the rearrangement of the incorporated Al during calcination at elevated temperature. Physical properties of the products are list in Table 4.3.

The Si/Al ratios obtained for the aluminated mesostructured silica by method I and method II were about 7.0, which is higher than the value of 2.8 for the composition of initial reaction mixture. This suggests that only a portion of the starting Al was retained in the solid after modification. It is clear that the incorporation of aluminum sacrifices the structure and the surface area and pore volume of the resulting materials.

^{27}Al MAS NMR spectra showed the presence of only tetrahedrally coordinated Al species in the aluminated silica solid by using the sodium aluminate as the aluminum source before and after calcination (Fig. 4.8), suggesting that all the incorporated Al are in the tetrahedron framework sites. This observation agrees with previous studies of the alumination of SBA-15,[24] SBA-16,[32] and MCM-41[22] using $NaAlO_2$ solution as the aluminum sources. In these studies, the ^{27}Al MAS NMR profiles also showed a main resonance with a chemical shift of 50 ppm, indicating that main coordination environment for aluminum to be tetrahedral.

$NaAlO_2$ solution has also been used as Al source for alumination for Al containing material Al-MSU-S.[30,31] In these works, the authors claimed that the presence of cetyltrimethylammonium bromide (CTAB) was critical to maintain the framework mesostructure. In this present work, no CTAB was used to maintain the mesostructure,

yet features typical of a mesostructure were observed for the nitrogen isotherms, even though the XRD results do not support the presence of an ordered mesostructure. The retention of mesopores, without mesopore order, may be a consequence of the ambient condition used to carry out the alumination reactions.

Figure 4.5. Low angle X-ray diffraction patterns of HMS-Al-I and HMS-Al-II materials before and after calcination at 600°C.
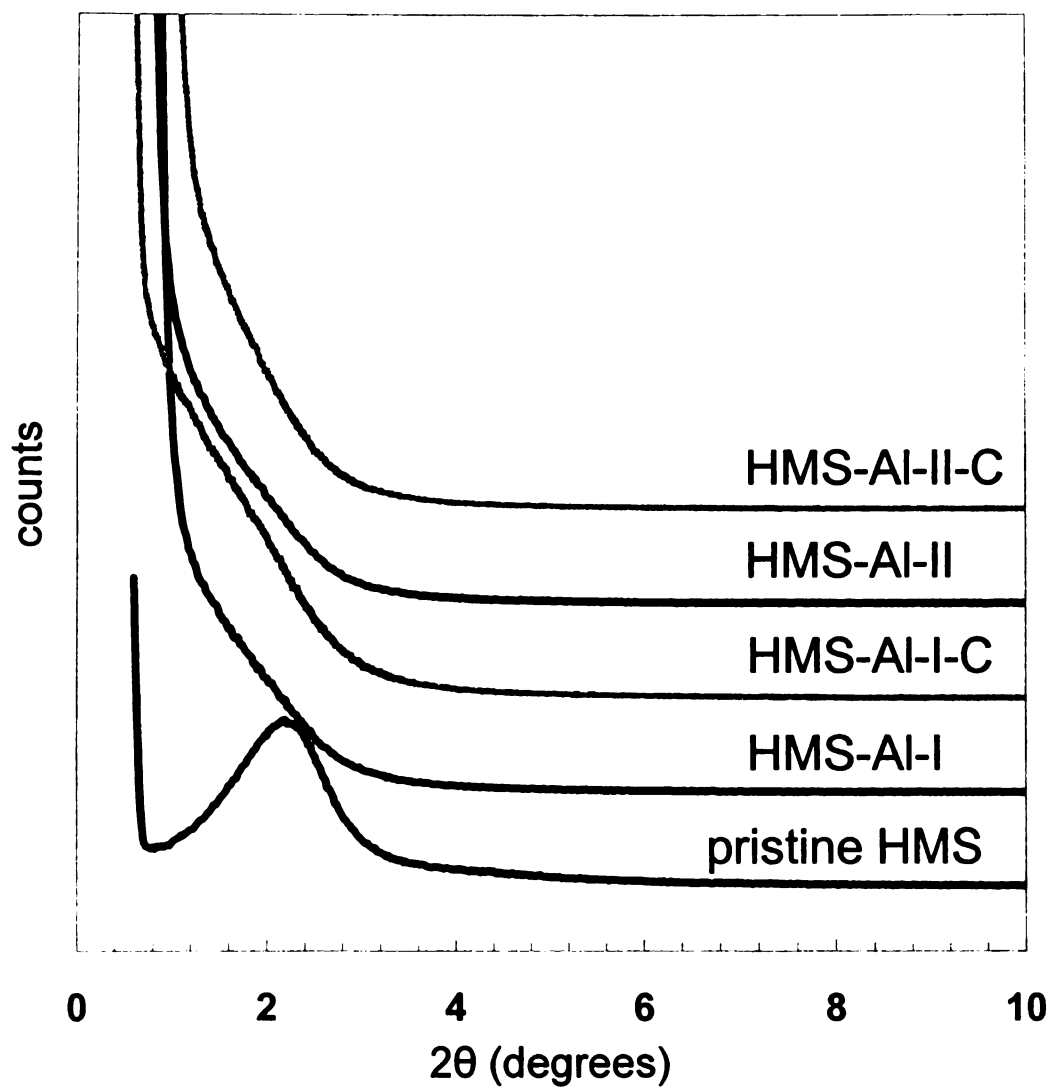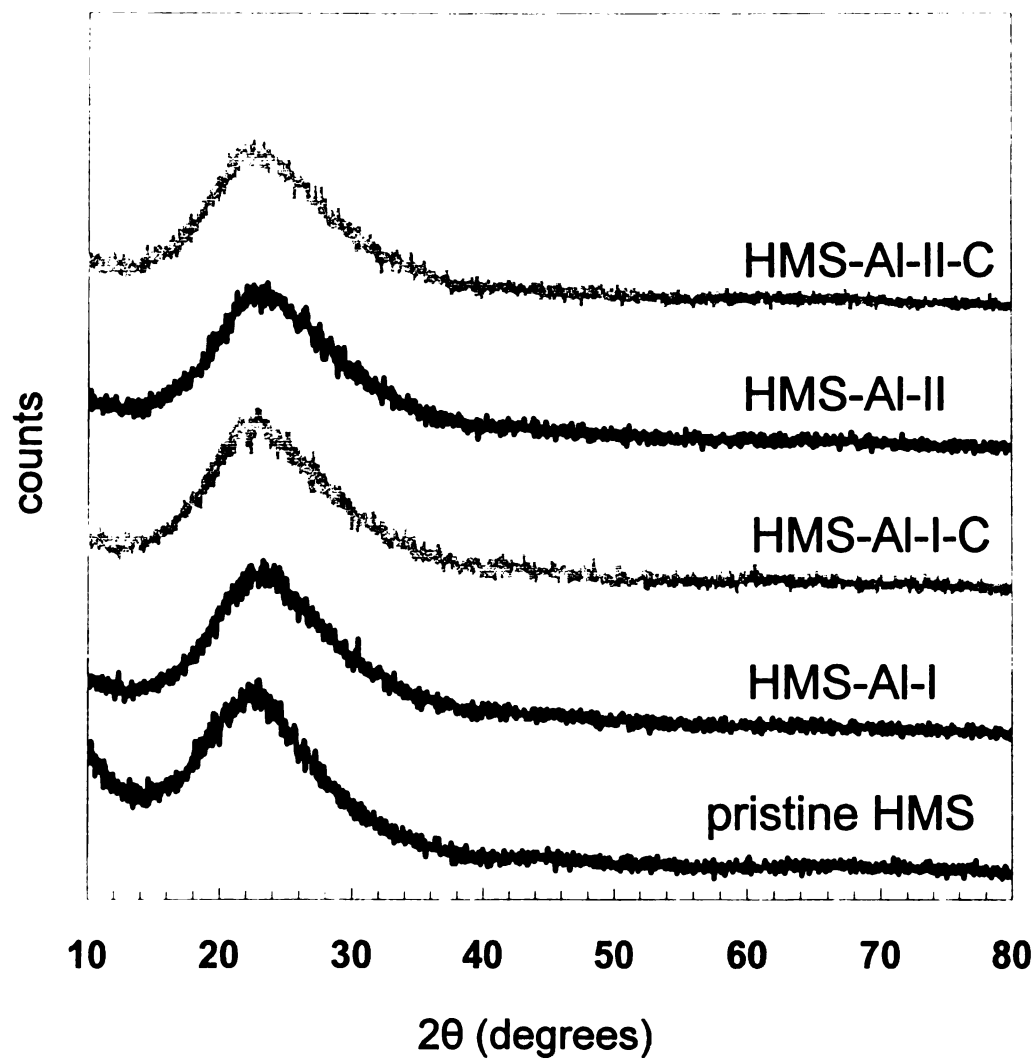
Figure 4.6. Wide angle X-ray diffraction patterns of HMS-Al-I and HMS-Al-II materials before and after calcination at 600°C.
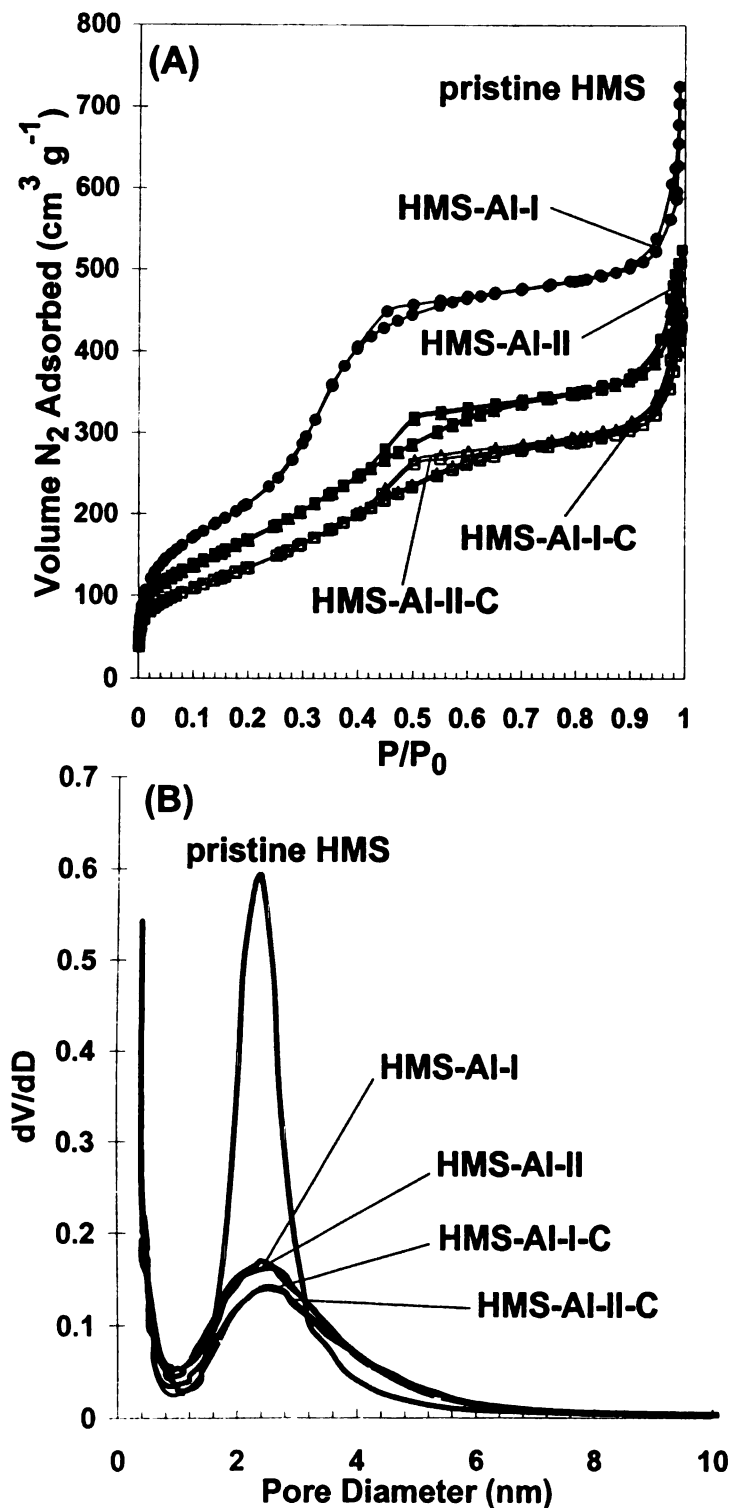
Figure 4.7. (A) N_2 adsorption–desorption isotherms and (B) BJH framework pore size distributions for pristine HMS (●), HMS-Al (filled marker) and HMS-Al-C (opened marker) synthesized by method I (square) and method II (triangular).

Table 4.3. Physical properties of aluminated mesostructured silicas using sodium aluminate prior to and upon calcination.

	pore size [a] (nm)	S_{BET} (m^2 g^{-1})	V_{tot} [b] (cm^3 g^{-1})	Si/Al ratio [c]
Pristine HMS	2.4	941	1.12	∞
HMS-Al-I	2.4	642	0.81	7.2
HMS-Al-I-C	2.5	513	0.69	7.3
HMS-Al-II	2.4	638	0.77	7.0
HMS-Al-II-C	2.6	512	0.71	6.9

[a] Pore size diameter was determined by the BJH model from the adsorption branches of the isotherms. [b] Total pore volume was determined at P/P$_0$=0.98. [c] Calculated from the ICP results.

Figure 4.8. (A) ^{27}Al MAS NMR spectra of aluminated mesostructure, HMS-Al-I and (B) the counterpart after calcination, HMS-Al-I-C.

4.3.3 Lead Adsorption experiment

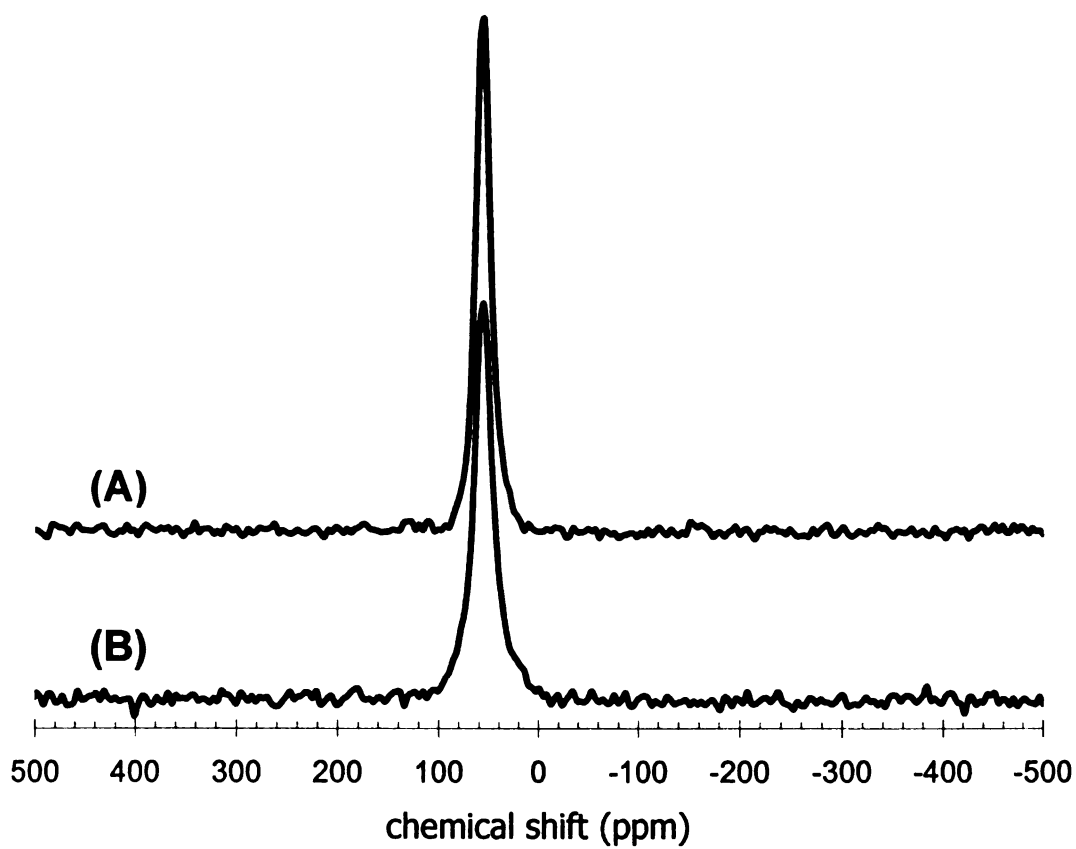Calcined HMS does not have a binding capacity towards Pb^{2+} from aqueous solution. So any trapping site was generated through the process of alumination. Aluminated HMS mesostructured materials made by using LAH and sodium aluminate as aluminum sources were evaluated for the lead adsorption performance. The results were listed in Table 4.4.

Aluminated HMS materials, made from LAH, whether calcinated or not, had Pb^{2+} trapping capacities of about 0.96 mmol g^{-1}, leaving the equilibrium concentration of lead near the detection limit of the AA instrument (which is 0.5 ppm). The HMS-LAH materials with different initial Si/Al ratio showed similar trapping capacities. This might be because the materials were not saturated with Pb^{2+} cations. If a higher initial lead concentration is used, the difference in trapping capacities for different Si/Al ratios may be observed.

Aluminated mesostructure silica materials from sodium aluminate by method II showed better lead adsorption capacity (0.90 mmol g^{-1}) in comparison with the derivatives obtained by method I (0.75 mmol g^{-1}), even though the physical properties of the materials made by two methods did not show any significant difference. Aluminated silica materials synthesized by using sodium aluminate solution as the aluminum sources showed relatively lower adsorption capacities in comparison to the derivatives aluminated by LAH. This is due to the high Si/Al ratio (lower aluminum content) in the former materials.

A yellow flame was observed during the AA analysis of the Pb^{2+} solution that came in contact with the HMS-Al-I and HMS-Al-I adsorbents. This suggests the

existence of sodium cation in the filtrate. No characteristic flame color was observed for filtrate after contact with HMS-LAH and HMS-LAH-C materials because the counter ions in these cases are Li^+. Therefore, it is suggested that the trapping property was base on an ion exchange mechanism.

In the aluminated materials, one aluminum tetrahedron site was electrostatically matched by one Li^+ or Na^+ counter ions. Each Pb^{2+} adsorbed on the adsorbent will replace two of the Li^+ or Na^+ counter ions during the trapping experiments. Therefore the maximum trapping capacities of an adsorbent would be half amount of the accessible tetrahedron Al sites within the material.

For the HMS-LAH (2.8) material, 46% of the Al is in the Td sites according to the ^{27}Al MAS NMR date. The maximum trapping capacity for lead divalent cation is about 0.9 mmol g^{-1}, which agrees with the 0.96 mmol g^{-1} trapping capacity result observed. HMS-LAH-C (2.8) material has a theoretical maximum trapping capacity of 1.8 mmol of lead per gram of the adsorbent, while the trapping capacity is 0.96 mmol g^{-1}. There are two possible explanations. First, the material is not totally saturated yet because the equilibrium concentration is near the detection limit of the AA instrument. Secondly, part of the tetrahedral Al sites in the HMS-LAH-C (2.8) are generated during the calcination process through the possible co-condensation of hydroxyl groups on the aluminum sites. The newly formed Al layer will make the first original Td Al layer not accessible anymore. Therefore the trapping capacity may not increase with the increasing tetrahedral Al sitesl.

The theoretical lead capacities of aluminated HMS materials made using sodium aluminate as Al sources are compatible with the observed trapping capacities. For

example, the sodium aluminate incorporated HMS-Al-II-C material after calcination shows a trapping capacity of 0.90 mmol g^{-1}, while the theoretical maximum trapping capacity calculated from tetrahedral Al amount is 0.95 mmol g^{-1}. It also further proves the ion exchange mechanism for heavy metal trapping and suggests that all the Td Al sites in the aluminated HMS by using sodium aluminate are available. In comparison to the low accessibility of aluminum site in MCM-41[34] and SBA-15[24] systems, the wormhole 3D structured showed an advantage with respect to the adsorption application.

Table 4.4. The lead trapping performance of aluminated HMS mesostructure silica materials made using LAH and sodium aluminate as the aluminum sources.

	Equilibrium Concentration (ppm)	Lead adsorbed capacity (mmol g^{-1})	Al content in adsorbents (mmol g^{-1}) [a]	Td Al sites in adsorbents (mmol g^{-1}) [b]	Theoretical trapping capacity for lead (mmol g^{-1})	Si/Al ratio expected	Si/Al ratio observed
HMS-LAH (2.8)	0.9	0.96	3.7	1.8	0.9	2.8	2.6
HMS-LAH-C (2.8)	0.5	0.96	4.3	3.6	1.8	2.8	1.9
HMS-LAH (1.4)	7.2	0.90	NM	NM	NM	1.4	NM
HMS-LAH-C (1.4)	0.8	0.96	NM	NM	NM	1.4	NM
HMS-Al-I	21.0	0.76	1.7	1.7	0.85	2.8	7.2
HMS-Al-I-C	22.5	0.75	1.7	1.7	0.85	2.8	7.3
HMS-Al-II	7.3	0.89	1.9	1.9	0.95	2.8	7.0
HMS-Al-II-C	6.9	0.90	1.9	1.9	0.95	2.8	6.9

[a] Calculated from the ICP test results. [b] Based on the integration results from ^{27}Al MAS NMR data. NM: not measured Initial Pb(NO$_3$)$_2$ concentration in all cases is 100 ppm. A 0.05 g quantity of adsorbent was dispersed in 100 mL Pb^{2+} solution for the trapping experiments.

4.4 Conclusion

Wormhole mesostructured HMS silica was synthesized and aluminated using different aluminum sources, namely lithium aluminum hydride (LAH), in-situ sodium aluminate ($NaAlO_2$) (method I) and sodium aluminate solution (method II). The incorporation of the aluminum into the framework by all the methods caused some structure disorder and sacrificed surface area and pore volume of the parent materials, though some mesopores were retained after alumination.

The aluminated HMS silica material by LAH showed some crystallinity according to the X-ray diffraction patterns at wide angle range. However, the low degree of crystallinity vanished after calcination. LAH aluminated HMS showed both tetrahedrally coordinated (framework) and octahedrally coordinated (non-framework) Al sites, and the fraction of framework Al site increased upon calcination. This is the first example of the alumination of a mesostructure silica material by using LAH as aluminum source. The resultant adsorbents showed excellent heavy metal ion (i.e. Pb^{2+}) trapping capacities, which is nearly 1 mmol g^{-1}. It was suggested that all the Td Al sites in the HMS-LAH materials are accessible, while only half of the Td Al sites in the HMS-LAH-C materials are accessible.

The aluminated HMS silica materials made using sodium aluminate by both method I and II showed nearly identical results. These materials only have tetrahedrally coordinated (framework) Al sites, indicating the efficiency of alumination by using the aqueous aluminum sources. The aluminated materials showed good trapping capacities towards lead in aqueous solution, 0.75-0.90 mmol g^{-1}. It was suggested that ion exchange is the mechanism for heavy metal adsorption and that all the tetrahedral Al sites are

available ion exchange sites. The 3D wormhole structure of HMS material is superior to the hexagonal arrayed channel 1D MCM-41 and SBA-15 systems with regards to the alumination of mesostructured silicas for heavy metal ion removal.

The aluminated materials presented in this work have very high percentage of tetrahedral coordinated framework Al in the aluminosilicate framework. It also proved that the accessibility of the Td Al sites is excellent. Besides applications as metal ion adsorbents, they also have the potential to serve as the acidic sites in catalytic reactions.

4.5 References

(1)   Beck, J. S.; Vartuli, J. C.; Roth, W. J.; Leonowicz, M. E.; Kresge, C. T.; Schmitt, K. D.; Chu, C. T. W.; Olson, D. H.; Sheppard, E. W.; et al. *J. Am. Chem. Soc.* **1992**, *114*, 10834-43.

(2)   Kresge, C. T.; Leonowicz, M. E.; Roth, W. J.; Vartuli, J. C.; Beck, J. S. *Nature* **1992**, *359*, 710-12.

(3)   Corma, A.; Fornes, V.; Navarro, M. T.; Perez-Pariente, J. *J. Catal.* **1994**, *148*, 569-74.

(4)   Luan, Z.; He, H.; Zhou, w.; Cheng, C.-F.; Klinowski, J. *J. Chem. Soc., Faraday Trans.* **1995**, *91*, 2955-9.

(5)   Luan, Z.; Cheng, C.-F.; Zhou, W.; Klinowski, J. *J. Phys. Chem.* **1995**, *99*, 1018-24.

(6)   Mokaya, R.; Jones, W.; Luan, Z.; Alba, M. D.; Klinowski, J. *Catal. Lett.* **1996**, *37*, 113-20.

(7)   Weglarski, J.; Datka, J.; He, H.; Klinowski, J. *J. Chem. Soc., Faraday Trans.* **1996**, *92*, 5161-5164.

(8)   Mokaya, R.; Jones, W. *J. Catal.* **1997**, *172*, 211-221.

(9)   Chen, L. Y.; Ping, Z.; Chuah, G. K.; Jaenicke, S.; Simon, G. *Microporous Mesoporous Mater.* **1999**, *27*, 231-242.

(10)   Xu, M.; Arnold, A.; Buchholz, A.; Wang, W.; Hunger, M. *J. Phys. Chem. B* **2002**, *106*, 12140-12143.

(11)   Choudhary, V. R.; Mantri, K. *J. Catal.* **2002**, *205*, 221-225.

(12)   Choudhary, V. R.; Mantri, K. *Microporous Mesoporous Mater.* **2002**, *56*, 317-320.

(13)   Mokaya, R.; Jones, W. *Phys. Chem. Chem. Phys.* **1999**, *1*, 207-213.

(14)   Landau, M. V.; Dafa, E.; Kaliya, M. L.; Sen, T.; Herskowitz, M. *Microporous Mesoporous Mater.* **2001**, *49*, 65-81.

(15)   Mokaya, R. *Chem. Commun. (Cambridge)* **1997**, 2185-2186.

(16)   Anwander, R.; Palm, C.; Groeger, O.; Engelhardt, G. *Organometallics* **1998**, *17*, 2027-2036.

(17)   Oumi, Y.; Takagi, H.; Sumiya, S.; Mizuno, R.; Uozumi, T.; Sano, T. *Microporous Mesoporous Mater.* **2001**, *44-45*, 267-274.

(18)   O'Neil, A. S.; Mokaya, R.; Poliakoff, M. *J. Am. Chem. Soc.* **2002**, *124*, 10636-10637.

(19)   Mokaya, R.; Jones, W. *J. Mater. Chem.* **1999**, *9*, 555-561.

(20)   Mokaya, R. *J. Catal.* **1999**, *186*, 470-477.

(21)   Mokaya, R.; Jones, W. *Chem. Commun. (Cambridge)* **1998**, 1839-1840.

(22)   Hamdan, H.; Endud, S.; He, H.; Nazlan, M.; Muhid, M.; Klinowski, J. *J. Chem. Soc., Faraday Trans.* **1996**, *92*, 2311-2315.

(23)   Kao, H.-M.; Ting, C.-C.; Chao, S.-W. *J. Mol. Catal. A: Chem.* **2005**, *235*, 200-208.

(24)   Luan, Z.; Hartmann, M.; Zhao, D.; Zhou, W.; Kevan, L. *Chem. Mater.* **1999**, *11*, 1621-1627.

(25)   Gomez-Cazalilla, M.; Merida-Robles, J. M.; Gurbani, A.; Rodriguez-Castellon, E.; Jimenez-Lopez, A. *J. Solid State Chem.* **2007**, *180*, 1130-1140.

(26)   Zeng, S.; Blanchard, J.; Breysse, M.; Shi, Y.; Shu, X.; Nie, H.; Li, D. *Microporous Mesoporous Mater.* **2005**, *85*, 297-304.

(27)   Mokaya, R. *Chem. Commun. (Cambridge, U. K.)* **2001**, 633-634.

(28)   Mokaya, R. *Chem. Commun. (Cambridge)* **2000**, 1541-1542.

(29)   Shen, S. C.; Kawi, S. *Langmuir* **2002**, *18*, 4720-4728.

(30)   Zhai, S.; Zheng, J.; Li, J.; Wu, D.; Sun, Y.; Deng, F. *J. Porous Mater.* **2005**, *12*, 107-112.

(31)   Zhai, S.; Zheng, J.; Li, J.; Wu, D.; Sun, Y.; Deng, F. *Microporous Mesoporous Mater.* **2005**, *83*, 10-18.

(32)   Klimova, T.; Lizama, L.; Amezcua, J. C.; Roquero, P.; Terres, E.; Navarrete, J.; Dominguez, J. M. *Catal. Today* **2004**, *98*, 141-150.

(33)   Isobe, T.; Watanabe, T.; d'Espinose de la Caillerie, J. B.; Legrand, A. P.; Massiot, D. *J. Colloid Interface Sci.* **2003**, *261*, 320-324.

(34)   Kolodziejski, W.; Corma, A.; Navarro, M. T.; Perez-Pariente, J. *Solid State Nucl. Magn. Reson.* **1993**, *2*, 253-9.